Czech Technical University in Prague
Faculty of Electrical Engineering
Department of Telecommunication Engineering

Efficient Energy Management System for Enhancing Quality of Service in Wireless Sensor Networks

Doctoral Thesis

Akeel Othman

Prague, February 2024

Ph.D. programme: P2612 Electrical Engineering and Information Technology
Branch of study: 2601V013 Telecommunication Engineering

Supervisor: prof. Ing. Dušan Maga, Ph.D.
Supervisor-Specialist: Ing. Jaromír Hrad, Ph.D.

Declaration

I declare that the work presented in this dissertation thesis is my work, and the achieved results are the findings of my research monitored and directed by my supervisors in parallel with the contributions of other co-authors in the corresponding published papers.

In Prague, February 2024

.....
Akeel Othman

Abstract

Wireless Sensor Network (WSN) is an important technology in the field of telecommunication offering a wide range of applications across various sectors. It is used for monitoring, data collection, and measuring physical signals in both natural and artificial environments. A WSN consists of numerous distributed sensors, strategically placed in various locations. These sensors work in unison to gather data from their surroundings and share this information via wireless connections. The collective data is then utilized for decision-making processes or continuous monitoring purposes. WSNs find their application in a range of scenarios, from compact system implementations to extensive environmental monitoring. Energy management in Wireless Sensor Networks (WSN) is crucial, given that the nodes are typically powered by batteries with limited energy capacity. The primary goal of WSN energy management systems is to extend the network's operational lifespan while maintaining its communication efficiency at acceptable levels. This is achieved by optimizing energy consumption through various strategies. Key methods include extending the sleep periods in the duty cycling approach, which alternates between active and inactive states to conserve power. Data aggregation from multiple sensors is employed to reduce the frequency of transmissions, thereby saving energy. Additionally, the implementation of energy-efficient routing protocols, such as LEACH (Low-Energy Adaptive Clustering Hierarchy), further contributes to minimizing energy expenditure during data transmission. Another pivotal aspect is the use of energy harvesting technologies, either to recharge the batteries or to facilitate battery-less operation of sensors, thus significantly enhancing the sustainability and endurance of the network. In this dissertation, a novel approach for an energy management system in Wireless Sensor Networks (WSN) is presented. This system uniquely integrates two energy harvesting methods: photovoltaic (PV) and mechanical vibration, specifically using piezoelectric PZT materials, alongside a conventional battery. This integration aims to significantly extend the battery's lifespan and enhance the communication efficiency of the network. By harnessing energy from two distinct renewable sources, the system effectively mitigates the issue of unreliability associated with individual renewable sources, as the energy harvesters rely on different types of renewable energy. The core of this system lies in its intelligent selection mechanism for the energy source powering each node. This selection is based on real-time data regarding the status of the PV harvester, the piezoelectric harvester, and the battery's state of charge (SoC). For the PV harvester, the dissertation introduces an innovative hybrid solar energy prediction algorithm. This algorithm combines statistical methods and deep learning techniques to forecast the availability of solar energy for the upcoming hour. This forecast is then compared with the energy data from the PZT harvester, derived from a lookup table based on vibration resources, alongside the current SoC of the battery. To optimize the Quality of Service (QoS) of the network, a novel algorithm is proposed. This algorithm dynamically adjusts the transmission power level, data rate, and duty cycle based on the available energy resources. It aims to maintain the minimum QoS requirements while simultaneously addressing a multi-objective optimization problem. This problem focuses on maximizing QoS and prolonging the battery's lifespan. The proposed system thus presents a holistic approach to energy management in WSNs, leveraging the synergy of multiple energy sources and advanced algorithmic strategies to achieve superior network performance and sustainability.

Keywords: Telecommunication, WSN, Energy Management System, Solare Energy Prediction, Energy Harvesting, Piezoelectric, Battery, QoS, Deep Learning.

Abstrakt

Bezdrátová senzorová síť (Wireless Sensor Network – WSN) je důležitou technologií pro monitorování, sběr dat a měření fyzikálních signálů v přírodních i umělých prostředích. WSN se skládá z mnoha distribuovaných senzorů, strategicky umístěných na různých místech. Tyto senzory společně pracují na sběru dat ze svého okolí a sdílení těchto informací prostřednictvím bezdrátových komunikačních prostředků. Sběr dat je poté využíván pro rozhodovací procesy nebo pro nepřetržitý monitoring. WSN nacházejí uplatnění v řadě scénářů, od kompaktních systémových implementací po rozsáhlý environmentální monitoring. Správa energie v bezdrátových senzorových sítích (WSN) je klíčová, vzhledem k tomu, že komunikující uzly jsou typicky napájeny bateriemi s omezenou kapacitou. Hlavním cílem systémů pro správu energie WSN je prodloužit operační životnost sítě při zachování její funkčnosti na přijatelné úrovni. Toho je dosaženo optimalizací spotřeby energie s využitím různých strategií. Klíčové metody zahrnují prodloužení doby spánku v přístupu duty cycling, který střídá aktivní a neaktivní stavy za účelem šetření energie. Agregace dat z více senzorů je použita k snížení frekvence přenosů, čímž se šetří energie. Dále implementace energeticky účinných směrovacích protokolů, jako je (Low-Energy Adaptive Clustering Hierarchy– LEACH), přispívá k minimalizaci energetických výdajů během přenosu dat. Dalším klíčovým aspektem je využití technologií pro sběr energie, buď pro dobíjení baterií, nebo pro usnadnění provozu senzorů bez baterií, čímž se významně zvyšuje udržitelnost a výdrž sítě. V této disertační práci je prezentován nový přístup k systému pro správu energie v bezdrátových senzorových sítích (WSN). Tento systém inovativním způsobem integruje dvě metody sběru energie: fotovoltaickou (PV) a z mechanických vibrací, konkrétně s využitím piezoelektrických materiálů PZT, v kombinaci s konvenční baterií. Tato integrace má za cíl výrazně prodloužit životnost baterie a zvýšit celkovou efektivitu sítě. Využíváním energie ze dvou odlišných obnovitelných zdrojů navrhovaný systém vhodně řeší problém nespolehlivosti spojený s jednotlivými obnovitelnými zdroji, jelikož sběrače energie spoléhají na různé, vzájemně se doplňující, druhy obnovitelné energie. Jádrem tohoto systému je inteligentní mechanismus pro volbu zdroje energie napájející každý uzel sítě. Volba je založena na reálných datech o stavu fotovoltaického sběrače, piezoelektrického sběrače a stavu nabití baterie (SoC). Pro fotovoltaický sběrač disertace navíc představuje inovativní hybridní algoritmus pro predikci dostupného výkonu.

Klíčová slova: Telekomunikace, WSN, systém pro správu energie, predikce solární energie, sběr energie, piezoelektrický, baterie, QoS, hluboké učení.

Acknowledgements

I am immensely thankful to my supervisors, Prof. Dušan Maga, and Prof. Jaromír Hrad, for steering me onto the right path. Their unwavering support, invaluable information, and guidance have been instrumental in my academic and personal growth. Their mentorship has shaped this thesis and profoundly impacted my approach to research and learning.

I extend my heartfelt gratitude to my mother Hanan, whose unwavering belief in me has been a constant source of inspiration and strength. Her encouragement to persevere in my studies to the very end has been invaluable. To the spirit of my father, whose presence never seemed to leave my side, offering solace and motivation throughout this journey.

I am deeply grateful to my soulmate and guiding light, the incomparably valuable Ghaidaa, who has given my life meaning and purpose. She spared no effort and worked tirelessly to provide me with the opportunity to complete this work. Her selflessness and dedication have been the foundation of my success.

To my little angels, Kamila and Valerie, your innocence and laughter have been a constant reminder of the beauty and joy in the world, fueling my determination to push forward even during challenging times.

This journey would not have been possible without the love, support, and guidance of each one of you. Your contributions to my life and this work are deeply appreciated and will always be remembered.

List of Tables

List of Figures

List of Acronyms

WSN	Wireless Sensor Network
IoT	Internet of Things
SN	Sensor Node
PMIC	Power Management Integrated Circuit
QoS	Quality of Service
EMS	Energy Management System
PV	Photovoltaic
PZT	Piezoelectric
SoC	State of Charge
LoRa	Long Range
TEG	Thermoelectric Power Generator
EM	Electromagnetic
MPPT	Maximum Power Point Tracking
PWM	Pulse Width Modulation Controlled
MIBC	Multiple Input Boost Converter
LDO	Low Drop Out
OCC	Open Circuit Conditions
DCM	Discontinuous Conduction Mode
BFC	Biofuel Cell
NiMH	Nickel-Metal Hydride
Li-Ion	Lithium Ion
LiPo	Lithium Polymer
EDLC	Electric Double-Layer Capacitor
AC	Alternative Current
DC	Direct Current
SoH	State of Health
ICA	Incremental Capacity Analysis
ARIMA	Autoregressive Integrated Moving Average
SEPAD	Solar Energy Predication based on Additive Decomposition
UD-WCMA	Universal Dynamic Weather Condition Moving Average
AnEn	Analog Ensemble
DL	Deep Learning
DNN	Deep Neural Network
RNN	Recurrent Neural Network
LSTM	Long Short-Term Memory
CNN	Convolutional Neural Network
ReLU	Rectified Linear Unit
FFNN	Feed-Forward Neural Network
MAE	Mean Absolute Error
RMSE	Root Mean Square Error
MAPE	Mean Absolute Percentage Error
GHI	Global Horizontal Irradiance
RNN	Recurrent Neural Networks

1 CONTENTS

1 INTRODUCTION

Wireless Sensor Network (WSN) is a set of distributed wireless sensors called nodes or motes collaborating to collect and share data from the surrounding area over wireless links. Its stimulation feature to the physical and chemical signals can measure and detect physical and chemical conditions like temperature, humidity, light, gases, etc., and convert them to data suitable for analysis and decision-making [1]. WSN is an integral component in the Internet of Things (IoT) applications in various domains like industry, healthcare, military, transportation, smart building, etc. [2]. The wireless sensor node consists of the sensing subsystem, which includes the physical sensors that capture data from the environment. The processing subsystem comprises a microcontroller and memory for processing and saving data. The communication subsystem consists of a transceiver module for transmitting and receiving that supports wireless protocols like Wi-Fi, Bluetooth, Zigbee, LoRa, etc. The power subsystem comprises energy sources (battery, supercapacitor, or energy harvesting) and a power management unit, which can be a simple circuit or a Power Management Integrated Circuit (PIMC).

WSN faces many challenges, like energy constraints, limited computing and storage resources, security and privacy, Quality of Service (QoS), etc. [3]. The common factor in most challenges is the energy constraints because the WSN nodes are commonly battery-powered, and the high number of WSN nodes makes replacing the battery costly and complex. This thesis is focusing on energy constraints and QoS problems.

For energy constraints problem researchers proposed providing another energy resource by using an energy harvesting system as an alternative to the battery or having a hybrid system that combines the energy from both resources. However, the battery has a significant disadvantage: degradation when its capacity decreases after each charging/discharging cycle. Also, the disrupted nature of renewable energy sources makes designing an efficient Energy Management System (EMS) critical. The efficient EMS combines energy from several renewable energy sources, leading to less battery use and consequently extending its life span. An efficient method to combine the energy of several resources is crucial since the portability of missing harvesting available energy is high. A prediction algorithm can forecast the available energy to be harvested is a good solution, and researchers proposed several methods for this goal that can be grouped into physical, statistical, hybrid, and adaptive methods. The

accuracy and computational requirements vary according to the application and environment. So, an accurate and optimal prediction algorithm is crucial to design an efficient EMS.

For QoS problem researchers proposed several methods: transmission power selection, data rate adjustments, duty cycle adaptation, data compression, sensing rate adjustment, channel selection, and signal power modification. All methods aim to minimize the QoS to save energy consumption in the WSN. An efficient adaptive QoS algorithm to maximize the QoS is crucial since accurate data demand is increasing with modern applications.

The thesis aims to maximize the network's QoS and extend the life span of the network by implementing an EMS combines the energy from two harvesters Photovoltaic (PV) and Piezoelectric (PZT) to provide a sustainable energy resource to the WSN node. The contributions in this thesis in brief:

- A novel Energy Management System combines the energy from two resources PV and PZT harvesters based on the prediction algorithm is introduced and validated. And, a new algorithm to estimate the battery's State of Charge (SoC) is introduced.

- A novel hybrid forecasting algorithm for solar energy using statistical and machine learning methods is introduced and optimized for embedded devices.

- A novel algorithm to maximize the QoS while efficiently using the battery to extend the operational life time and lifespan of the IoT device and consequently the WSN.

1.1 Objectives

The general objective of this thesis is to enhance the Quality of Service (QoS) and extend the lifespan of the Wireless Sensor Network (WSN) by designing an efficient Energy Management System (EMS) for the WSN node and an adaptive control of the QoS. The detailed objectives of the thesis are as follows:

Objective 1: To design a novel Energy Management System (EMS) that combines the energy from two harvesters, Photovoltaic and Piezoelectric, to extend the life span of WSN node batteries.

Objective 2: To study various solar energy forecasting methods, including physical, statistical, adaptive, and hybrid models, focusing on their effectiveness and accuracy, mainly through machine learning and deep learning techniques.

Objective 3: To develop and validate a novel hybrid forecasting algorithm that integrates a Random Forest classifier with a Convolutional Neural Network (CNN) model, aiming to enhance the precision and efficiency of solar energy predictions, focusing on optimizing the model for potential deployment in Wireless Sensor Network node.

Objective 4: To develop an algorithm and a framework that ensures high Quality of Service QoS while efficiently using the battery to extend the operational life and lifespan of the wireless sensor node. And validate the proposed algorithm with actual data using realistic Energy Management System (EMS) hardware and Wireless Sensor Network.

1.2 Thesis Overview

This thesis consists of seven chapters as follows:

Chapter 1 is an introduction to WSN technology and the challenges facing this technology. The necessity to enhance the quality of service and the energy management system is addressed. The main contributions and the thesis objectives are presented.

Chapter 2 presents the theoretical background of the WSN technology and the energy management system for WSN. The theory of energy storage devices and their characteristics, pros, and cons are illustrated. The theoretical background of a single energy harvesting system as a power supply for IoT devices is presented, and a comparison between the different kinds of this technology and their characteristics, advantages, and disadvantages are illustrated. The state of the art of combining multiple energy harvesting techniques is presented with comparisons between the variant techniques is done.

In Chapter 3, the requirements of EMS for IoT devices are mentioned. The theoretical background of the PV, PZT harvesters, and battery management system are explained. The novel EMS for IoT device is presented, which combines the energy from PV and PZT harvester to extend the life operational time of the IoT device and prolong the lifespan of the battery. The dynamic behavior of the EMS is illustrated.

In Chapter 4, an analysis of photovoltaic energy forecasts is done using multiple models and methods with a focus on the common approaches to solar energy forecasting over the short term, including physical, statistical, adaptive, and hybrid methods, and their advantages and disadvantages. A study of the effectiveness of deep learning techniques in solar energy forecasting, including Deep Neural Networks (DNN), Recurrent Neural Networks (RNN), Long Short-Term Memory (LSTM), and Convolutional Neural Networks (CNN), is presented. To improve the CNN model's precision and effectiveness, a novel hybrid approach that combines a Random Forest classifier with a CNN model is designed. The validation results are presented, which show that the hybrid approach reduced errors by about 7% when compared to the CNN model used alone. The optimization of the CNN model size while maintaining its performance, making it appropriate for Internet of Things (IoT) devices, is performed.

In Chapter 5, the study of Quality of Service (QoS) in Wireless Sensor Networks (WSNs) is done with a focus on the duty cycle and transmission power. A novel algorithm is presented for adaptive management of power transmission and duty cycle, based on the availability of energy from multiple sources, which can enhance QoS in IoT devices without compromising energy conservation. A solution for a multi-objects optimization problem is presented to provide the balance between QoS and energy sustainability in WSN.

In Chapter 6, The validation is done over 15 years for the proposed EMS and adaptive management of power transmission and duty cycle is done for different values of channel pathlosses. The results are shown for different used energy resources scenarios: battery only, PV harvester only, PZT harvester only, and Hybrid system (battery, PV, and PZT).

In Chapter 7, The experiments with real hardware are done. The results for one week with the same scenarios in discussed and compared to simulation.

In Chapter 8, the conclusion is presented with a summary of the thesis results. And the future work in the field of enhancing the QoS and EMS in WSN is suggested.

2 STATE OF THE ART

2.1 Wireless Sensor Network (WSN)

Wireless Sensor Network (WSN) is a group of small embedded devices with sensing features called nodes or motes. Each node has a location in the sensing area, which can be small or vast according to the application requirements to collect the required data. The nodes can communicate wirelessly to collaborate and deliver the data to the sink and then to the goal network for processing as shown in Figure 2.1. Its stimulation feature to the physical signal can measure and detect physical and chemical conditions and convert them to data suitable for analysis and decision-making [1]. WSN is an integral component in IoT applications and has applications in various domains like:

- In industry, it provides real-time and self-work for industrial operations, monitoring the "health state" of the machines and integrating the physical properties and the control system to reduce power consumption and gas emissions, increasing efficiency and productivity [4].

- In military and security applications, the WSN allows monitoring the boundaries of countries, detecting and classifying parasitic objects to reduce soldiers' workload. Also, they help break into restricted areas and spy operations [5].

- In the intelligent building, WSN introduces complete control, monitoring, and management of lighting, temperature, humidity, and all other user requirements to make their life much easier and safer and minimize efforts and energy consumption [6].

- In the healthcare field, WSN monitors the atmosphere and the temperature in the hospital. Also, it reports and observes the health status of the patients [7].

- In the environment and agriculture, the WSN plays a critical role in observing the different physical and chemical data to decrease pollution, study the behavior of the organisms, and early detect disasters [8]. Also, it contributes to improving crops by providing the ability to implement automated agriculture, which is more efficient and productive than traditional agriculture [9].

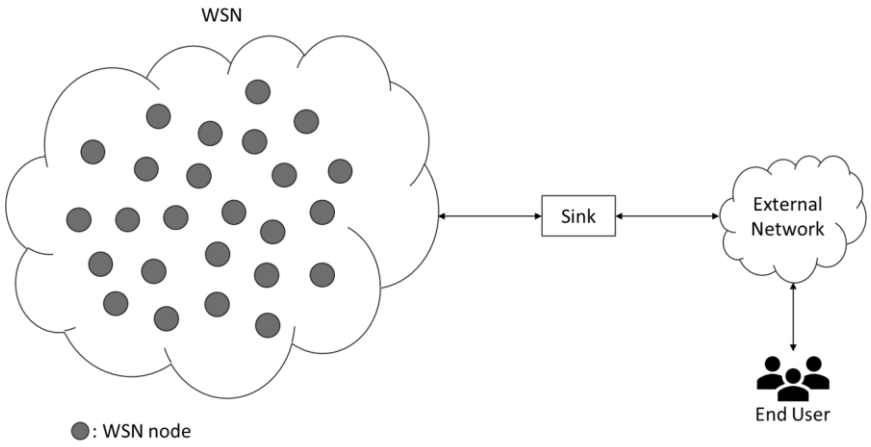

Figure 2.1 Wireless Sensor Network (WSN) Architecture

The architecture of WSN node as shown in Figure 2.2 consists of:

- **Sensing subsystem** includes the physical sensors that capture data from the environment. It may involve various types of sensors, such as temperature, humidity, light, motion, gas, etc.

- **The processing subsystem** consists of a microcontroller or microprocessor responsible for executing instructions and processing the sensor data.

- **The communication subsystem** enables wireless communication between nodes and facilitates data exchange. It includes a transceiver module for transmitting and receiving that supports wireless protocols like Wi-Fi, Bluetooth, Zigbee, or Long Range (LoRa).

- **The power subsystem** provides the necessary electrical power to the WSN node for its operation. It typically includes a power source, such as batteries or energy harvesting modules

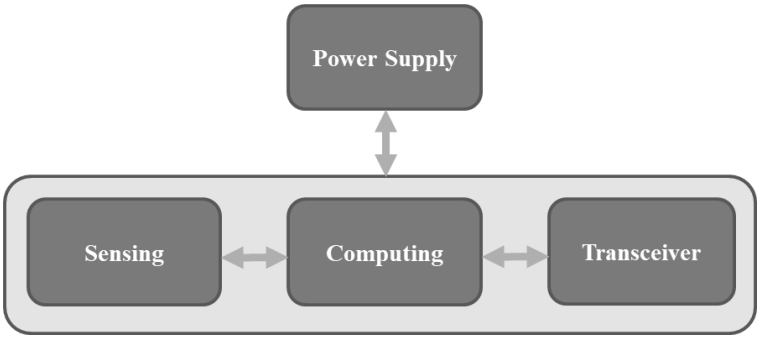

Figure 2.2 WSN Node Architecture

2.2 Energy Management of WSN

Energy Management System Definition

Energy management in Wireless Sensor Networks (WSN) is a group of policies and strategies managing the network's operation. These are designed to align with the application's requirements to adapt the network's behaviour based on the currently available energy level, guarantee the optimal operation of the WSN, and protect it from energy depletion or inefficiencies. Energy management is essential in maintaining the balance between operational demands and energy conservation, consequently ensuring the high efficiency and sustainability of the WSN. The complexity of this task comes from the efficiency required for a high quality of service (QoS), where the price is high energy consumption.

Energy Management System Techniques

Energy Management System (EMS) techniques is classified into two main groups based on the dealing with the energy either for providing or consume it as show in Figure 2.3 [10]:

1- Energy Consumption: This method focuses on saving the energy and optimizing the energy usage by following one or more of the following techniques:

   a. Duty Cycle: This method involves managing the active, idle sleep time of devices to conserve energy. It regulates the intervals during which a device operates and the periods when it rests in order to optimize the energy consumption [11].

   b. Mobility Based: This technique leverages the movement patterns of mobile devices to optimize energy consumption. By understanding and predicting mobility, it can manage the energy usage of devices more efficiently [12].

   c. Data Driven: This approach uses data analytics to optimize energy consumption. It predicts the data in a certain level of accuracy to save the energy required for measuring it [13].

2- Energy Provision: This method focuses on energy resources and increase its efficiency by following one or more of the following techniques:

a. Harvesting: This involves using one or more harvester to capture and convert the ambient energy from the environment, such as solar, vibration, wind, or thermal energy, into electrical energy. This method is increasingly popular for powering small devices and sensors [14].

b. Storage Device: This technique focuses on choosing and optimizing the energy storage device which can be a battery (fixed, replicable, rechargeable), supercapacitor, or ultracapacitor [15].

c. Transferring: This method deals with transfer the energy from the resource to the sensor node using wire or wireless technique [16].

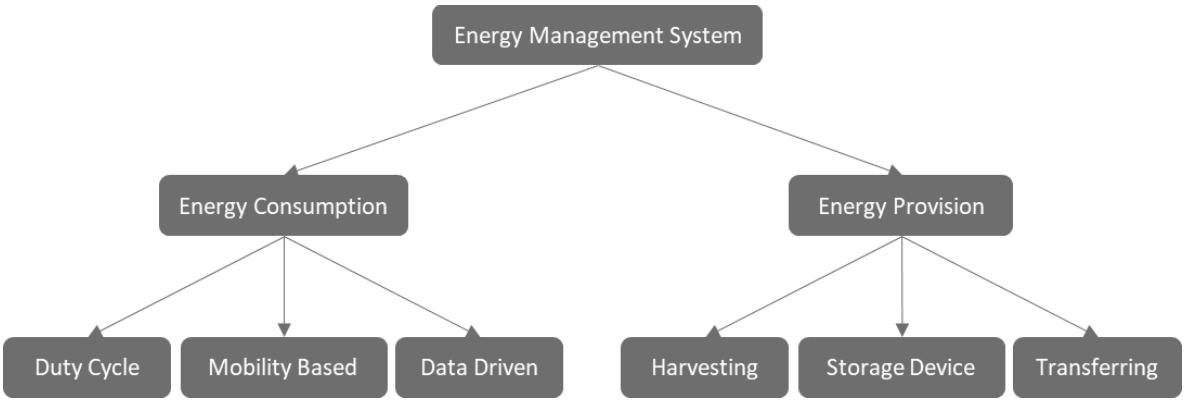

Figure 2.3 Energy Management System Techniques in WSN

Energy management in WSN can be performed in two levels: the network level, and sensor node level. In the network level EMS focuses on the overall energy of the network involving routing (LEACH, PEGASIS), and data aggregation [17]. While in the sensor node level, the focus on optimizing the energy usage of the individual node to increase its and life span extension by using techniques like duty cycling, power management, and energy harvesting.

This thesis focuses on Energy Management System control the energy consumption where adapting the Duty Cycle based on the level of available energy and Energy Provision where a multi-input energy harvesting is used and Battery Management System for the storage Device provides the protection for the battery and prolong its life span.

2.3 Energy Storage Devices

Energy storage in portable devices like sensor nodes is critically important. The efficiency of energy storage significantly influences the size, cost, and lifespan of a sensor node. Broadly, there are two primary energy storage technologies used in sensor nodes:

1. Supercapacitors: Ideal for energy harvesting systems in low-powered and compact applications due to their specific characteristics in charge storage density, lifespan, discharging rate, leakage, and size.

2. Rechargeable Batteries: More suited for long-lasting and task-intensive implementations, offering different trade-offs in terms of energy density and operational longevity.

Additionally, a hybrid approach combining both supercapacitors and rechargeable batteries can be employed. This method leverages the strengths of both technologies to meet specific requirements. Choosing the most effective energy storage method for a particular application necessitates a thorough understanding of the differences between these energy storage technologies, considering factors like charge storage density, lifecycle, discharge capabilities, potential leakage, and physical dimensions [15].

2.3.1 Batteries

Batteries are the most traditional form of energy storage in wireless sensor networks (WSNs). They are favoured for their excellent high-energy density and availability in a wide range of sizes. Another advantage of batteries is their ability to supply energy at specific voltage levels directly aligning with the requirements of IoT device, eliminating the need for external voltage converters. There are various types of batteries being developed specifically for WSN applications. Among the most advanced are Nickel-Metal Hydride (NiMH), Lithium Ion (Li-Ion), and Lithium Polymer (Li-polymer) batteries. These types have been refined for optimal performance in WSN contexts [15].

1. Nickel-Metal Hydride (NiMH)

Nickel-Metal Hydride (NiMH) batteries consist of an anode made of nickel metal hydride, a cathode composed of a hydrogen storage alloy or metal hydride, and an electrolyte primarily containing hydroxide potassium. Advantages of NiMH batteries include a 30-40% higher capacity compared to

standard Nickel-Cadmium (NiCd) batteries. They don't require special regulations for storage and transport. However, NiMH batteries have their drawbacks. They necessitate complex charging algorithms and are sensitive to overcharging. Rapid charging and excessive discharging can cause an increase in heat. They also suffer from high self-discharge rates and have a limited-service life. NiMH batteries are a suitable choice in scenarios where low energy density, short service life, and affordability are key requirements [18].

2. Lithium Ion (Li-Ion)

A Lithium Ion (Li-Ion) battery is composed of an anode made from carbon, a cathode from Li-transition metal oxide, and a separator. During the charging phase, Lithium hex carbide (LiC6) is formed due to the intercalation of lithium ions between the graphene layers of the anode. In the discharge phase, lithium ions migrate into the cathode, as illustrated in Figure 2.4**Error! Reference source not found.**. Advantages of Li-Ion batteries include high energy density and a low self-discharge rate. They don't require priming after the initial charge and need minimal maintenance. However, Li-Ion batteries also have several disadvantages. They are sensitive to overcharging, and high charging currents can be detrimental. Overload discharging is another concern, and they require special care during transportation, particularly by air. Moreover, these batteries have a limited lifecycle and are relatively expensive. Li-Ion batteries are an optimal choice in scenarios where high energy density and medium service life are priorities, and cost is not a major concern [19].

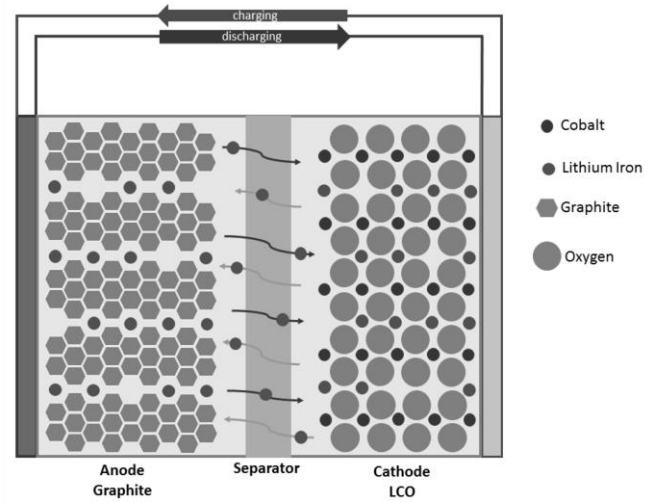

Figure 2.4 Lithium Ion: Structure, Charging and Discharging

3. Lithium Polymer (Li-polymer)

The Lithium Polymer (Li-polymer) battery shares a similar structure to standard lithium batteries, with a crucial distinction being its polymer-based separator, as depicted in Figure 2.5. It has a nominal voltage of 3.6 V and can sustain up to 500 charging cycles. The load current is below 1C, and it boasts an energy density of about 160Wh/kg. Typically, a full charge takes around four hours, and the discharge rate is approximately 10 percent per month when in storage. Advantages of Li-polymer batteries include their slim profile, flexibility in form, lightweight nature, and enhanced resistance to overcharging and overload discharging. These features make them particularly suitable for applications where space and weight are critical factors. However, there are notable disadvantages to Li-polymer batteries. They tend to have a shorter service life compared to other types and are more expensive to manufacture. Additionally, they usually have a larger volume, which might be a limiting factor in compact device designs [20].

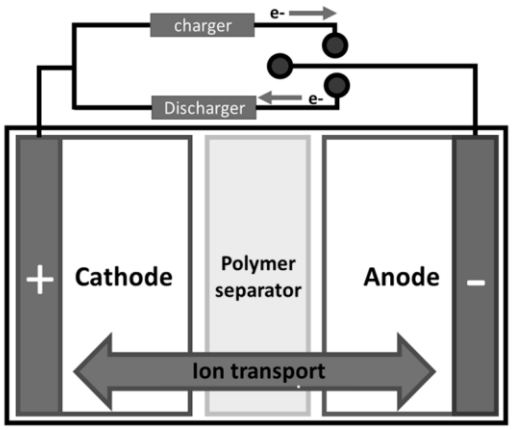

Figure 2.5 Lithium Plymer: Structure, Charging and Discharging

Choosing the proper battery is based on the application requirements and the operational environment. The comparison between the batteries is presented in Table 2.1:

- Recharge Cycles: These refer to the number of total charges (0 to 100%) and discharge (100% to 0) cycles a battery can operate before its total capacity degrades to a specific percentage (for lithium-ion batteries, 80%) of its original capacity.

- Efficiency: It is the ratio of the energy delivered by the battery to the energy put into it during charging.

- Nominal Voltage in Volts is the output voltage of the battery when it is connected to the load.

- The Capacity in mA is the amount of electric charge which a battery can deliver. The higher capacity, the longer the battery can power the load before the need for recharging.

- Energy in W is the total amount of energy a battery can store and deliver over time. It's calculated by multiplying the battery's voltage (in volts) by its capacity (in ampere-hours). This value indicates the battery's performance than just voltage or capacity.

- Self-Discharge Percentage: It refers to the rate at which a battery loses its charge when the load is disconnected. A lower self-discharge rate means the battery keeps its charge longer when no load is connected.

- Recharge Cycles: These refer to the number of total charges (0 to 100%) and discharge (100% to 0) cycles a battery can operate before its total capacity degrades to a specific percentage (for lithium-ion batteries, 80%) of its original capacity.

- Efficiency: It is the ratio of the energy delivered by the battery to the energy put into it during charging.

Table 2.1 Rechargeable Batteries Comparison

Battery	Nominal voltage(V)	Capacity [mA]	Energy [W]	Self discharge	Recharge Cycle	Efficiency
NiMH	1.2	2500	3.0	5% /month	500-2000	66%
Li-ion	3.7	730	2.7	1.5% /month	400-1200	99%
LiPo	3.7	930	3.4	5% /month	500-1000	99%

2.3.2 Supercapacitor

Supercapacitor also knew as ultracapacitor or Electric Double- Layer Capacitor (EDLC) is an electrochemical capacitor with a large capacitance [21]. The supercapacitor has a construction like the

battery. It has two conductor electrodes immersed in an electrolyte with a porous membrane separator between the electrodes. The electrodes are manufactured from a high surface area; porous material of the separator has pores of diameter in the nanometre (nm) range. The electrode in ultracapacitor is fabricated from a material which its surface area is greater than the surface area of the material which is used in battery electrodes being 500–2000 m^2/g as shown in Figure 2.6. Supercapacitors are divided into two different types:

1. Electrochemical double-layer capacitors: which stores its charge electrostatically, so the electrical energy is stored in the static electric field in the micropores between the electrodes and the ions in the electrolyte.

2. Supercapacitors based on pseudo-capacitance That is counted on the adsorption of the active ions or appears from Faradaic redox reaction that is located at a transition metal oxide surface or in a doped electrically conducting polymer.

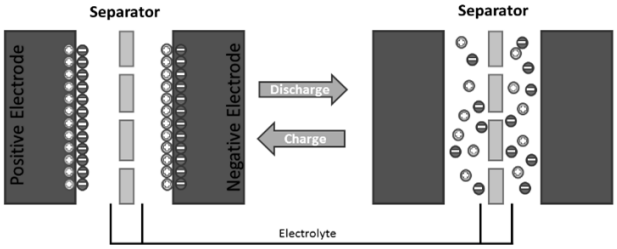

Figure 2.6 Supercapacitor Structure

There are three types of pseudo-capacitance:

1. The ions adsorption from the electrolyte by the surface.

2. The second one involves the ions from the electrolyte by redox reactions.

3. The third one is doping electrically conducting polymers in the electrode.

The comparison between different types of supercapacitors is presented in Table 2.2. For some applications where self-discharge is not considered, a supercapacitor is a good alternative solution to batteries due to its long lifetime.

Table 2.2 Supercapacitors Used in IoT Devices

Supercapacitors	Capacity (F)	Nominal voltage (V)	Specific energy (Wh/L)	Self-discharge per day	Weight (g)	Cyclelifetime
Maxwell BCAP0350	350	2.5	5.73	20%	60	500,000
Maxwell PC10	10	2.5	1.4	30%	6.3	500,000
Green-cap EDLC(DB)	50	2.7	4.4	50%	10	>100, 000
NEC TokinFT0H105Z	1	1	NA	10min	10	1000

Conclusion

Batteries and supercapacitors are simple solutions for applications where the lifespan and operational time of Wireless Sensor Networks (WSN) are not critical so they can lead to network degradation and eventual failure. Also, they have environmental drawbacks. Their environmental impact is also significant due to complex recycling processes and high carbon emissions from production and raw material mining [22].

2.4 Energy Harvesting

For years, many researchers have presented energy harvesting as a power supply for IoT devices to overcome the limitations of batteries and supercapacitors and reduce their harmful environmental side effects. Energy Harvesting refers to collecting energy from the surrounding environment to charge energy storage devices or serve as an alternative to them. This technology is gaining prominence due to its cost-effectiveness and environmental friendliness. As illustrated in the Figure 2.7, IoT devices are equipped with various energy harvesters and are categorized based on the nature of the energy they harvest. This diversity allows for harnessing different forms of ambient energy, such as thermal,

mechanical, or solar, making energy harvesting a versatile and sustainable solution for various applications.

Mechanical Energy Harvesting

This process involves converting mechanical energy into electrical energy by various means, such as vibrations, mechanical stress, and pressure [23]. The most common types of mechanical harvesters are piezoelectric, electrostatic, or electromagnetic.

1. Piezoelectric Energy Harvesting

This method generates electrical energy through the piezoelectric effect. Mechanical energy from pressure, force, or vibrations is converted into electrical energy by straining a piezoelectric material. Typically, a cantilever structure with a seismic mass attached to a piezoelectric beam is used. When strained, the piezoelectric material produces an electric field due to charge separation, with the generated voltage being proportional to the stress [24].

2. Electromagnetic Energy Harvesting

Based on Faraday's law of electromagnetic induction, this method uses an inductive spring mass system to convert mechanical energy into electrical energy. Movement of a magnetic material through a stationary magnetic field induces voltage. The vibration of a magnet attached to a spring within a coil alters the flux, generating voltage [25].

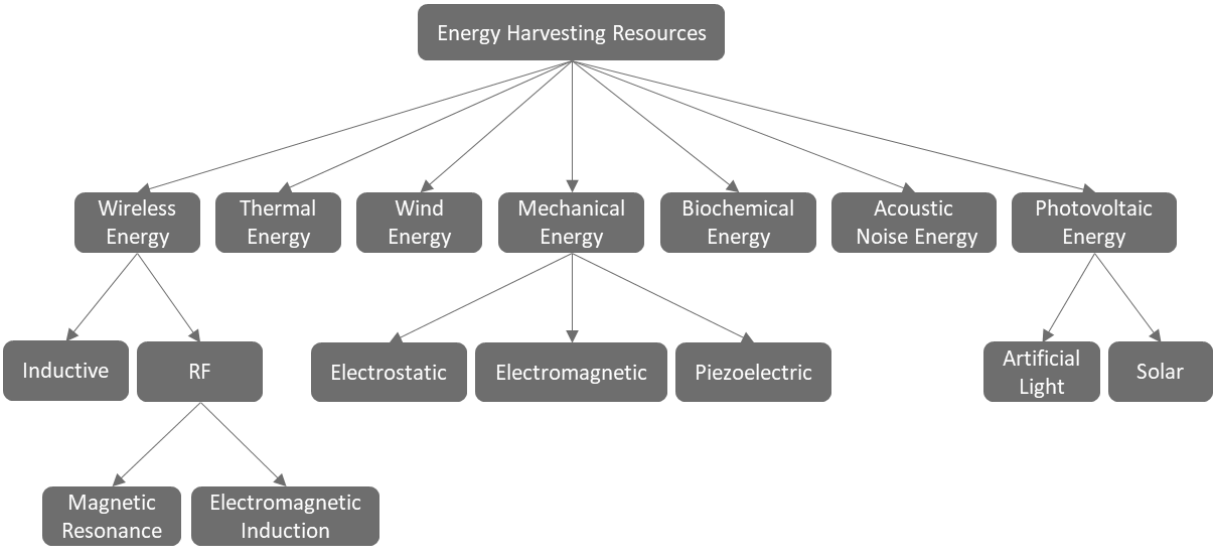

Figure 2.7 Energy Harvesting Resources

Photovoltaic Energy Harvesting

Photovoltaic energy harvesting involves transforming light photons from the sun or artificial sources into electrical energy. This process utilizes photovoltaic (PV) cells, composed of two types of semiconducting materials: N-type and P-type. At the junction of these materials, known as the P-N junction, an electrical field is created. When light hits the photovoltaic cell, electrons are released, facilitating energy conversion [26].

Thermal Energy Harvesting

Thermal energy is harvested through two primary methods: thermoelectric and pyroelectric energy harvesting.

1. Thermoelectric energy harvesting

The main component of this harvester is the Thermoelectric Power Generator (TEG), which use thermal gradients to generate electrical power. TEG includes a thermopile made of p-type and n-type semiconductors connected in series between hot and cold plates. The Seebeck effect causes the generated electrical energy and is proportional to the temperature difference between the plates. [27].

2. Pyroelectric Energy Harvesting

Pyroelectric energy harvesting generates voltage by heating or cooling pyroelectric materials. Unlike thermocouples, which require a temperature difference, pyroelectric materials rely on time-varying temperature changes. These changes modify the atomic positions within the crystal structure of the pyroelectric material, resulting in voltage generation [28].

Wireless Energy Harvesting

This technique falls into two primary categories:

1. RF Energy Harvesting

This method involves the use of a rectifying antenna, commonly known as a rectenna, to transform Electromagnetic (EM) waves into electrical energy. Energy can be harvested from various surrounding RF sources such as cell phones, radio and television broadcasts, Wi-Fi communications, and microwaves. It can also be drawn from EM signals emitted at specific wavelengths [29].

2. Resonant Energy Harvesting

Resonant energy harvesting is a method of wirelessly transferring and harvesting electrical energy through two coils resonating at the same frequency. This process involves an external inductive transformer device connected to a primary coil, capable of transmitting power through the air to a device equipped with a secondary coil. The primary coil generates a time-varying magnetic flux, which passes through the secondary coil and induces a voltage [30].

Wind Energy Harvesting

This method involves transforming the kinetic energy of airflow into electrical energy. It uses a wind turbine, appropriately sized, to harness the linear motion produced by wind [31].

Biochemical Energy Harvesting

This technique involves converting oxygen and endogenous substances into electrical energy through electrochemical reactions. Biofuel cells, utilizing active enzymes and catalysts, can harness the biochemical energy in biofluids and convert it into electrical energy [32].

Acoustic Energy Harvesting

This technique utilizes an acoustic transformer or resonator to convert continuous, high-intensity acoustic waves from the surrounding environment into electrical energy [33].

2.4.1 Energy Harvesting Techniques comparison

When selecting the optimal energy harvester, both the application and the surrounding environment play pivotal roles. The choice can generally be made by comparing energy harvesting techniques based on two key factors as presented in Table 2.3:

1. Power Density: This refers to the amount of energy harvested per unit volume, area, or mass. It's expressed in watts per cubic centimeters, watts per square centimeters, or watts per gram. This metric measures the intensity of energy generation in relation to the size or mass of the energy harvester.

2. Conversion Efficiency: This is the ratio of the electrical power harvested to the total power available for harvesting. It's a unitless metric and ranges from 0 to 100. This measure indicates how effectively the energy harvester can convert the available energy (like mechanical, thermal, or solar energy) into electrical energy.

Table 2.3 Energy Harvesting Comparsion

EH Technique	**Power Density**	**Conversion Efficiency**
Photovoltaic	Outdoors (direct sun): 15 mW/cm^2 Outdoors (cloudy day): 0.15 mW/cm^2 Indoors: <10 µW/cm^2	Highest: 32 _ 1:5% Typical: 25 _ 1:5%
Piezoelectric	250 µW/cm^3 330 µW/cm^3	Maximum power and efficiency are source dependent
Thermoelectric	Human 30 µW/cm^2 Industrial 1 to 10 mW/cm^2	±0:1% ± 3%
Pyroelectric	8.64 µW/cm^2 at the temperature rate of 8.5º C/s	3.5%

Electromagnetic	Human motion: 1 to 4 $\mu W/cm^3$ Industrial: 300 $\mu W/cm^3$	Maximum power and efficiency are source dependent
Electrostatic	50 to 100 $\mu W/cm^3$	Maximum power and efficiency are source dependent
RF	GSM 900/1800 MHz: 0.1 $\mu W/cm^2$ WiFi 2.4 GHz: 0.01 $\mu W/cm^2$	50% Excluding transmission efficiency.
Wind	380 $\mu W/cm^3$ at speed of 5 m/s	5%
Acoustic noise	0.96 $\mu W/cm^3$ at 100 dB 0.003 $\mu W/cm^3$ at 75 dB	Noise power densities are theoretical values.

According to Table 2.3, photovoltaic and piezoelectric energy harvesting technologies demonstrate the highest values in both power density and conversion efficiency. This implies that they are particularly efficient in converting available energy into electrical power and do so with a high intensity relative to their size or mass.

2.4.2 Energy Harvesting Challenges

Energy harvesting techniques face several challenges, but the most important one is the instability of the energy source to be harvested [34]. The photovoltaic energy harvesting system accounts mainly for solar irradiation, which varies during the day and disappears at night, creating a nonsecure energy source for the IoT device. The Figure 2.8 shows the irradiation during the 24 hours when the PV harvester can gather available solar energy from 7:00 AM to approximately 15:00 where the data is gained form [35].

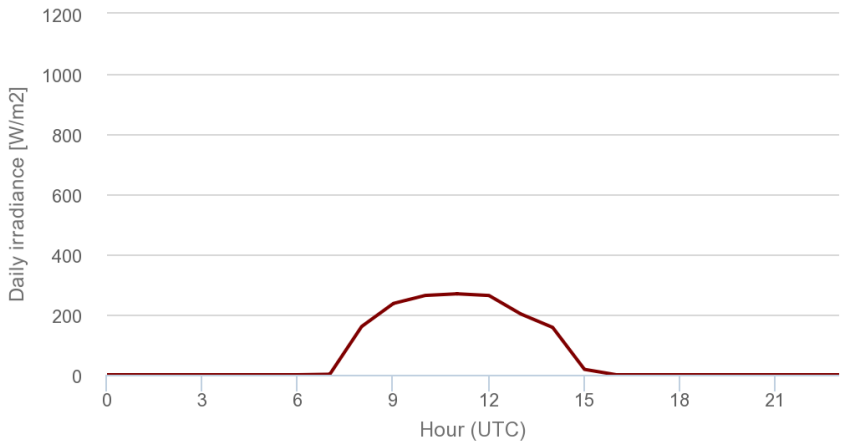

Figure 2.8 Daily Irradiance in 24 Hours

The piezoelectric harvester can also harvest the energy from vibration when available. Still, as shown in the Figure 2.9, which is the magnitude of the vibrational acceleration on Chicago North Suspension Bridge, the data is gained from Real Vibrations database [36], the vibration is intermittent. Hence, the piezoelectric harvester is not a stable energy source for the IoT device.

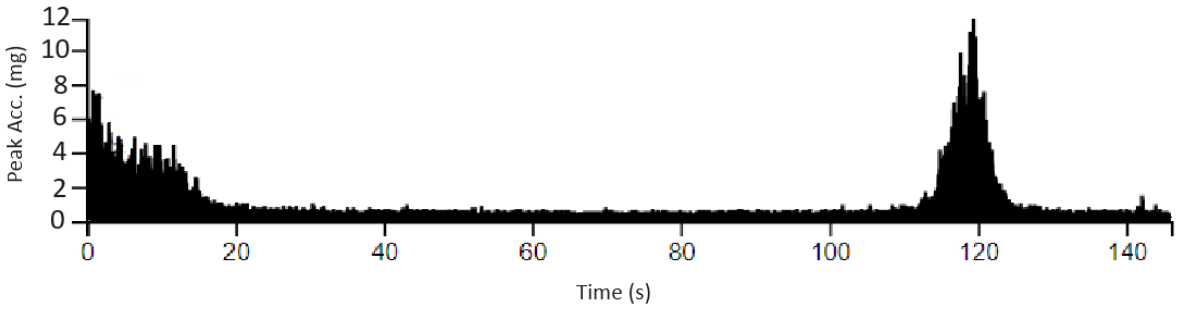

Figure 2.9 Magnitude of the Vibrational Acceleration on Chicago North Bridge

The energy harvesting system architecture which is used as a power supply for IoT device consists of the harvester, conditioning and interfacing, and energy storage device as shown in Figure 2.10. The energy storage device can be a buffer like capacitor and supercapacitor to use the accumulated energy in the near future in the battery less systems. Or, it can be a rechargeable battery which will be keep the energy for long time due to its low leakage current comparing to capacitor and supercapacitor as presented in Table 2.1

Figure 2.10 Single Energy Harvesting System for IoT Device

The minimum capacity of the energy storage device to power the IoT device can be calculated as:

$$C_{ST,min} = \frac{I_{discharge} . t_{discharge}}{V_{ST,max} - V_{ST,mim}} \quad (1)$$

Where:

- $C_{ST,min}$ is the capacity of the energy storage device.
- $I_{discharge}$ is the current consumption of the IoT device.
- $t_{discharge}$ is the time period of current consumption which can be the duty cycle period.
- $V_{ST,max}$ is the maximum output voltage of the energy storage device.
- $V_{ST,mim}$ is the minimum output voltage of the energy storage device.

The minimum time required to charge the energy storage device to be ready to operate with its maximum voltage level can be calculated as:

$$t_{charging\ min} = \frac{C_{ST,min} . (V_{ST,max} - V_{ST,mim})}{I_{charging}} \quad (2)$$

Where:

- $t_{charging\ min}$ is the minimum charging time to reach to the maximum output voltage level
- $I_{charging}$ is the charging current.

In case of energy storage device is a buffer (capacitor, supercapacitor) a stable charging current $I_{charging}$ required to reach the maximum output voltage $V_{ST,max}$ of the energy storage device so if the PV harvester is used then the IoT device will operate during the irradiation period. If the PZT harvester

is used then there is risk to reach the maximum output voltage $V_{ST,max}$ or the IoT device will work on short periods.

In case of energy storage device is a battery the operational life time of IoT device will be increased but the lifespan of the battery will decrease since the main limitation of the battery is the limited number of life cycles. The battery capacity degrades after each complete life cycle then the battery will not be able to store the harvested energy.

Conclusion

Using a multiple energy harvesting with battery is a good solution to extend the life span of the battery especially when the harvesters are gathering the energy from different ambient resources. Which will ensure the availability of energy resource and reduce the relay on the battery as a result the lifespan of the battery will be extended [37].

2.5 Multi Input Energy Harvesting

The multi-input energy harvesting technique is an energy management method that prolongs batteries' lifetime and lifespan. This technique combines energy from various sources in the ambient environment (light, wind, mechanical, wireless, etc.) to reduce reliance on a single resource and increase the consistency of energy supply. Consequently, it enhances IoT devices' reliability, efficiency, and sustainability [38].

Supplementary Use of Different Energy Sources

The concept of utilizing supplementary energy resources in wireless sensor networks involves employing a primary energy harvester, complemented by one or more secondary harvesters. These secondary harvesters either contribute energy directly to certain system components or enhance the efficiency of the primary harvester. This technique's primary advantage is its straightforward design, though it requires careful tailoring to align with specific application needs and environmental conditions. A case study in reference [39] demonstrates this approach. Here, a photovoltaic transducer is employed as the main energy harvester, charging a supercapacitor via a DC–DC converter. Additionally, a piezoelectric transducer serves as a secondary energy source. This secondary harvester primarily supplies power for the system's self-start-up phase, a period characterized by higher energy

consumption due to the initial requirements of the electronic components. Another application of this technique is reported in [40]. In this instance, a thermal generator functions as the primary energy harvester, powering a battery-less sensor. Complementing this, a piezoelectric transducer is used as the secondary energy source. Its role is to provide the necessary bias for the rectifier circuit, which is integral to the operation of the thermal generator. It also supplies energy to certain components of the wireless sensor node. This example illustrates the versatility and adaptability of using supplementary energy harvesters in enhancing the energy efficiency and operational reliability of wireless sensor networks.

Power Oring

The Power ORing topology connects multiple energy sources in parallel, utilizing conventional diodes, Schottky diodes, or MOSFETs. This design combines the energy from different harvesters, isolates each power source and provides protection against problems from shunt-connected sources and other detrimental factors. The principle of this technique is that the energy source with the highest output voltage will supply power to the load, while the others remain isolated. A key advantage of Power ORing is its capability to link an unlimited number of resources. Additionally, it can be used with MPPT circuits or a rectifier in series with each energy source, enhancing the system's overall redundancy, reliability, stability, and effectiveness, as illustrated in Figure 2.11. In study [41], researchers employ conventional diodes to amalgamate energy from solar, heat, and wind harvesters for charging a supercapacitor. Similarly, in study [42], this approach is adapted to merge energy from various piezoelectric harvesters. In another instance, study [43] also utilizes this design but incorporates an independent Maximum Power Point Tracking (MPPT) circuit for each harvester, enhancing the efficiency of energy collection. In research [44], a Power ORing topology is developed by combining energy from thermal and light harvesters using Schottky diodes. This setup benefits from a low forward voltage drop and simplicity in the circuit design. However, it still experiences energy wastage when other connected harvesters have lower voltage outputs, a challenge common to similar configurations. Conversely, in study [45], researchers opt for Power MOSFETs in their Power ORing system due to their lower forward voltage drop compared to both Schottky and conventional diodes. Additionally, this arrangement allows for full control over switching thresholds and speeds. Despite these advantages, the main drawback of using Power MOSFETs is the increased complexity and size of the circuit.

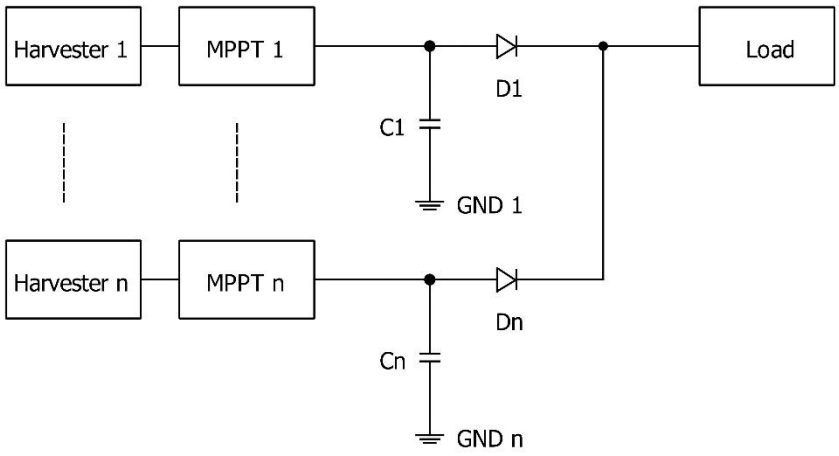

Figure 2.11 Power ORing Scheme

Voltage Level Detection Method

The voltage level detection technique employs a controller to manage switches connected to individual energy harvesters. This controller can implement various algorithms and methods, designed to the specific application and type of harvester used. The complexity of this system increases with the number of components involved. In some instances, this complexity can adversely affect efficiency due to the high energy consumption of the system's components. Typically, voltage level detection operates by comparing the output voltage of each harvester against a predetermined threshold, ensuring efficient energy management [46] [47].

Multiple-Input Boost Converter (MIBC)

A boost converter is a DC-DC power converter specifically used to step up the output voltage. Also, it can be used in integrating energy from diverse sources. Various topologies of this converter can be customized to align with specific application needs. This adaptability allows for efficient energy management in systems that require elevated voltage levels from multiple energy inputs.

1. Serial Form:

In research [48], a DC-DC converter topology is introduced for merging wind and photovoltaic energy. This involves connecting two switch-mode, Pulse Width Modulation Controlled (PWM) step-up converters in series. This series connection caters to the low voltage outputs of wind and photovoltaic harvesters (illustrated in Figure 2.12Figure 2.12), providing an output voltage equal to the input voltage,

which enhances switch utilization compared to parallel connections. However, a significant drawback of this topology is its sensitivity to voltage drops at either source, which can lead to an unregulated output state. Maintaining input voltage variation is crucial for producing a regulated output in a boost converter.

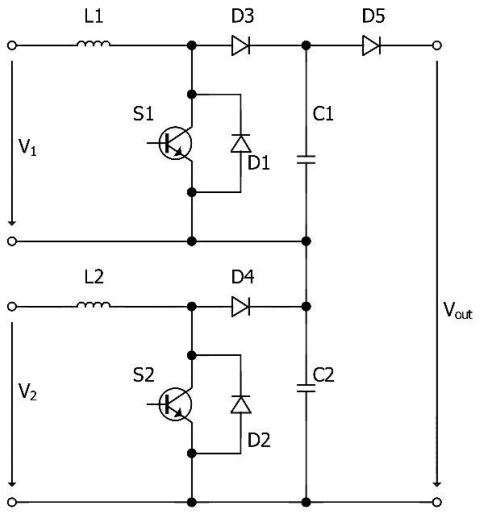

Figure 2.12 Multiple Input Boost Converter Scheme – Serial Form

2. Magnetic Form:

Study [49] suggests using a multiple-input DC-DC converter to merge energy from two sources in magnetic form. This converter is based on flux additivity, utilizing phase-shifted PWM control to combine input DC sources in the magnetic core through the addition of produced magnetic flux. This topology (shown in Figure 2.13Figure 2.13) offers advantages such as combining energy from two sources irrespective of their input voltage magnitudes and the ability for each input to independently and simultaneously deliver energy. The downsides include limitations on the input sources and a larger size of the setup.

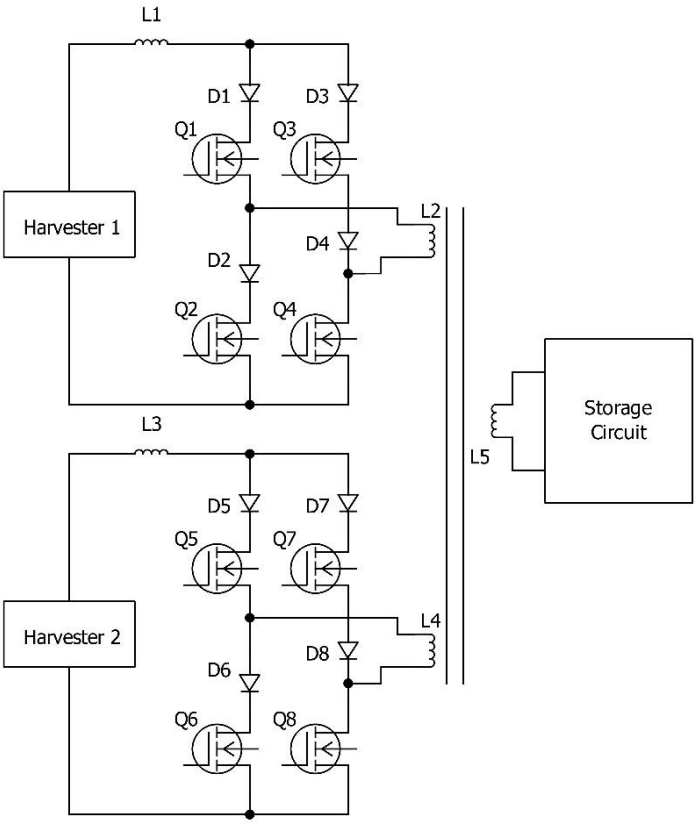

Figure 2.13 Multiple Input Boost Converter Scheme – Magnetic Form

3. Parallel Form:

Research [50] and [51] explore a topology that combines energy from two sources connected in parallel via a Multiple Input Boost Converter (MIBC). The control strategy is based on alternating time division between the sources. A significant limitation of this strategy is energy wastage, as the sources cannot deliver energy simultaneously.

Linear Regulator

A Low Drop Out (LDO) regulator is responsible for regulating output voltage. These regulators are notable for their lack of switching noise, compact size, and straightforward design as shown in Figure 2.14. However, a primary drawback of LDO regulators is their tendency to produce waste heat. The energy combining technique involving LDO regulators works by ensuring that each energy harvester outputs the same voltage value, allowing for simultaneous charging of the storage device. However, this approach necessitates an LDO for each input, leading to increased heat production and higher costs, which are directly proportional to the complexity of the device. Research [52] presents a design for

energy harvesting that combines four sources: indoor light, mechanical vibration, electromagnetic fields, and thermal energy. In this design, each energy branch is equipped with an LDO (Low-Dropout regulator), a conditioning circuit, and a storage device. The system is battery-less and capable of simultaneously collecting energy from all these resources. However, the application of this system is limited to a maximum voltage of 2.5V. Additionally, the use of LDOs in each branch leads to the generation of high temperatures, which is a notable limitation of this design.

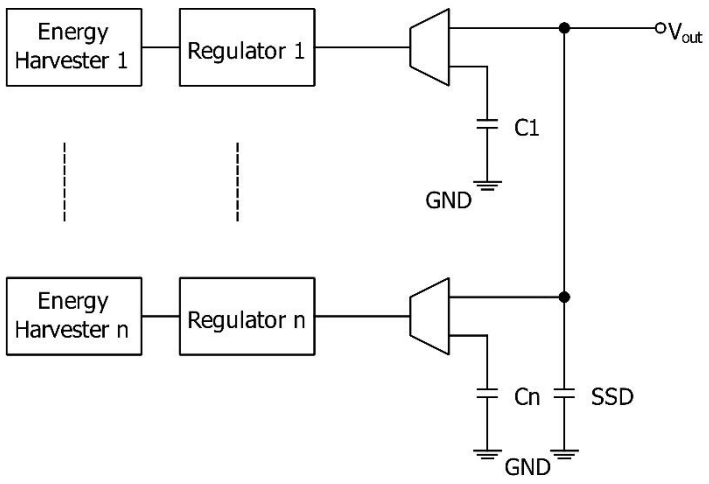

Figure 2.14 Linear Regulator Scheme

Multiplexing Techniques

A multiplexing technique involves merging energy from various sources by sequentially allowing each harvester to charge the storage device for predetermined time intervals. This process is governed by a control algorithm and utilizes a combination of a controller, controllable switches, and a synchronization oscillator to facilitate the multiplexing. The efficiency of this method is closely tied to the specific algorithm used. However, a notable drawback of this technique is the increased complexity of the system and the additional energy consumed by the components responsible for executing the multiplexing process. In study [53], researchers introduce a system that combines energy from two harvesters using Maximum Power Point Tracking (MPPT). This system operates by time-division, allocating specific intervals for each resource to efficiently transfer energy to an inductor. The setup includes four PMOS and NMOS transistors for switching, five capacitors, an inductor, and a controller. The controller establishes three distinct time periods: ON-time (TON) for energizing the inductor, OFF-time (TOFF) to transfer energy to the load, and idle-time (TIDLE) where the inductor is set to float, minimizing energy leakage. Additionally, the system features three operating modes: single-source

mode (SSM), dual-source mode (DSM), and backup mode (BM), each with a unique switch configuration. The choice of mode is contingent on the availability of energy resources, with SSM activated for one available resource, DSM for two, and BM in the absence of resources. This approach allows the system to adapt to varying ambient environmental conditions, optimizing energy harvesting and usage.

Switched Capacitors

A switched capacitor is a simple electronic circuit consisting of switches and capacitors, illustrated in Figure 2.15. Its basic configuration includes two switches (S1 and S2) and a capacitor, operating in two phases: the charging phase, where S1 is closed and S2 is open, allowing energy storage in the capacitor, and the discharging phase, where S1 opens and S2 closes, releasing the stored energy. This technique of using a switched capacitor for energy combination involves converting the current from one harvester to AC, merging it via the capacitors, and then rectifying it with transistors. In study [54], a design using the switched capacitor technique is proposed. This system comprises five primary subsystems: a passive start-up (PSU), ranking and level detection, Maximum Power Point Tracking (MPPT) control, a combiner core, and control logic. An external under-voltage lockout (UVLO) circuit is also included to enable operation. The energy storage is managed with two capacitors: a high-capacity main capacitor for storing harvested energy for the load, and a secondary capacitor to expedite the start-up process. The PSU initially charges the secondary capacitor using the harvester generating the most energy. Upon full charging, the UVLO generates a power good (PG) signal to activate the system. The system then reassesses the inputs during a brief waiting cycle, identifying Open Circuit Conditions (OCC). The control logic selects two out of four inputs to connect them to the combiner core, where a differential low-power oscillator converts the current (I2) of the second harvester to AC. This pulse-shaped current is coupled by charging capacitors C1 and C2. The switched capacitor's output charges one capacitor, resulting in the voltage (VC) being equal to the sum of V1 and V2. The switched capacitor offers the advantage of concurrent energy combining, eliminating the need for time-division multiplexing. Additionally, it represents an integrated solution, characterized by its compact size and ease of packaging. This makes it a practical and efficient choice for systems where space-saving and integration are priorities.

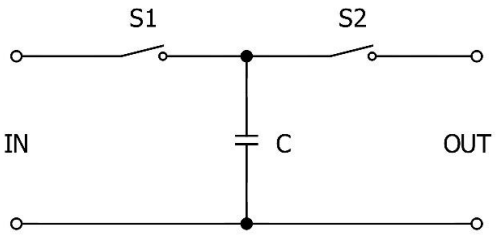

Figure 2.15 Switched Capacitors Scheme

Shared Inductor

The shared inductor method for energy combining uses a single inductor within a buck-boost converter to accumulate energy from different sources, as shown in Figure 2.16. This buck-boost converter can operate in Discontinuous Conduction Mode (DCM), with the potential to implement Maximum Power Point Tracking (MPPT) by controlling the frequency of the converter's switches. While this method is effective in low-power applications, a notable drawback is the size of the inductor, which increases the overall circuit size and, consequently, the total costs. In study [55], a design is proposed to merge energy from three harvesters: a thermoelectric generator (TEG), a Biofuel Cell (BFC), and a photovoltaic (PV) panel, using a single-stage shared inductor. This design includes controllable switches, a shared MPPT controller, a shared output regulator, the shared inductor, a battery, and a controller. The control method allocates a charging interval (T1) to each harvester branch for charging the shared inductor, with a switching frequency determined by the harvester output comparator, based on MPPT and ambient energy availability. After T1, a zero-current detector (ZCD) checks for zero inductor current, and the controller then assesses other harvesters, giving the selected branch a second charging interval (T2) if necessary. If both remaining harvesters have low output, the process restarts. Another design in [56] combines energy from three sources: vibration, PV, and RF. It includes controllable switches, comparators, an MPPT circuit, oscillators, a shared inductor, and capacitors. The aim is to achieve DCM in three phases: energizing the inductor, dumping stored energy into a capacitor to maintain constant peak inductor current, and a waiting phase for charging each transducer's capacitor.

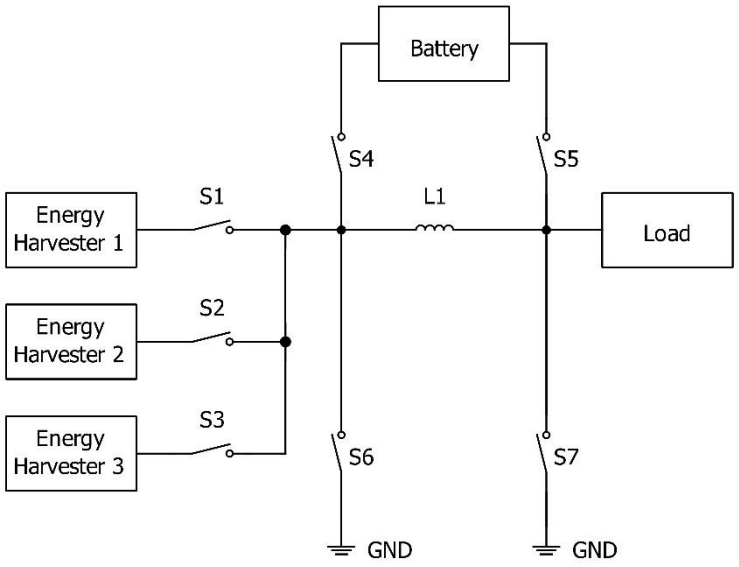

Figure 2.16 Shared Inductor Scheme

2.5.1 Multi Input Energy Harvesting Techniques Comparison

A comparison of multi-input energy harvesting techniques is presented in Table 2.4 based on the following criteria:

1. Complexity: define the level of system complexity. The possible values are High, Medium, and Low, where High indicates difficulties with the device introduced by its size, price, reliability, etc.

2. Simultaneity states refer to the ability of the system to harvest the energy from the input resources at the same time (binary criterion – Yes/No).

3. A typical number of inputs indicates the maximum number of resources that can be connected to the system.

4. The typical efficiency of an energy harvester is based on the ratio between the input and output energy, considering losses.

5. MPPT indicates whether Maximum PowerPoint Tracking can be implemented in the system.

The application and environment play an important role in choosing the optimal techniques. Also, the typical efficiency is varying based on the used control algorithm.

Table 2.4 Multi Input Energy Harvesting Techniques Comparison

Method	Complexity	Simultaneity	Typical number of inputs	Typical Efficiency	MPPT	References
Supplementary use of energy sources	Low	Yes	2	90.5%	No	[39], [40]
Power ORing	Low	No	unlimited	80-94%	Yes	[43], [44]
Voltage level detection	High	No	unlimited	72- 94.67%	Yes	[46]
Multiple-input boost converter	Medium	Yes	2	85%	Yes	[48], [49], [50], [51]
Linear regulator	Medium	Yes	3	80%	Yes	[52]
Multiplexing techniques	High	No	3	80-90%	Yes	[47]
Switched capacitors	High	Yes	2	72-87.2%	Yes	[54]
Shared inductor	High	No	3	87-89%	Yes	[55], [56]

Conclusion

The main disadvantages of combining energy harvested from different resources are the delay in choosing the energy resource and the waste of harvested energy since all the proposed energy combining systems rely on sensors to measure the voltage level, which leads to delay in energy waste. In this thesis, I propose a novel technique based on forecasting the available energy from PV harvesters and a lookup table of available PZT harvesters to choose the primary source of energy to be harvested.

3 ENERGY MANAGMENT SYSTEM

This chapter introduces the system requirements for the Energy Management System (EMS) in IoT device. The architecture of the EMS is proposed to meet these requirements, drawing insights from the comprehensive review in Chapter 2. The sizing of the PZT and PV harvesters for this purpose is detailed, and techniques for battery management within the EMS are implemented. A novel energy combine technique is proposed based on multi-input buck boost converter. Additionally, a novel algorithm is introduced to calculate battery degradation. The chapter also covers the design of the dynamic behavior of the EMS, showcasing how it adapts to varying conditions and requirements.

3.1 System Requirements

The requirements of EMS for IoT device:

- PV harvester output power is sufficient to power the IoT device Then the PV harvester is the power resource in order to extend the battery' SoC and lifespan.
- PZT harvester output power is sufficient to power the IoT device Then the PV harvester is the power resource in order to extend the battery' SoC and lifespan.
- Battery output power is sufficient to power the IoT device.
- Battery's SoC will never drop below 40% to avoid deep discharging.
- If the battery's voltage exceeds 4.20V, then the EMS must stop the charging process.
- If the battery's voltage drops below 2.5V to 3.0V, then the EMS must disconnect the load and prevent further discharge.
- If any battery's voltage falls below 2.5V, then the EMS must disconnect the battery from the load and prevent further discharge.

- If the discharge current exceeds the battery's maximum continuous discharge rate, then the EMS must disconnect the battery to prevent damage.

- If the discharge current is abnormally low, indicating a potential fault, then the system must alert the user and initiate a diagnostic check.

- If the battery temperature exceeds a safe limit (45°C to 60°C), then the EMS must suspend charging or discharging.

- If the battery temperature is below 0°C, then the EMS must prevent charging to avoid damage due to lithium plating on the anode.

3.2 Energy Management System Architecture

The proposed energy management system will provide the following features:

- Combine the renewable energy from two harvesters.

- Manage the energy flow from battery and the harvesters to the load based on the available energy and the application requirements QoS.

- Provide the protection to the battery, load, and harvesters.

The proposed energy Management system consist of:

- Photovoltaic branch which is the photovoltaic harvester

- Piezoelectric branch which consists of a Piezoelectric harvester and rectifier since the output of the Piezoelectric harvester is Alternative Current (AC) while it is required a Direct Current (DC) to power the sensor node and charge the battery.

- Buck Boost Converter which will combine the harvested energy from the Photovoltaic and Piezoelectric harvester and extract the maximum power from the harvesters to charge the battery.

- Sensors which are voltage, current, and temperature sensors to provide information about the state of the harvesters, battery, and atmosphere.

- Switches which will connect and disconnect the branches, resources and battery according to the control signals to perform the energy management operations.

- Regulator that will regulate the voltage according to the IoT device energy specifications.

- Controller that will perform the following tasks:

    1. Choosing the harvester based on the input from sensors, PZT output power lookup table and PV output power prediction data.

    2. Choosing the energy source to power the load.

    3. Perform Maximum Power Point Tracking (MPPT) algorithm.

    4. Perform Battery Management System (BMS) operations.

The Energy Management System (EMS) architecture is presented in the Figure 3.1.

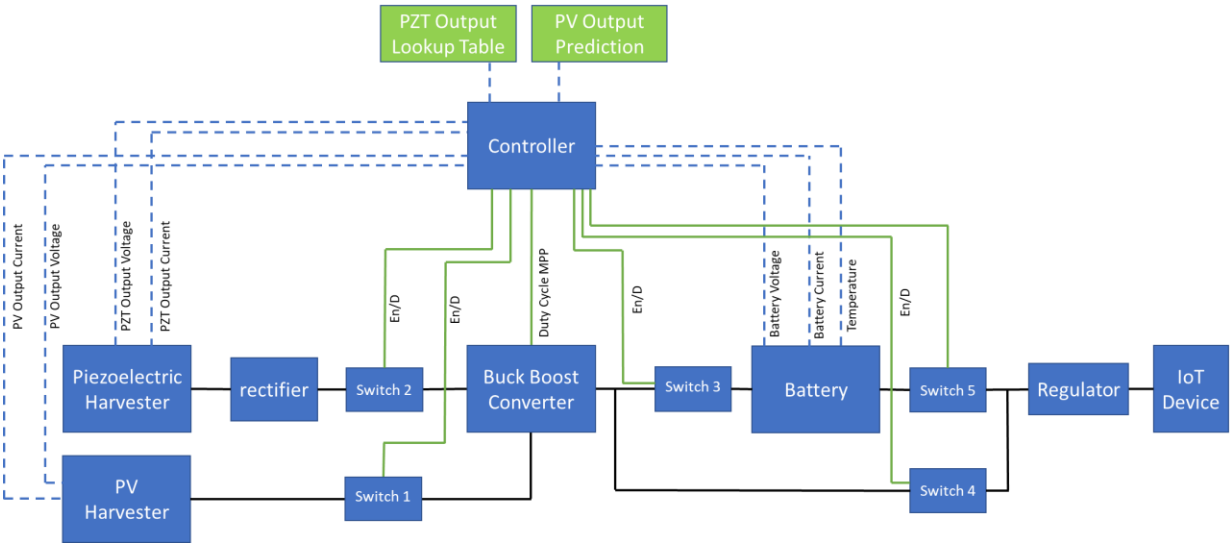

Figure 3.1 EMS Architecture

3.3 Piezoelectric Energy Harvesting

Piezoelectric Converter Theory

Piezoelectric converters are devices that convert mechanical energy into electrical energy. They generate an electric charge on their surface in response to external forces that cause distortion or mechanical stress. There are two main types of piezoelectric effects:

- Direct Piezoelectric Effect: In this effect, the polarity of the induced charge reverses when the direction of the applied stress is reversed. This property not only enables the piezoelectric transducer to generate electricity but also makes it useful as a sensor.

- Converse Piezoelectric Effect: This effect involves changes in the dimensions of the material due to surface deformation when an electric field is applied. It allows the piezoelectric material to function as an actuator.

The direct piezoelectric effect, which facilitates both electricity generation and sensing capabilities, is illustrated in Figure 3.2.

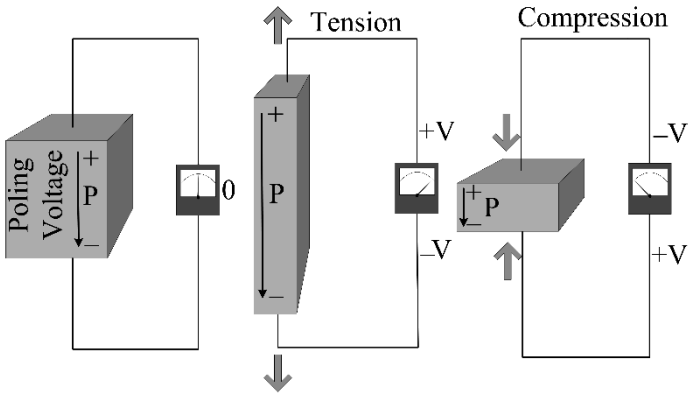

Figure 3.2 Piezoelectric Effect

In its normal state (without any external force), a piezoelectric material generates zero voltage. However, when subjected to tension or compression, it produces voltage. Piezoelectric materials are a subset of ferroelectric materials, which are crystals characterized by their inherent polarity even without an applied electric field. This piezoelectric effect is commonly found in piezoceramics like PbTiO3 (Lead Titanate), PbZrO3 (Lead Zirconate), PVDF (Polyvinylidene Fluoride), and PZT (Lead

Zirconate Titanate). Among these materials, PZT is particularly noteworthy in the ceramic piezoelectric category. It is preferred over PVDF due to its significantly higher piezoelectric coefficient, which is about ten times greater than that of PVDF. This superior characteristic makes PZT a more effective choice for use in various models and applications. The behaviour and properties of piezoelectric materials are further defined by the constitutive relations set out in the IEEE Standard of 1987 [18].

Direct piezoelectric effect:

$$D_i = e_{ij}^{\sigma} E_j + d_{im}^{d} \sigma_m \tag{3.1}$$

Converse piezoelectric effect:

$$\varepsilon_k = d_{jk}^{c} E_j + s_{km}^{E} \sigma_m \tag{3.2}$$

And, it could be written in the form

$$\begin{bmatrix} D \\ \varepsilon \end{bmatrix} = \begin{bmatrix} e^{\sigma} & d^{d} \\ d^{c} & S^{E} \end{bmatrix} \begin{bmatrix} E \\ \sigma \end{bmatrix} \tag{3.3}$$

Where:

- D is the electric displacement vector of size (3×1) (Coulomb/m²).
- ε vector (6×1) is the is the strain (without unit).
- E vector (3×1) (Volt/m) is the applied electric field.
- σ_m vector (6×1) (N/m²) is the stress.
- e_{ij}^{σ} is the dielectric permittivity of size (3×3) (Farad/m) – Piezo electric constant
- d_{im}^{d} is the piezoelectric coefficient (3×6) – Piezo electric constant
- d_{jk}^{c} is the piezoelectric coefficient (6×3) (Coulomb/N or m/Volt) – Piezo electric constant

- s_{km}^{E} is the elastic compliance of size (6×6) (m²/N) – Piezo electric constant.

- d_{jk}^{c} is the piezoelectric coefficient (m/Volt) which defines strain per unit field at constant stress

- d_{im}^{d} is the electric displacement per unit stress at constant electric field (Coulomb/N).

The equivalent circuit of a piezoelectric transducer, as depicted in Figure 3.3, includes both mechanical and electrical components. On the mechanical side, the circuit represents elements such as mechanical mass, stiffness, and losses. These are connected to the electrical part of the circuit through a transformer, which serves the function of converting mechanical strain into electrical current.

In the electrical domain, the piezoelectric material is modeled as a plate capacitor. When the harvester operates within its self-resonant frequency (SRF) range, which is optimal for inducing maximum charge, the total equivalent circuit can be simplified and represented purely in electrical terms. In this representation, it consists of an alternating current source connected in parallel with a resistance and a capacitor. This configuration effectively captures the electrical behavior of the piezoelectric transducer under resonant conditions.

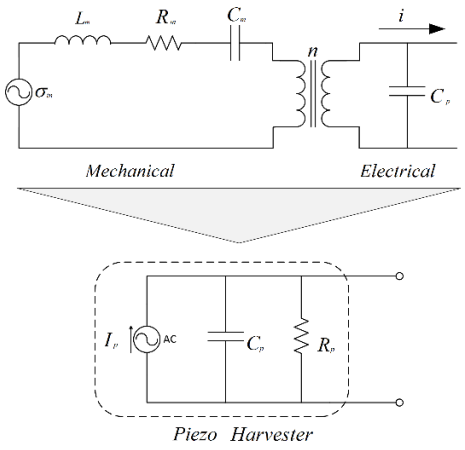

Figure 3.3 Equivalent Circuit of Piezoelectric Transducer

3.3.1 Piezoelectrical Element Model

The model of the piezoelectric harvester describes the mechanical and electrical behavior,

A. Mechanical model:

a. Cantilever Beam Dynamics:

It is Modeled as a spring-mass-damper system. The natural frequency can be represented in the following equation:

$$f_n = \frac{1}{2\pi}\sqrt{\frac{k}{m}} \tag{3.4}$$

Where:

- k is the effective stiffness of the beam
- m is the effective mass.

b. Vibration Response

The strain (ϵ) in the piezoelectric material due to deflection under vibration can be represented in the following equation:

$$\epsilon = \frac{\delta}{d} \tag{3.5}$$

Where:

- δ Is the defection
- d is the thickness of the piezoelctric

B. Piezoelectric Energy Conversion

a. Piezoelectric Effect

The strain produces and electric charge (q) in the piezoelectric material can be represented in the following equation:

$$q = d_{31}.\epsilon.A \tag{3.6}$$

Where:

- d_{31} is the piezoelectric charge constant
- A is the area of the piezoelectric layer

b. Generated Voltage

The voltage (V_p) across the piezoelectric material can be calculated as:

$$V_p = \frac{q}{C_p} \tag{3.7}$$

Where (C_p) is the capacitance of the piezoelectric material.

c. Output Current

The output current can be calculated as:

$$I_p = C_p \frac{dV_p}{dt} \tag{3.8}$$

d. Electrical Output to Load

The electrical power output (P) to a resistive load (R) is:

$$P = \frac{V^2}{R} \tag{3.9}$$

C. Complete System Model

The complete model of the piezoelectric harvester is the coupling of the differential equations of the mechanical vibration and the piezoelectric effect and it is expressed as:

$$m\ddot{x} + c\dot{x} + kx = F_{ext} - d_{31}.A.V \quad (3.10)$$

Where:

- x is the displacement
- $\ddot{x}$ is the acceleration
- $\dot{x}$ is the velocity
- c is the damping coefficient
- F_{ext} is the external force (vibration source)

3.3.2 Voltage Rectifier

The output from a piezoelectric harvester is in alternating current (AC), which necessitates conversion to direct current (DC) to power a load or charge a battery. Assuming the use of an ideal rectifier, then the rectifier's output voltage (V_{DC}) can be approximated as being equal to the amplitude of the AC output voltage from the piezoelectric element. This approximation is based on the principle that an ideal rectifier efficiently converts the peak AC voltage to a corresponding DC voltage, with minimal loss. Consequently, the peak AC voltage becomes a key determinant of the DC output voltage level after rectification.

The DC output voltage (V_{dc}) can be calculated as:

$$V_{dc} = |V_p| \quad (3.11)$$

The output power of the rectifier is:

$$P_{out} = \eta_{rect} \times P_{max} \quad (3.12)$$

Where:

- P_{out} is the power delivered to the load

- η_{rect} is rectifier efficiency.

3.4 PV Energy Harvesting

3.4.1 Single PV Cell Model

The equivalent circuit of the PV cell consists the of several components as shown in Figure 3.4.

1. Current source represents the generated electric current by the incident solar light I_L connected in parallel with a forward biased diode represent the behavior of the semiconductor material of the PV panel.

2. Shunt resistance R_{sh} models the leakage current path because of the imperfections in the cell's material

3. Series resistance R_s models the internal resistance of the PV panel. This represents the semiconductor material resistance and the metal connections.

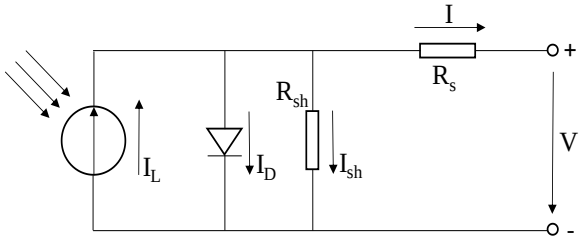

Figure 3.4 Equivalent Circuit of the Photovoltaic Panel

The light current is proportional to the incident solar irradiance (G) and the area of the PV panel. It can be represented as:

$$I_L = G * A * I_{Lref} \tag{3.13}$$

Where:

- G is the solar irradiance (W/m^2)

- A is the area of the PV panel (m^2)

- I_{Lref} is the reference light current at the standard test conditions (STC) which are usually at 25°C and 1000 W/m^2

The behaviour of the diode in the PV panel can be described in the diode equation which relates the diode current to the cell's voltage and temperature as:

$$I_D = I_O * \left[e^{\left(\frac{qV_D}{akT}\right)} - 1\right] \quad (3.14)$$

Where:

- I_D is the diode current.

- I_O is the reverse saturation current of the diode.

- q is the charge of an electron (= $1.6 \times 10^{-19}\ Coulomb$).

- V_D is the diode voltage.

- a is the ideality factor (=1 for indirect semiconductor, =2 for direct semiconductor).

- k is the Boltzmann's constant (= $1.38 \times 10^{-23}\ J/K$).

- T is the absolute temperature (in Kelvin)

The model of the single PV cell can be expressed in the following equation:

$$I = I_L - I_D - I_{sh} \quad (3.15)$$

Where:

- I is the output current of the PV cell

- I_{sh} is the current through the shunt resistance, representing leakage currents in the cell

3.5 Multi Input Buck-Boost DC-DC Converter

The Buck-Boost converter is a circuit which can step up or step down [57]. The proposed topology combines the output energy of photovoltaic (PV) and piezoelectric harvesters. These harvesters are connected to a shared capacitor and inductor via switches as shown in the Figure 3.5. A predictive algorithm controls the state of switches (open or close) which is designed to select the energy source with the highest output based on prediction for the next hour. The converter's output is then directed to a load, which could be a sensor node or a battery. This topology ensures a unidirectional flow of energy, from the sources to the load. In steady-state operation, the system goes into Continuous Conduction Mode (CCM) when the inductor current stays above zero. This condition guarantees that either a switch or a diode is continuously conducting, allowing for current flow through the inductor, thereby keeping the inductor current consistently above zero during the switching cycle. The output voltage (V_{out}) is given by:

$$V_{out} = V_{in} \cdot \frac{D}{1 - D} \tag{3.16}$$

Where:

- V_{out} is the output voltage of the converter
- V_{in} is the input voltage form the PV cell or Piezoelectric harvester.
- D is the duty cycle of the Buck-Boost converter which is the ratio of the ON time to the total switching period.

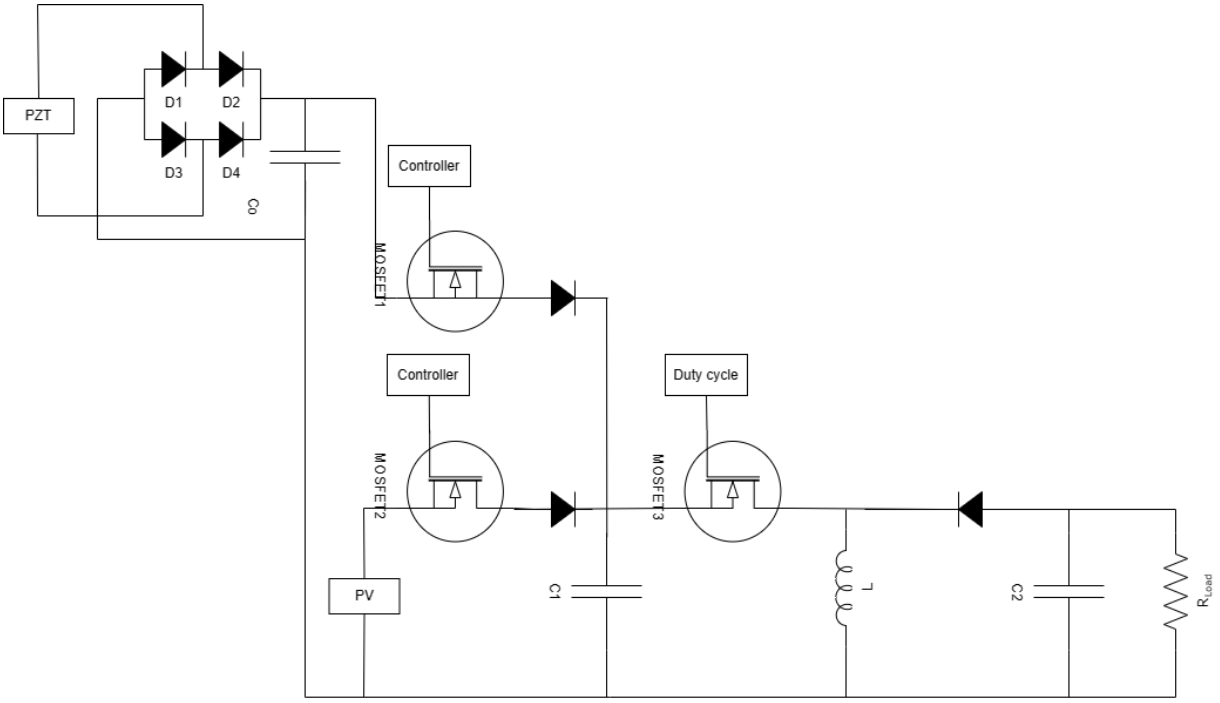

Figure 3.5 Multi Input Buck Boost Converter

Sizing DC-DC Converter

The inductor is sized to limit the ripple in the inductor current (ΔI_L), The equation for the inductor is:

$$L = \frac{V_{in}.(1-D).D}{f_{sw}.\Delta I_L} \tag{3.17}$$

- f_{sw} is Switching frequency.
- ΔI_L is desired peak to peak ripple current in the inductor.

A large inductor reduces the current ripple, which can improve efficiency and minimize voltage spikes, but at the same time, it leads to an increase in the dimensions of the inductor component.

The capacitor size affects the ripple in the output voltage (ΔV_{out}). The equation for the capacitor is:

$$C = \frac{I_{out}.D}{f_{sw}.\Delta V_{out}} \tag{3.18}$$

- ΔV_{out} is desired peak to peak ripple voltage in the output.

- I_{out} is output current

A large capacitor minimizes output voltage ripple. As a result, the output is more stable, but at the same time, it increases the capacitor component's dimensions.

Working Principle of Buck-Boost Converter

The Buck-Boost Converter operates in two primary modes based on the state of switches:

1. Switches is Closed (ON):

- The input voltage is applied on the inductor so the current through the inductor is rising.
- The diode is preventing current flow to the output

2. Switches is open (OFF):

- The inductor current flows through the capacitor to the load via the diode.
- The energy stored in the inductor is transferred to the capacitor and the load.

The duty cycle (D) of the switch controls the converter's operation and define if the converter increasing the voltage or decreasing it.

Maximum Power Point Tracking (MPPT)

Maximum Power Point Tracking (MPPT) is a technique used to extract the maximum output power from the harvester to power the load or charge the battery [58] [59].

The MPPT algorithm adjusts the duty cycle (D) to maximize the output power as:

$$P_{max} = V_{mpp} \times I_{mpp} \tag{3.19}$$

Where:

- V_{mpp} is the voltage at the MPP

- I_{mpp} is the current at the MPP

Power Efficiency:

By taking into consideration the efficiency of the Buck-Boost converter. The the output power can be expressed as:

$$P_{out} = \eta \times P_{max} \tag{3.20}$$

Where:

- P_{out} is the power delivered to the load
- η is the efficiency foactor of the Buck-Boost converter

3.6 Battery Mangment System (BMS)

The Battery Management System (BMS) plays a crucial role within the broader scope of an Energy Management System (EMS), particularly in systems where battery usage is a significant component. The BMS is dedicated to overseeing the state and health of the battery, a task it accomplishes by continuously monitoring critical battery parameters such as voltage, current, temperature, and State of Charge (SoC). This monitoring is vital for implementing safeguards against conditions like overcharging, deep discharging, and overheating, which can compromise both the performance and longevity of the battery. Additionally, the BMS actively manages the charging and discharging processes, ensuring they are conducted in a manner that optimizes battery life and maintains operational safety. The data and control inputs provided by the BMS are integral to the functionality of the EMS. By delivering real-time insights into the battery's condition and operational parameters, the BMS enables the EMS to make informed decisions regarding energy distribution, storage, and utilization across the system. This synergy is especially critical in systems powered by a combination of energy harvesters and batteries.

3.6.1 Battery

The equivalent circuit model (ECM) of battery is illustrated in the Figure 3.6. It represents the electrical characteristics. The work voltage of the battery is presented as follow:

$$U_L = \begin{bmatrix} -1 & -1 \end{bmatrix} . \begin{bmatrix} U_b \\ U_P \end{bmatrix} - R_0 . I_L + U_{oc} \tag{3.21}$$

Where:

- U_L is the battery voltage.
- U_P is capacitance terminal voltage.
- I_L is the battery current.
- R_0 is the internal resistance.
- The work current is presented as follow:

$$I_L = \frac{U_T - \sqrt{(U_T)^{1/2} - 4R_0P_L}}{2R_0} \tag{3.22}$$

Where P_L is the load power.

In the circuit, the voltage

$$U_p = R_p . I_p \tag{3.23}$$

$$I_{p,k} = 1 - \frac{\theta}{T} + e^{-T} . I_{p,k-1} + \left\{ \frac{\theta}{T} - e^{-T} \right\} . I_{L,k-1} \tag{3.24}$$

Where:

- $I_{p,k}$ is the current value of a variable (or signal) at iteration k

- $I_{p,k-1}$ is the value of the same variable at the previous iteration $(k-1)$
- $I_{L,k-1}$ is the value of another variable (or signal) at the previous iteration $(k-1)$
- θ and T are parameters of the system, $\Delta t/\tau = -e^{-T} + 1T$, $\tau = RC$, and Δt is the simulation step.

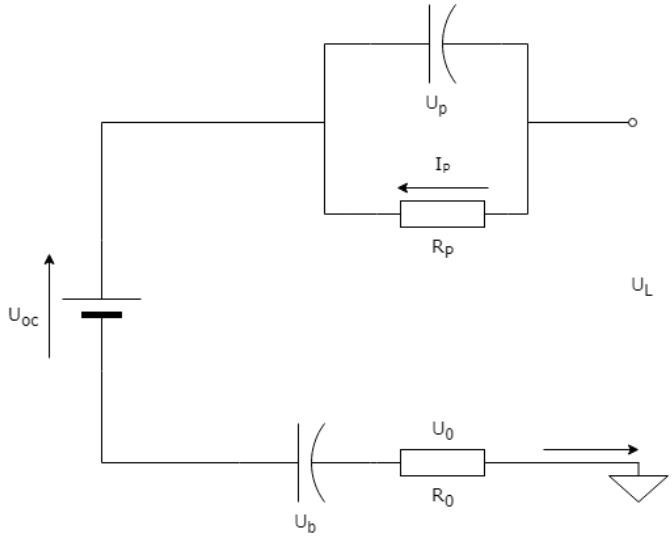

Figure 3.6 The Equivalent Circuit Model for Modeling the Battery

3.6.2 State of Charge (SoC) Calculation

The State of Charge (SoC) of a battery is a critical metric, quantitatively defined as the ratio of the remaining capacity of the battery to its total capacity, typically expressed as a percentage. Mathematically, this relationship can be represented as:

$$SoC = \left(\frac{Remaining\ Capacity}{Total\ Capacity}\right) \times 100\% \tag{3.25}$$

Accurate estimation of SoC is akin to a fuel gauge in various applications, offering essential insights into the battery's current state and its readiness for use. To calculate SoC, several methodologies have been developed, each with unique advantages and limitations, tailored to different application requirements.

1. Open Circuit Voltage (OCV) Method: Relies on the correlation between the battery's rest voltage and its (SoC). While it provides good accuracy without significant computational load, it requires

the battery to be in a no-load condition for an accurate measurement, which may not always be practical.

2. Coulomb Counting Method: Involves the integration of current over time to track the charge flowing in and out of the battery. This method is straightforward but can accumulate errors over time, particularly if not periodically recalibrated.

3. Model-Based Methods (Kalman Filter and Extended Kalman Filter): These sophisticated methods use mathematical models of the battery to estimate (SoC). The Kalman Filter and its non-linear variant, the Extended Kalman Filter, are particularly notable for their ability to provide accurate SoC estimates even in the presence of system uncertainties and measurement noise. However, they require more computational resources and careful tuning of model parameters.

4. Artificial Intelligence (AI) Methods: AI and machine learning techniques are emerging as powerful tools for SoC estimation, capable of learning complex battery behaviors and adapting to changes over time. While they can offer high accuracy, they often require extensive training data and computational power, which might be a constraint in resource-limited applications.

Given these constraints, the Coulomb Counting Method emerges as the most suitable algorithm for SoC estimation in WSN nodes. This method's primary advantage is its straightforward approach, which involves measuring the incoming and outgoing current to and from the battery. It provides real-time SoC estimation without imposing significant computational demands. The fundamental principle of Coulomb Counting is based on the accumulation of charge over time, with the SoC calculated using the following equation:

$$SoC(t) = SoC(t_0) + \frac{1}{Q}\int_{t_0}^{t} I(t)dt \tag{3.26}$$

Where:

- $SoC(t)$ is the State of Charge at time t.
- $SoC(t_0)$ s the initial State of Charge at the starting time t_0.
- Q is the total capacity of the battery (in ampere-hours).
- $I(t)$: is the net current flowing into or out of the battery at time t.

- The integral $\int_{t_0}^{t} I(t)dt$ represents the total charge transferred in or out of the battery over the time interval from t_0 to t.

The real-time capability, combined with its minimal processing requirements, makes the Coulomb Counting Method particularly well-suited for WSN nodes. It effectively balances the need for accurate SoC estimation with the inherent limitations of embedded systems in terms of processing power and energy efficiency.

3.6.3 Capacity and Health Monitoring

Capacity and Health Monitoring is the prediction the lifespan of a battery by assessing its current state and overall health. Various algorithms have been developed for this purpose, each with its specific advantages and disadvantages, making them suitable for certain applications.

1. Voltage Recovery Method: This method is observing information about the battery's internal resistance which is an indicator of battery health. It is based on disconnecting the load and then measure the time open circuit voltage. It is not a practical method for WSN application since disconnecting the load is a condition for this method.

2. Impedance Spectroscopy: This technique measures the internal impedance of the battery at various frequencies. It involves applying an AC signal and measuring the response, which varies in relation to the battery's State of Health (SoH). Effective for gaining insights into the internal status of the battery, reflecting its health. The special conditions like applying AC signals with different frequencies make it complicated to be performed in application such as WSN.

3. Incremental Capacity Analysis (ICA): It focuses on identifying capacity fade and degradation. It analyses the differentiation of the charge capacity curve with respect to voltage. This analysis is instrumental in detecting changes in the battery’s capacity over time, indicative of its aging process. This method requires additional computing and energy resources to be performed which make it not suitable for application where the resources are limited.

4. Machine Learning-Based Health Estimation: Utilizes historical data, including voltage profiles, charge/discharge cycles, temperature, and overall performance to predict the battery’s state using machine learning techniques. It offers adaptive predictions based on evolving data, providing a dynamic view of the battery's condition. Like (ICA) it is not suitable for WSN due to the restrictions of energy and computing resources.

Coulomb Counting: This method is calculating the current battery capacity by measuring the incoming and outcoming current of the battery and compare it with the original battery capacity. By adding a life cycle counter this method will be a practical solution in WSN application since the same data can be used for calculation the (SoC) and Capacity Fade.

Coulomb Counting Combined Life Cycle Counter Algorithm

To estimate the current capacity of the battery and calculate its degradation over time a combined algorithm of Coulomb Counting and battery life cycle counter is proposed.

A. Capacity Fade Estimation

Capacity Fade is used to estimate the battery's age by comparing the current capacity of the battery to its original capacity. To calculate the Capacity Fade the following equation is used:

$$Capacity\ Fade = \left(1 - \frac{Q_{current}}{Q_{original}}\right) \times 100\% \tag{3.27}$$

Where:

- $Q_{current}$ is the current maximum charge capacity
- $Q_{original}$ is the original capacity of the battery

By knowing the typical degradation rate for the battery based on the type or historical data. The estimated Cycles can be calculated. For instance, if the used battery is lithium ion, then the typical degradation is 20% over 500 cycles then the remaining cycles can be calculated as:

$$Estimated\ Cycles = \frac{Capacity\ Fade}{Typical\ Degradation\ per\ Cycle} \times 500 \tag{3.28}$$

For calculation the current Capacity, the degradation should be taken into consideration. Let's Assume a linear degradation model for simplicity then:

$$Q_{current} = Q_{max} - degradation\ rate \times N \tag{3.29}$$

N: Number of complete charge-discharge cycles

Update Q_{max} periodically based on N

B. Generalized Cycle Counting Approach:

Let's define the variables and the formula:

- C_{start}: State of Charge (SoC) at the start of the charging.
- C_{end}: State of Charge (SoC) at the end of the charging.
- D_{start}: State of Charge (SoC) at the start of the discharging.
- D_{end}: State of Charge (SoC) at the end of the discharging.
- Q: Total capacity of the battery.
- $partialCycle$: Accumulator for the fractional cycles.
- $fullCycleCount$: Total count of full cycles.

Each charging or discharging event contributes a fraction of a cycle calculated as:

- For charging:

$$Fraction\ of\ Cycle = |\frac{C_{end-}\ C_{start}}{Q_{original}}| \tag{3.30}$$

- For discharging:

$$Fraction\ of\ Cycle = |\frac{D_{end-}\ D_{start}}{Q_{original}}| \tag{3.31}$$

The absolute value is taken since the magnitude of charge or discharge is needed for this method.

- The general equations:

- For charging:

$$partialCycle += |\frac{C_{end-} C_{start}}{Q_{original}}| \quad (3.32)$$

- For Discharging

$$partialCycle += |\frac{D_{end-} D_{start}}{Q_{original}}| \quad (3.33)$$

- Full Cycle Calculation

    1. If $partialCycle \geq 1$:

        1. $fullCycleCount += 1$

        2. $partialCycle -= 1$

3.6.4 The Proposed Algorithm

- Assumptions:

    1. The battery (SoC) is 100%.

    2. The total Capacity of the battery is known $Q_{original}$.

    3. Battery's current is measured at the calculation time.

    4. Battery $fullCycleCount$ is zero.

    5. Battery $partialCycle$ is zero.

- Steps:

    1. Initialization:

        1. Set the initial (SoC) to 100% when the battery is full of charge.

2. Initialize a variable to count the $fullCycleCount$ starting with zero value.

3. Initialize a variable to count the $partialCycle$ starting with zero value.

4. Initialize a variable to keep track the current charge state (delivered/extracted) since the last full charge

2. Measurements:

1. Measure the current flowing into or out of the battery at regular intervals ($I(t)$).

2. Record the time interval (Δt) for charging and discharging

3. Charge Integration (Coulomb Counting):

1. For each interval calculate the charge transferred using

$$Q = I(t) \times \Delta t. \tag{3.34}$$

2. Add this value to the total charge counter, adjusting the sign based on whether the battery is charging or discharging

3. Update the (SoC) as follows:

$$SoC = SoC_{previous} + \frac{Q}{Q_{original}} \times 100\% \tag{3.35}$$

4. For charging update $partialCycle$ as follows:

$$partialCycle += |\frac{C_{end-} C_{start}}{Q_{original}}| \tag{3.36}$$

5. For Discharging update $partialCycle$ as follows:

$$partialCycle += |\frac{D_{end-} D_{start}}{Q_{original}}| \tag{3.37}$$

6. Check full Cycle as follows:

- If $partialCycle \geq 1$:
    - $fullCycleCount += 1$
    - $partialCycle -= 1$
    - Update the capacity of the battery by taking into consideration the degradation due to the life cycle increment as follows:

$$Q_{current} = Q_{original} - degradation\ rate \times fullCycleCount \quad (3.38)$$

4. Resetting and Continuation:

1. After a full charge cycle, reset the total charge counter and SoC to 100%

2. Continue the measurement and calculation process

3.6.5 Protection Mechanisms

BMS provides many protection mechanisms for the battery according to the application for ensuring the safety, reliability, and the extension the life span of the battery. The most common protection mechanisms are:

1. Overcharge/ over-discharge Protection: prevent the battery form exceeding the maximum/ minimum voltage limits.

2. Over Current Protection: keeps the flowing current into or out of the battery in the safe limits.

3. State of Charge (SoC) Monitoring: Keeps the battery SoC in the safe range.

3.7 EMS Dynamic Behaviour

The EMS's dynamic behaviour illustrates the system's response to various scenarios, with the energy flow paths depicted in the figures under specific conditions. These scenarios include:

Case 1: PV harvester output power is high and sufficient to QoS requirements & PZT harvester power is low & Battery SoC is greater than 40%. Then switches (1,3,4) are close and switches (2,3) are open. The energy flow from PV Harvester through the Buck Boost converter to the load (IoT device) as shown in Figure 3.7.

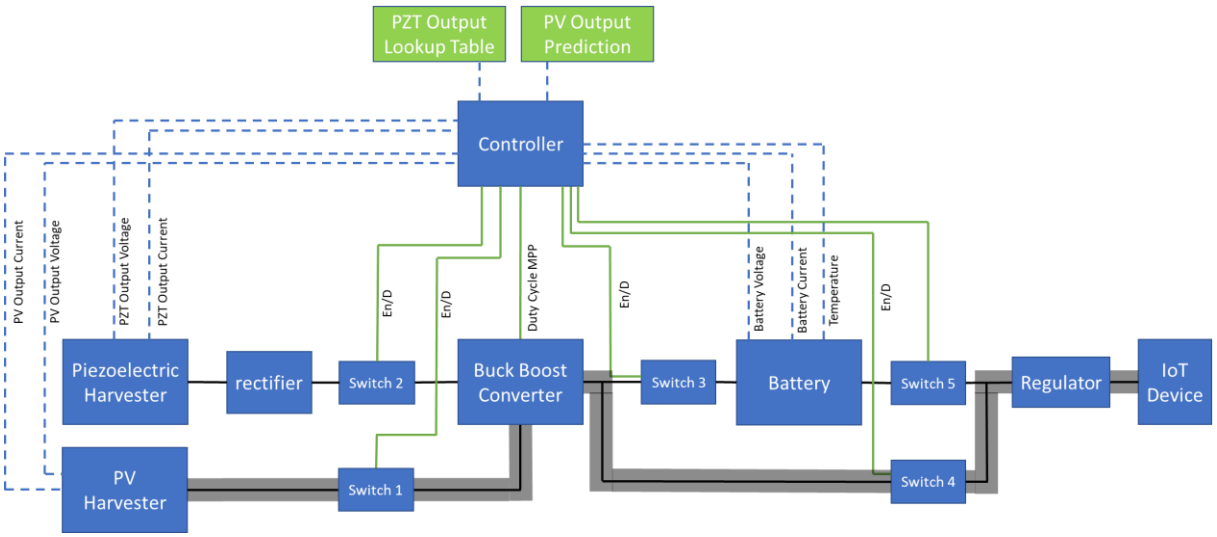

Figure 3.7 Case1: PV Feeding the IoT Device

Case 2: PZT harvester output power is high and sufficient to QoS requirements & PV harvester power is low & Battery SoC is greater than 40%. Then switches (1,2,4) are close and switches (2,3) are open. The energy flow from PZT Harvester through the Buck Boost converter to the load (IoT device) as shown in Figure 3.8.

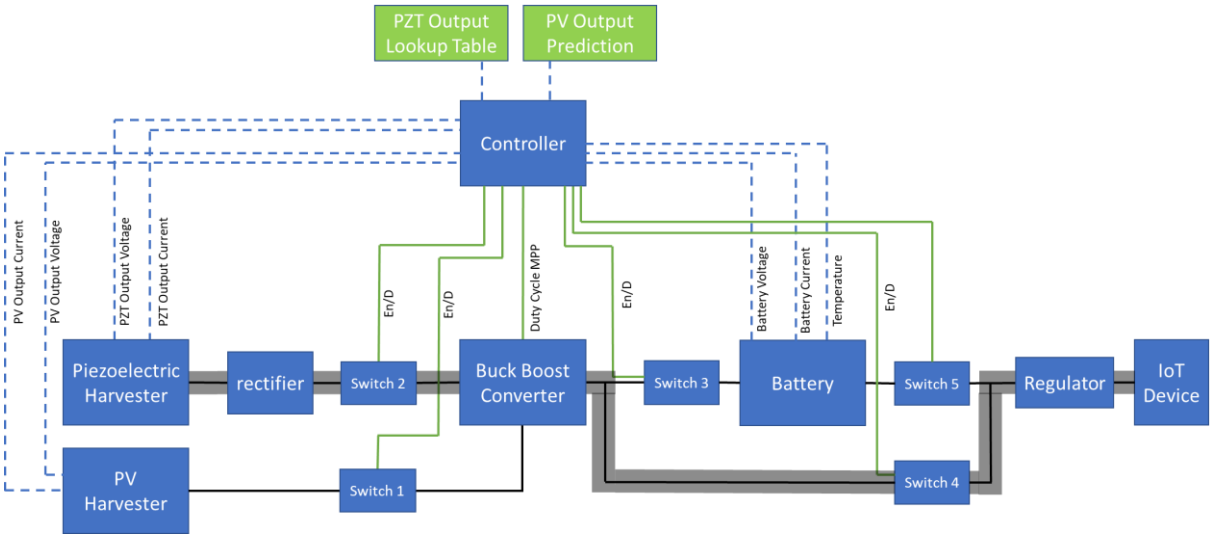

Figure 3.8 Case2: PZT Feeding the IoT Device

Case 3: PV harvester output power is low & PZT harvester power is low & Battery SoC is greater than 40%. Then switch (5) is close and switches (1,2,3,4) are open. The energy flow from the battery to the load (IoT device) as shown in Figure 3.9.

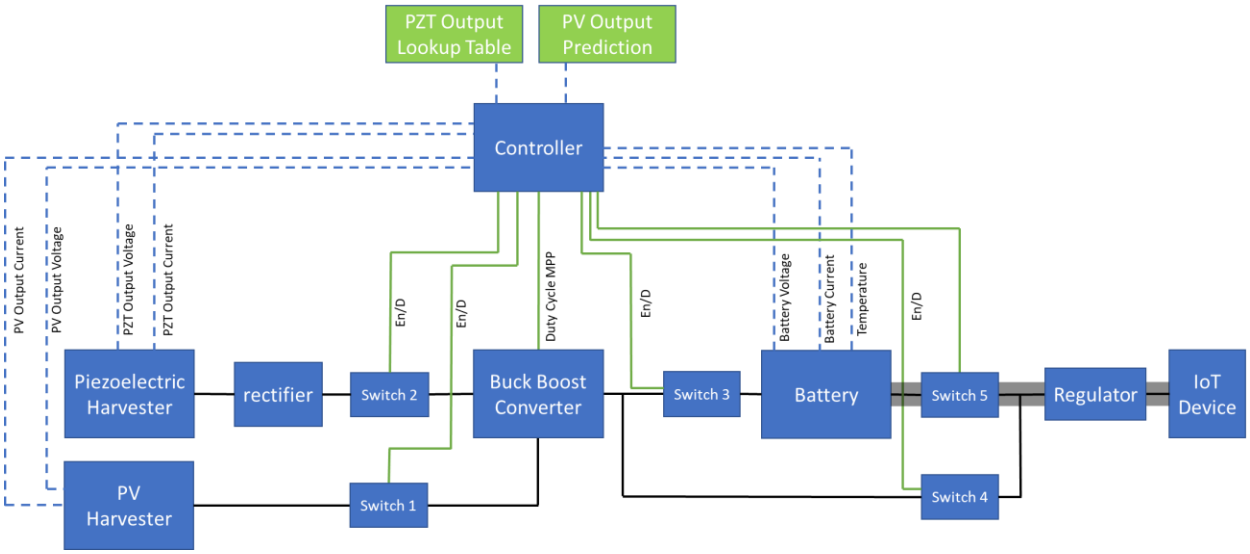

Figure 3.9 Case3: Battery Feeding the IoT Device

Case 4: PV harvester output power is high & PZT harvester power is low & Battery SoC is equal or lower than 40%. Then switches (1,3) are close and switches (2,4,5) are open. The energy flow from PV Harvester through the Buck Boost converter to charge the battery as shown in Figure 3.10.

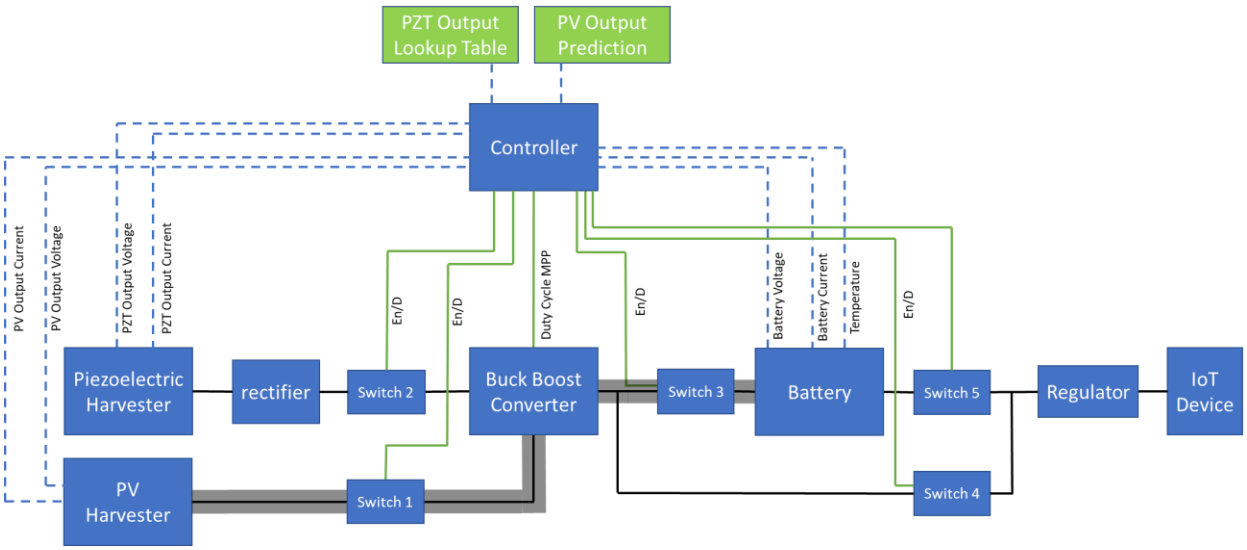

Figure 3.10 Case4: PV Charging the Battery

Case 5: PV harvester output power is low & PZT harvester power is low & Battery SoC is greater than 40%. Then switches (2,3) are close and switches (2,4,5) are open. The energy flow from PZT Harvester through the Buck Boost converter to charge the battery as shown in Figure 3.11.

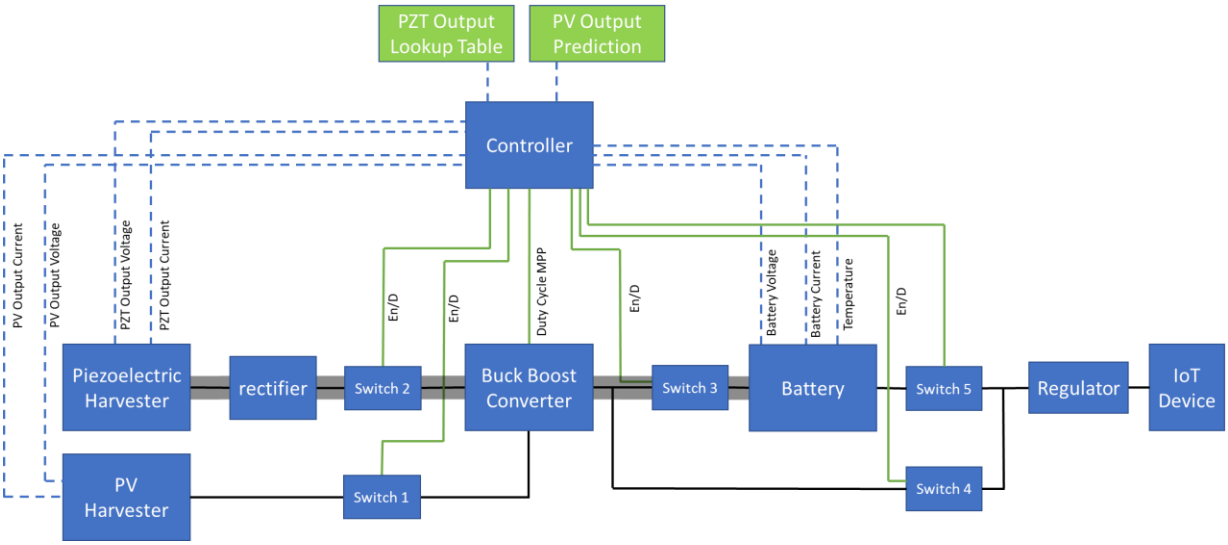

Figure 3.11 Case5: PZT Charging the Battery

4 PV ENERGY PREDECTION

4.1 Introduction

One of the most promising and rapidly evolving fields within renewable energy is photovoltaic (PV) energy harvesting. This advancement underscores the importance of short-term PV harvester output forecasting models. Developing accurate forecasting models is crucial for maximizing the benefits offered by this alternative energy source. Nowadays, short-term solar energy output forecasting lacks a fully established and validated technique and is frequently linked to significant forecast mistakes, which can occasionally approach 60–65%. Simultaneously, an area forecast with more points produces a less accurate result; similarly, a forecast for a longer period of time yields a more accurate outcome. The amount of solar radiation that solar panels will actually receive is forecasted, not the amount of electricity that a solar power plant will produce. This is influenced by many factors, the primary ones are the weather and climate, including the sun's position in the sky, the length of daylight, precipitation, cloud cover, wind speed, etc.

Various forecasting models are available, each with unique features constructed within the parameters of the chosen short-term forecasting techniques. Evaluating the most commonly used forecasting methods is the first step, and then the most promising method will be studied. The accuracy evaluation of each short-term forecasting method is essential to decide on the viability of applying and enhancing the various techniques.

4.2 Short-Term Forecasting Methods and Their Classification

The existing short term forecasting methods is divided into four main groups shown in Figure 4.1. Physical models elucidate the correlations between weather conditions and solar irradiance, derived through numerical weather forecasting and the generated electrical energy at the PV station. Statistical approaches define the relationship between the flux density of solar radiation, ascertained via numerical weather forecasting, and generated electrical energy at the PV station through statistical examination of historical data time series, disregarding physical factors. Adaptive techniques employ artificial intelligence systems to identify the linkage between forecasted weather conditions and the

generated electrical energy at the PV station. Predominantly, hybrid methods integrate physical and statistical models, offering a comprehensive framework for analysis.

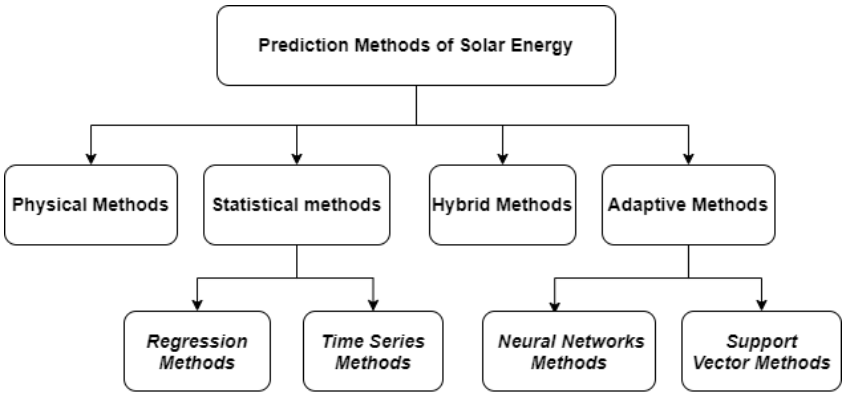

Figure 4.1 Solar Energy Prediction Methods

4.2.1 Physical Methods

In physical method, the input variables of the model include numerical weather forecasts, local meteorological observations, information on terrain and land surface type, and historical data regarding the generated energy of the PV station. Also, a satellite systems is used to track the direction and speed of cloud movement in some applications [60], which provides the opportunity to forecast solar radiation in real time. However, the accuracy of these methods is sensitive to the sudden changes in the weather condition and it is high with stable weather [61], [62]. Moreover, the practical application of physical models often presents a significant challenge. This is primarily due to their inherent complexity and the extensive array of parameters they require for accurate operation [62]. Furthermore, these models necessitate the use of sophisticated and costly equipment. Unfortunately, such resources are not readily accessible or even available in many regions across the globe, thereby limiting the widespread adoption and utilization of these physical models [62]. Thus, these models are not as well suited for incorporation into IoT devices. Therefore, for efficient solar energy prediction in this context, different approaches that are more compatible with the limitations of IoT devices need to be investigated.

The practical use of various physical models in predicting the generation of electrical energy is shown in works [63], [64], [65]. In [63], the influence of the value of aerosol optical depth on the quality of forecasting solar radiation using numerical weather forecast models MM5 or Eta is considered. As a result of the work, it is shown that when the value of the aerosol optical depth is less than 0.1, the

forecasting error is acceptable and is about 3-4%, and when the value of the aerosol optical depth is more than 0.1, the average deviation is about 100 W/m2.

In [64], one of the physical forecasting models is presented, which is based on short-term changes in the scale of Oktas and temperature changes to determine the average hourly output power of photovoltaic systems at small solar power plants located in the cities of Sanandaj and Rasht. This model has acceptable accuracy in predicting the generation of solar energy in cloudy weather, while in sunny weather it gives much worse results.

The study presented in [65] applies physical methods that rely on numerical weather predictions and satellite-based cloud motion vectors. The findings indicate that the accuracy of these pure physical methods, when used independently without integration with other methods, ranges between 15% and 21%.

4.2.2 Statistical Methods

For statistical forecasting models, the input data are numerical weather forecast data, in particular information about solar radiation and retrospective data on the generation of electrical energy by a solar power station.

Regression Methods

One of the widely used statistical methods for predicting electrical energy is regression methods. They allow taking into account a large number of factors affecting the forecast, including meteorological ones. When using regression methods, it is possible to estimate causal relationships and dependencies in the data. In addition, the advantage of these methods is that they allow predicting the value of the dependent variable by the values of the independent ones, but it is necessary that the feature values be uncorrelated.

The equation of linear regression has the following form:

$$\boldsymbol{Y = a + b_1 x_1 + b_2 x_2 + \cdots + b_n x_n + \mathcal{E}} \quad (4.1)$$

Where Y is the resulting feature, $x_1, \dots, x_n$ are the factor features, $b_1, \dots, b_n$ are the regression coefficients, a is the free term of the equation, and $\mathcal{E}$ is the “error” of the model.

The advantage of regression methods lies in the simplicity of their implementation, and the main disadvantage is the unpredictability of the parameters that affect the actual values. When sharp changes occur in the available retrospective data, the reliability of the forecast will be violated. The use of regression methods is well applicable for finding patterns in data and for determining significant factors of the model, but they do not provide high accuracy when building short-term models for forecasting the generation of electricity output.

Methods Based on Time Series

One of the most frequently used methods of time series is the Box-Jenkins ARIMA (Autoregressive Integrated Moving Average) model. This model is applied to non-stationary time series, brought to stationary, by taking the difference of a certain order from the original values of the time series. For a non-stationary time, series X, the ARIMA model has the following form:

$$\Delta^{\mathrm{d}}\mathrm{X_t} = \mathrm{c} + \sum_{\mathrm{i=1}}^{\mathrm{P}} \mathrm{a_i}\,\Delta^{\mathrm{d}}\mathrm{X_{(t-1)}} + \sum_{\mathrm{j=1}}^{\mathrm{q}} \mathrm{b_j}\mathcal{E}_{\mathrm{t-j}} + \mathcal{E}_{\mathrm{t}} \tag{4.2}$$

where $\mathcal{E}_t$ is a stationary time series, $c, a_i, and\ b_j$ are the parameters of the model, Δ^d is the difference operator of the time series of order d (sequential taking d times differences of the first order - first from the time series, then from the obtained differences of the first order, then from the second order, etc.) Also, this model is interpreted as ARMA$(p + d, q)$ - a model with d unit roots. When d = 0, the usual ARMA models are used.

Methods based on time series theory are widely used in building short-term forecasts for electrical energy generation, as companies have a large amount of historical data on electrical energy generated by PV plants, and methods in this group are aimed at processing large data arrays and allow finding patterns in them, as well as using these patterns when building forecast models. The main disadvantage of these methods is that they do not provide the required forecasting accuracy. But when using time series methods in combination, for example with adaptive models, the required accuracy is achievable, but the methods used in this case will belong to hybrid methods.

In works [66], [67], [68], [69], [70], [71], [72], [73], [74], [75], the practical application of statistical models to forecasting electricity generation is shown. In [66], a two-stage method for forecasting solar

power plant electricity is described. At the first stage, statistical normalization of solar energy is performed utilizing a clear sky model [74]. During the second stage, forecasts for normalized solar energy are derived through time series models, explicitly using an autoregressive model and an autoregressive model with exogenous input, into which numerical weather forecasts are fed. As a result of the work, it is shown that the use of an autoregressive model with an exogenous input gives a 12% better result than using a simple autoregressive model when forecasting a short horizon and 23% when forecasting the next day.

In [67], a model for forecasting solar energy is proposed, taking into account the stochasticity of clouds by applying various parameters that take into account power attenuation. Based on the statistical behavior of the parameters, a simple process of switching between three classes was proposed: “sunny”, “cloudy”, “variable cloudiness”. The forecast is built by identifying the current mode and assuming it will remain in this mode. In [68], The authors propose a very short-term solar energy forecast using the classic concept of “seasonality,” with the allocation of the average value or trend and rapid fluctuations around it. The feature of this work is a very short time horizon of 1, 15 and 60 minutes.

Different statistical models, that aim to predict the solar energy of solar panels that are deployed in wireless sensing network, were proposed. In [69], an algorithm known as Solar Energy Predication based on Additive Decomposition (SEPAD) is designed to predict solar energy harvesting. It does this by identifying the key terms involved in the prediction of solar energy harvesting and analyzing each one individually, which are solar diurnal cycle, seasonal effect and recently trend on current day. Once this is done, the terms are then amalgamated to determine the predicted energy. In a manner akin to basic statistical methods, the day is segmented into timeslots. Within each of these timeslots, the three terms can be computed. The performance evaluation results show that SEPAD algorithm achieves higher accuracy, lower complexity, and lower communication overhead than the other statistical methods, namely EWMA [70], WCMA [71] and AEM [72].

In [75], a new energy estimation and forecast scheme for solar powered wireless sensor networks was proposed. The scheme is called UD-WCMA (Universal Dynamic Weather Condition Moving Average) and it aims to improve the energy efficiency and reliability of wireless sensor networks that use solar energy as the power source. The scheme forecasts the future energy level of each sensor node using a weighted cumulative moving average method that dynamically adjusts the weights according to the uncertainty of the solar energy and the sensor node’s workload. The scheme is evaluated through simulations and experiments using real-world data. The results show that the scheme can achieve higher accuracy and lower error rate than existing schemes such as Pro-Energy [73] and WCMA [71].

4.2.3 Adaptive Methods

Adaptive models have a learning process based on historical data analysis. Contrary to statistical models, adaptive models can implicitly capture complex nonlinear relationships between weather conditions and the generated electrical energy by PV harvester. The accuracy of the forecast primarily depends on the sample size and structure of the original data utilized in constructing the model.

Methods Using Neural Networks

Methods using artificial neural networks have recently become widespread not only in solving short-term forecasting tasks for solar energy generation, but also in medium- and long-term forecasting. Artificial neural networks consist of many neurons of input, hidden, and output layers, interacting with each other. Neurons have an activation function that depends on the weight coefficients of the connections between neurons and the bias.

To get a forecast, it is necessary to train the neural network. In the process of training, the values of biases and weights are selected for each neuron so that the output signal of the neural network is as close as possible to the actual value. There are a large number of neural network training methods, which have found application in forecasting the generation of electricity by solar power plants. The advantages of neural networks are fast learning algorithms and the ability to work in the presence of noisy input signals. Compliance with the requirements for building the structure of a neural network, considering neuron redundancy and the quantity and selection of informative attributes developed for training a neural network, guarantees the network's high reliability.

Support Vector Method

The support vector method is one of the popular methodologies for learning from precedents. The support vector method belongs to the family of linear classifiers and is used in regression analysis and classification tasks. The main idea of the method is to translate vectors into a space of larger dimension and search for a separating hyperplane with the maximum gap in it. From the hyperplane separating the classes on both sides, two parallel hyperplanes are constructed. The hyperplane, which has the maximum distance between the two parallel planes, will be separating. The primary advantages of the support vector method are the ability to derive an accurate solution to the problem in the existence of incomplete and distorted data and the ability to consider a large number of additional factors affecting

the quality of forecasting. The disadvantage is the need for training and increased requirements for hardware and software resources.

The use of adaptive models for forecasting power generation is shown in works [76], [77], [78], [79]. In work [76], the application of decision trees for very short-term forecasting of power generation by a solar power plant is demonstrated. The work shows that the accuracy of the forecast using gradient boosting was 75-65%. The forecast is built 1 hour ahead. The use of a support vector machine (SVM) algorithm to classify clouds into six types based on their shape, color, and texture features extracted from total sky images was proposed [80]. The cloud classification results can be used as inputs to a PV power forecasting model.

In [77], The application of an artificial neural network, an adaptive network employing a fuzzy inference system, and a generalized neural network. The input variables for the proposed model encompass solar radiation level, ambient temperature, wind speed, and module temperature. The findings demonstrate that employing a generalized neural network yields the most favorable outcome. In [78], the authors use a radial basis function network to forecast solar energy. The input data used are measurements of power and meteorological forecasts of solar radiation, relative humidity, and temperature at the location. The feature of this work is the preliminary classification of the type of weather (sunny, cloudy, rainy) and the use of a different network structure for each class.

In [79], the use of a deep trust network is proposed for predicting solar energy generation. The input parameters for the network are data on the level of solar radiation, ambient temperature, relative humidity, and retrospective data on solar energy generation five days before the forecast. The work also showed that wind speed has little effect on solar energy generation. As a result of the work, it was shown that the model based on a deep trust network shows a better result than the model based on a neural network with backpropagation of error.

4.2.4 Hybrid Methods

Hybrid methods combine various combinations of methods from other groups. For example, combinations of physical, statistical, and adaptive models are often encountered. The application of physical models is not always justified due to the complexity of accurately accounting for certain factors, which requires the introduction of a statistical approach to their determination Statistical methods have greater precision in calculating average solar radiation values over long periods (day, month, year). However, their accuracy diminishes over shorter spans (minutes, hours) where physical conditions like

cloud cover cannot be averaged effectively within these intervals. The statistical model is adjusted to constantly changing conditions that are described by physical models to enhance hybrid models' accuracy. The authors [81] propose a novel method that combines KNN algorithm with weather classification and physical model. The method first classifies the weather into different types based on historical data, then applies KNN algorithm to find the most similar days in each weather type, and finally uses a physical model to adjust the forecast based on the current weather conditions. The simulation results show that using a hybrid physical-statistical method can improve the accuracy of solar forecasting by 10% to 20% in comparison with physical model. The work in [82] initially analyzes previous PV power plant production data to determine the technical parameters of the PV power station. The forecasting model then takes past data and estimated physical parameters into account.

Combining various methods from statistical and adaptive models is also another hybrid methods that have prospects, as they allow taking into account the specifics of the physical process and using the capabilities of adaptive methods. The methods of this group are developing, and experts find various combinations of methods that provide the necessary accuracy.

In [83], a two-stage model is used, combining the autoregressive integrated moving average model, the least squares support vector model, an artificial neural network, and an adaptive network based on a fuzzy inference system with a genetic algorithm working at the first stage. The error of the method as a result of the study was about 3.43%.

The authors [84] use ANN to model the nonlinear relationship between weather variables and PV power output. They also use an Analog Ensemble (AnEn) technique to generate multiple forecasts from different weather scenarios and select the most likely one based on similarity measures. The results show that using a hybrid AnEn + ANN model yields best results.

In [68], the authors present a short-term forecasting procedure for continuous time series using regression techniques and machine learning models. The procedure is particularly useful in situations where the number of significant independent variables depends on the interval to which the observation belongs. A multivariate regression is used to identify relationships in the time series, dividing observations into several intervals. The proposed procedure is flexible and can predict the next value of the clearness index using independent significant identified variables. The results show a significant improvement over classical dynamic regression.

4.2.5 Statistical Adaptive Methods

Table 4.1 summarizes the previous analysis of different prediction methods. Putting physical models to use in real-world scenarios can be quite difficult [62], especially when using constrained IoT devices. However, the analysis shows that, using neural networks and statical-adaptive hybrid methods gives the best forecasting results and is the most promising direction in the field of building predictive models for electricity generation. Moreover, According to the most current published research, deep learning models outperform almost all other traditional forecasting methods in terms of yielding precise and promising results for solar forecasting with the highest level of accuracy [85]. Therefore, in the coming section I discuss the different types of DL networks and their usage in solar energy prediction.

Table 4.1 - Short-term Prediction Methods and Their Accuracy

Method		**Prediction error (%)**	**Presented Models**
Physical		3-45	[39]-[41], [57]
Statistical		7-40	[42]-[51]
Adaptive		5-10	[76], [77], [78], [79]
Hybrid	**physical-statistical**	18-35	[81], [82]
	statistical-adaptive	3-9	[68], [83], [84]

4.3 Deep Learning for Short-Term Prediction

While typical ML algorithms use a relatively shallow architecture that modifies the input data only once or twice, deep learning (DL) is a novel approach that uses a deep architecture to generate exact models. Specifically, DL approaches work well in time-series analysis because the input data is changed multiple times by a linear or non-linear process, and the output is then recovered from deep architecture. The use of DL methods for solar radiation forecasting has attracted a lot of attention lately. The DL techniques that have significantly improved solar energy forecasting are given in this section.

4.3.1 Deep Neural Networks (DNNs)

While a neural network with a single layer can still make approximate predictions, additional hidden layers can help optimize the results [86]. DNN are neural networks with a certain level of complexity,

a neural network with more than two layers. These neural networks are designed to simulate the behavior of the human brain, so that it can “learn” from large amounts of data.

DNNs are typically feedforward networks in which data flows from the input layer to the output layer without looping back, as shown in Figure 4.2Table 4.2.Figure 4.2 At first, the system is trained with a lot of data. During training, the weights and biases of the network are iteratively adjusted through backpropagation. Once trained, DNNs can be used to predict outcomes based on new sets of input data [87].

Let x be the input vector, a hidden layer h_i, for $i = 1,2, \dots, n$ where n is the number of hidden layers, is calculates using the input from the previous layer (either input layer or another hidden layer). This is done using the following formula:

$$h_i = \sigma_i(W_i h_{i-1} + b_i) \tag{4.3}$$

where $\boldsymbol{W_i}$ is the weight matrix for the $i - th$ layer, b_i is the bias and σ_i is the activation function. The output y is calculated using the final hidden layer using the following formula:

$$\boldsymbol{y = \sigma_{n+1}(W_{n+1} h_n + b_{n+1})} \tag{4.4}$$

where $\boldsymbol{W_{n+1}}$ is the weight matrix for the output layer and $\boldsymbol{b_{n+1}}$ is the bias. During training, the DNN uses the error of its predictions to determine the optimal values for the weights and biases. A loss function is used to compute the error, and stochastic gradient descent or other optimization algorithms are used to update the weights and biases. Backpropagation is the process of changing the weights and biases to lower the error. Usually, a type of gradient descent is used to train the network, where the derivative of each nested function is determined in relation to its input.

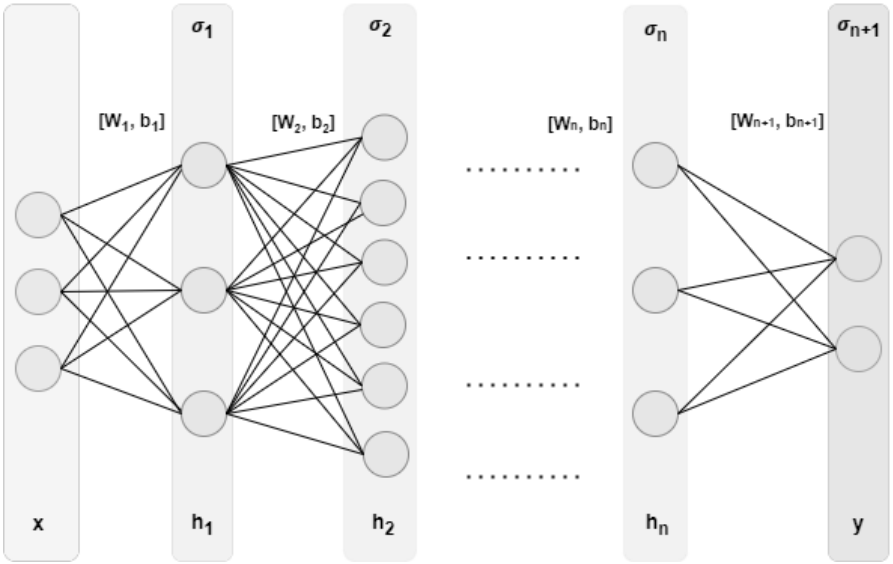

Figure 4.2 - DNN Structure

4.3.2 Recurrent Neural Networks (RNNs):

Inspired by the ANN family, Recurrent Neural Networks (RNNs) are DL-based architectures in which a link between nodes results in a graph that allows the network to exhibit dynamic activity. This makes them applicable to tasks such as unsegmented, connected handwriting recognition or speech recognition [88].

In an RNN, the information cycles through a loop. Unlike feedforward neural network, each neuron in hidden RNN layer has a recurrent connection or a recurrent edge. This loop allows information to be passed from one step in the sequence to the next, creating a form of memory, as shown in Figure 4.3. When it makes a decision, it considers the current input and also what it has learned from the inputs it received previously. Let x_t be the input vector of the input layer in RNN model, where t is the time step. The hidden layer h_t at time step t is calculated using the input at the same time step x_t and the hidden layer at the previous time step h_{t-1} using the following formula:

$$\boldsymbol{h_t = \sigma(W_{hh} h_{t-1} + W_{xh} x_t + b_h)} \quad (4.5)$$

where W_{hh} and W_{xh} are weight matrices, b_h is the bias and σ is the activation function. The output y_t at time step t is calculated using the hidden layer at the same time step. This is done using the following formula:

$$\boldsymbol{y_t = \sigma(W_{hy} h_t + b_y)} \quad (4.6)$$

where $\boldsymbol{W_{hy}}$ is the weight matrix for the output layer and b_y is the bias.

In theory, RNNs can make use of information in arbitrarily long sequences, but in practice they are limited to looking back only a few steps due to the problem known as “vanishing gradients”. The problem was explored in depth by Hochreiter [89] and Bengio, et al. [90], who found some pretty fundamental reasons why it might be difficult. This might be resolved by implementing what are known as "Long Short-Term Memory (LSTM)" networks, which include explicit memory.

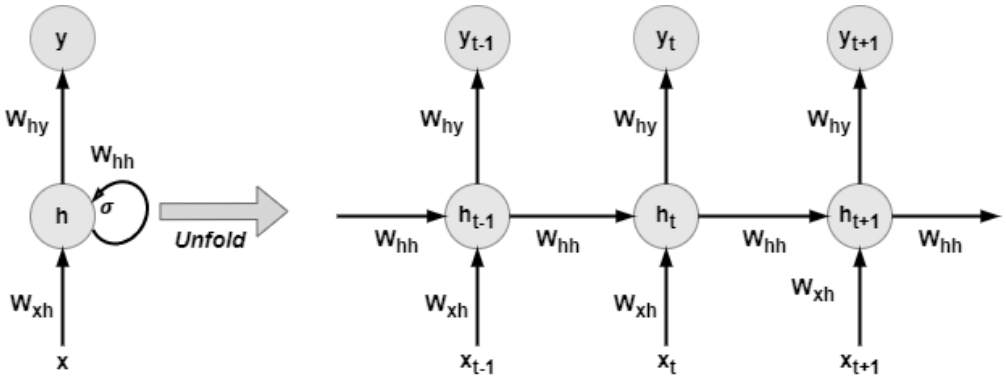

Figure 4.3 - RNN Structure

4.3.3 Long Short-Term Memory (LSTM)

They are a type of RNN capable of learning order dependence in sequence prediction problems. This is a behavior required in complex problem domains like machine translation, speech recognition, and more. LSTMs are a complex area of deep learning. It involves lots of theory and time to understand and get comfortable with [91].

Unlike traditional feedforward neural networks, LSTM has feedback connections. It can not only process single data points like image, but also entire sequences of data like video. LSTM networks are well-suited to classifying, processing and making predictions based on time series data, since there can be lags of unknown duration between important events in a time series. LSTMs were developed to deal with the exploding and vanishing gradient problems that can be encountered when training traditional RNNs. Relative insensitivity to gap length is an advantage of LSTM over RNNs, hidden Markov models and other sequence learning methods in numerous applications [92].

In order to determine whether or not the input information is meaningful, the LSTM approach incorporates a "processor" into the algorithm. The processor item that has all of the features of LSTM

modules is called a "cell", as shown in Figure 4.4. Determining what data from the cell state will be discarded is the first stage in the LSTM. The "forget gate layer" is a sigmoid layer that makes this determination. It looks at h_{t-1} and x_t and outputs a number between 0 and 1 for each number in the cell state C_{t-1}. A 1 denotes "keep this completely," whereas a 0 denotes "get rid of this completely." This can be expressed mathematically as:

$$f_t = \sigma\left(W_f . [h_{t-1}, x_t] + b_f\right) \tag{4.7}$$

where $\boldsymbol{W_f}$ and $\boldsymbol{b_f}$ are the weights and biases for the forget gate layer, the dot represents the dot product operation and $[h_{t-1}, x_t]$ represents the concatenation of the vectors h_{t-1} and x_t. Choosing the new data to be stored in the cell state is the next stage. There are two components to this. First, the values to be updated are selected via a sigmoid layer known as the "input gate layer." A vector of fresh candidate values is then produced by a hyperbolic tangent activation function (tanh) layer, $\check{C}_t$, that could be added to the state. I combine these two components to produce a state update in the following step. In terms of math, this is expressed as:

$$i_t = \sigma(W_i . [h_{t-1}, x_t] + b_i) \tag{4.8}$$

$$\check{C}_t = tanh(W_C . [h_{t-1}, x_t] + b_C) \tag{4.9}$$

$$C_t = f_t * C_{t-1} + i_t * \check{C}_t \tag{4.10}$$

where C_t is the new candidate values, scaled by how much I decided to update each state value, $\boldsymbol{W_i}$ and $\boldsymbol{b_i}$ are the weights and biases for the input gate layer and $\boldsymbol{W_C}$ and $\boldsymbol{b_c}$ are the weights and biases for the tanh layer.

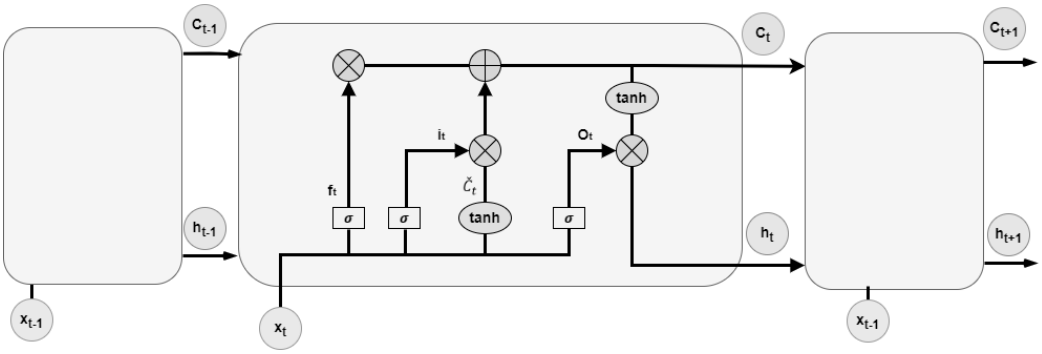

Figure 4.4 - LSTM Cell Structure

Lastly, I have to select the output to be generated. Cell state will serve as the basis for this output, which will be filtered. To determine which portions of the cell state to output, I first run a sigmoid layer. Next, in order to output only the portions, I multiply the cell state by the sigmoid gate's output after running it through tanh (which pushes the values to be between -1 and 1). This is expressed mathematically as:

$$o_t = \sigma(W_o.[h_{t-1}, x_t] + b_o) \tag{4.11}$$

$$h_t = o_t * tanh(C_t) \tag{4.12}$$

where W_o and b_o are the weights and biases for the output gate layer.

4.3.4 Convolutional Neural Networks (CNNs)

Convolutional Neural Networks (CNNs) are a cutting-edge method in the field of deep learning (DL) that may uncover hidden structures and information inside a dataset in addition to its conceptual properties. Because of the shared-weight architecture of the convolution kernels or filters, which slide along input features and produce translation equivariant responses known as feature maps, they are also referred to as shift invariant or space invariant artificial neural networks. They have applications in image and video recognition, recommender systems, image classification, medical image analysis, natural language processing, and financial time series [93].

Like a typical multilayer neural network, CNNs are made up of one or more convolutional layers, followed by one or more fully linked layers, as shown in Figure 4.5. The input layer to the CNN is a matrix x, which could be an image or a feature map from a previous layer. A collection of learnable filters, or kernels, K, are applied to the input by the convolutional layer C. To create a feature map, each filter is convolved across the input's width and height (also known as an activation map). This is done using the following formula:

$$C_{i,j} = \sum_{m,n} x_{m,n} . K_{i-m,j-n} + b \tag{4.13}$$

where the sum of the values is over the kernel's spatial extent, and b represents the bias. The result is a feature map that represents the filter's responses at each spatial position. The feature maps are subjected to a nonlinear function by the activation layer. Usually, this is the element-wise application of the Rectified Linear Unit (ReLU) function:

$$A_{i,j} = \max(0, C_{i,j}) \tag{4.14}$$

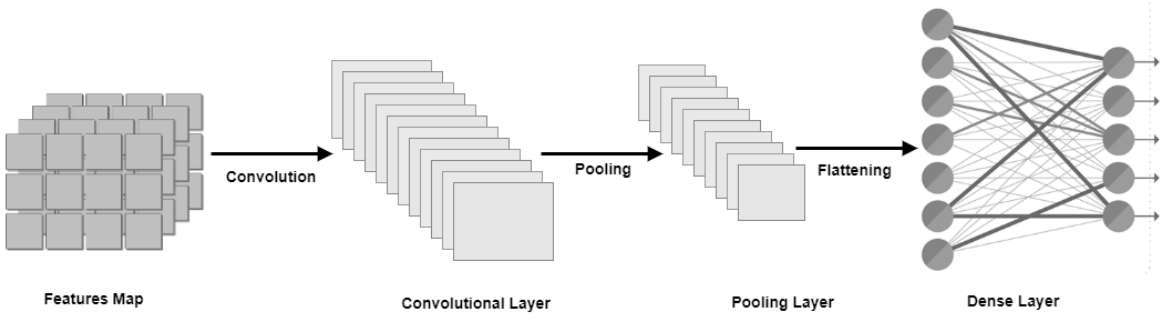

Figure 4.5 - CNN Structure

To minimize computational complexity, control overfitting, and reduce spatial dimensions, the feature maps are down sampled by the pooling layer. Max pooling is a popular method that takes the maximum value of each subregion (such as 2x2-pixel tiles) extracted from the feature map and discards all other values:

$$\boldsymbol{P_{i,j}} = \max_{\boldsymbol{m,n}} \boldsymbol{A_{m,n}} \tag{4.15}$$

The CNNs uses fully connected layers to do high-level reasoning after multiple convolutional, activation, and pooling layers. As observed in typical neural networks, neurons in a completely linked layer have complete connections to all activations in the preceding layer. As a result, their activations can be calculated using matrix multiplication and bias offset.

Related Work

The authors [94] propose a model to forecast day-ahead solar irradiance using only weather data, such as temperature and humidity, without historical solar irradiance data. They use a deep LSTM-RNN to learn the nonlinear relationship between the weather data and the solar irradiance. They use six datasets from four different countries with diverse climate types and compare their model with FFNN and persistence models. They use RMSE, MAE, and forecast skill as performance metrics. They also simulate a one-year operation of a commercial building microgrid to demonstrate the usefulness of their model. They achieve an average RMSE of $60.31\ W/m^2$ across the six datasets and show that LSTM-RNN outperforms FFNN and persistence models. They also show that their model increases the annual energy savings by 2% compared to FFNN.

The authors [95] proposes a hybrid deep learning method that combines the clustering techniques, CNN, LSTM, and attention mechanism with the wireless sensor network to overcome the existing difficulties of the PV energy generation forecasting problem. Their proposed method consists of three stages: clustering, training, and forecasting. In the clustering stage, correlation analysis and self-organizing mapping are employed to select the highest relevant factors in historical data. In the training stage, a CNN, LSTM, and attention mechanism are combined to construct a hybrid deep learning model to perform the forecasting task. In the testing stage, the most appropriate training model is selected based on the month of the testing data.

A combined approach utilizing CNN and LSTM network is proposed for predicting the thermal power of a solar power tower system, referred to as "Solar Two" in [96]. For this study, three distinct models were constructed: a standalone LSTM model, a standalone CNN model, and a combined CNN-LSTM model. These models were built for different seasons within a year. The combined CNN-LSTM model demonstrated superior performance, yielding a Root Mean Square Error (RMSE) of $5.061\ MWt$. This approach resulted in a 2.154% improvement in RMSE, a 5.503% improvement in MAE, and a 1.324% improvement in RMSE, and a 2.995% improvement in MAE when compared with the standalone CNN and LSTM models.

The authors [97] present a scheme for predicting the amount of solar radiation that reaches the earth's surface in different time horizons (3/6/24 hours ahead) using a deep learning model. The model uses LSTM to capture the dependence between hours of the same day and other variables such as direct horizontal irradiance, direct normal irradiance, relative humidity, dew point, temperature, wind speed, and wind direction. The model is applied to forecast solar radiation for four locations in the Thar desert region of Rajasthan, India. The model is optimized in terms of number of neurons and is evaluated using standard statistical indicators: RMSE and MAPE. The results show low values of RMSE and MAPE, indicating the efficacy of the proposed model.

The authors [98] propose a deep learning model based on LSTM networks for short-term forecasting of global horizontal irradiance (GHI), a proxy for solar energy. The authors investigate four design choices for LSTM, such as pre-processing, temporal order, batch size, and prediction horizon, and how they affect the forecasting performance. The authors use data from three solar stations in India across two climatic zones and two seasons. They compare their LSTM model with three recent benchmark methods based on random forest, RNN, and LSTM, respectively. They find that their LSTM model outperforms the benchmark methods in terms of forecasting accuracy. They also provide some

recommendations for better LSTM design, such as using raw data, preserving temporal order, choosing appropriate batch size, and considering input data variability.

The authors in [99] expanded upon the work of [100] by integrating Photovoltaic (PV) output data with sky images into a unified network to predict solar PV values 15 minutes ahead, averaged minute-wise. The input sky images were collected using the FSH-EYE camera installed at Stanford University, and the PV-based data was collected using poly-crystalline panels located at the Jen-Hsun Huang Engineering Center, Stanford's, for a one-year period between 1st March 2017 and 1st March 2018. The performance of the proposed model was evaluated by comparing it with the model in [100], an autoregressive model, two models developed using clear sky index values as inputs, a model built with PV data, a model developed with sky images input, and a persistence model that assumes constant clear sky index values and applies them as input. The proposed model demonstrated significantly superior performance with a forecast skill of 15.7% and a RMSE of 2.51. This indicates that the proposed model outperformed the other models in terms of both forecast skill and RMSE.

The authors [101] present a method for predicting the power output of a solar photovoltaic (PV) system in Cyprus using a single-layer LSTM model. The network uses only historical PV production data as input and forecasts up to 1.5 hours ahead. The performance of their single-layer LSTM network was tested using various metrics such nRMSE, mean bias error (MBE), and MAE. They also compare their model with a more complex 5-layer LSTM network that was previously developed using the same data. The single-layer LSTM model achieved an nRMSE of 10.7%, which is similar to the 5-layer LSTM network and lower than most of the published models for solar forecasting.

In an attempt to identify seasonal trends and diurnal patterns throughout time, the authors in [102] The first model, LSTM-1, is engineered to comprehend both short-term and long-term patterns of PV power outputs. The second model, LSTM-2, is constructed using meteorological data, excluding any information pertaining to seasonal factors. The dataset for this study was procured from a PV operator in Gumi, South Korea, spanning a period of 39 months from June 1, 2013, to August 31, 2016. The proposed LSTM-1 model was juxtaposed with an ANN, two Deep Neural Network models (DNN, DNN2), and ARIMA, S-ARIMA, and LSTM-2 models for comparison. Upon evaluation based on seasons, the LSTM model exhibited superior accuracy with a Root Mean Square Error (RMSE) of 0.563 for the summer season.

The recent studies that use deep learning models, especially LSTM networks, to forecast solar energy generation or irradiance were introduced in Table 4.2. The studies use different datasets, methods, and

performance metrics to evaluate their models. The study shows that LSTM and CNN networks are able to capture the complex and nonlinear relationship between solar energy and various factors, such as weather, time, and location. LSTM networks also outperform other models, such as FFNN, ARIMA, and persistence models, in terms of forecasting accuracy.

Table 4.2 Solar Power Prediction Works Using Deep Learning

Reference	**Input parameters**	**DL architecture**	**Performance**
[94]	dry-bulb temperature, dew point temperature, relative humidity, hour of the day and the month of the year	LSTM and RNN	RMSE: $60.31\ W/m^2$
[95]	Alternating Current 2 (AC2)	CNN and LSTM	(Time Interval: 30 min) RMSE: 2.04 MAPE: 32.39 MAE: 1.38
[96]	Atmospheric pressure, Global Horizontal Irradiance (GHI), Direct Horizontal Irradiance (DHI), Direct Normal Irradiance (DNI), wind speed, wind direction, global tilted irradiance, relative humidity, ambient temperature, sun altitude angle, and sun azimuth angle.	CNN and LSTM	RMSE: $5.061\ MWt$ MAE: $2.871\ MWt$

[97]	Global Horizontal Irradiance, temperature, relative humidity, wind direction, dew point, Horizontal Irradiance (DHI) and Direct Normal Irradiance (DNI),	LSTM	(3-hour forecasting) RMSE: 0.099 MAE: 4.54%
[98]	Solar irradiation data	LSTM	In winter: nRMSE: 0.023,0.021, 0.027
[99]	Sky images	CNN	RMSE: 2.51
[101]	Energy production data from a single PV system	LSTM	RMSE: 10.7%
[102]		LSTM	RMSE: 0.563

4.4 Prediction Algorithm

In this section I conduct a deep analysis of the dataset that provide historical data of a solar panel with temperature, wind and irradiance sensors. Then I develop a prediction algorithm using deep learning method. To improve the accuracy of developed model, I combine a statistical method with the developed model to remove the noise and reduce the prediction error.

4.4.1 Dataset Analysis

The dataset contains the 8 different features. They were collected every one hour from 2005-01-01 to 2020-12-31 from Photovoltaic Geographical Information System database [35]. To gain insights into the data trends and understand the impact of various features on the system power, I conducted a comprehensive analysis. The features are:

- P: PV system power (W)
- Gb(i): Beam (direct) irradiance on the inclined plane (plane of the array) (W/m2)
- Gd(i): Diffuse irradiance on the inclined plane (plane of the array) (W/m2)
- Gr(i): Reflected irradiance on the inclined plane (plane of the array) (W/m2)
- H_sun: Sun height (degree)
- T2m: 2-m air temperature (degree Celsius)
- WS10m: 10-m total wind speed (m/s)
- Int: 1 means solar radiation values are reconstructed

I plotted the harvested power and other features for January 2015. In Figure 4.6, I present the power, solar irradiance and sun height. My analysis reveals that higher values of irradiance (Gb(i), Gd(i), and Gr(i)) are generally associated with increased system power output. This finding suggests that solar irradiance plays a crucial role in determining the amount of harvested power. Interestingly, I observed that sun height values exhibit a periodic pattern without a direct effect on the harvested power. Thus, sun height does not directly impact power generation and I will not consider it for predicting the solar energy.

In, the power, temperature, and wind speed features are presented. The Int feature is consistently zero and will not be taken into account during the prediction process. Both temperature and wind speed have an impact on the harvested power. Any alteration in the power is accompanied by corresponding changes in the temperature and wind speed. Based on this analysis, the solar irradiance, temperature,

and wind speed (Gb(i), Gd(i), Gr(i), T2m, WS10m) will be considered as potential factors in predicting the solar power.

In Figure 4.7 the context of solar power generation, seasonality refers to the predictable and recurring fluctuations in solar power output that occur within each year. These fluctuations can be attributed to various factors such as the angle of the sun, length of the day, and weather patterns, which all follow a seasonal cycle. To capture this seasonality, I utilized the Fast Fourier Transform (FFT) to analyze the system power values denoted as P. This transformation is critical as it enables us to identify the dominant frequencies in the used dataset, which essentially represent the main cycles or patterns in the used data. The results of this transformation are visually represented in Figure 4.8. It is evident that the dominant frequency occurs at the daily level. This observation is of significant importance as it suggests a strong daily cycle in the harvested power values. This study implies that the power values that were harvested during the previous 24 hours may be a good indicator of the power value that would be generated in the next hour.

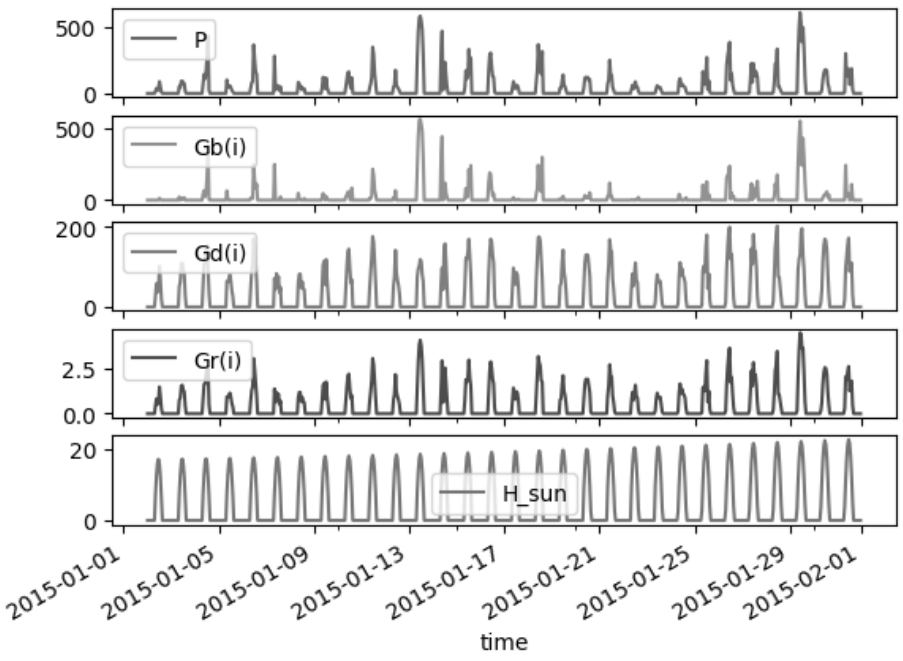

Figure 4.6 - Harvested Power, Sun Irradiance and Height Values in January, 2015

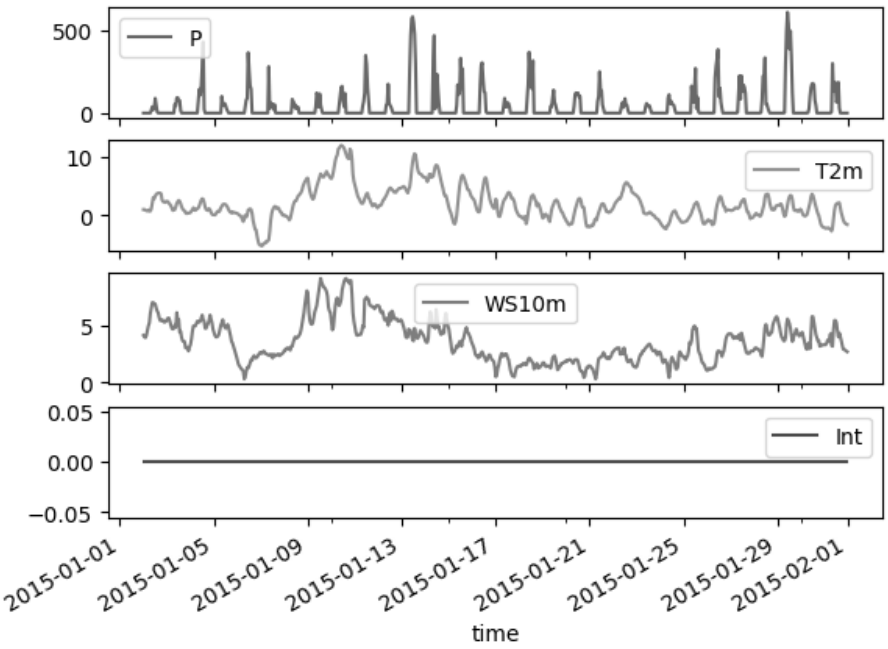

Figure 4.7 Harvested Power, Temperature, Wind Speed and Int Values in January, 2015

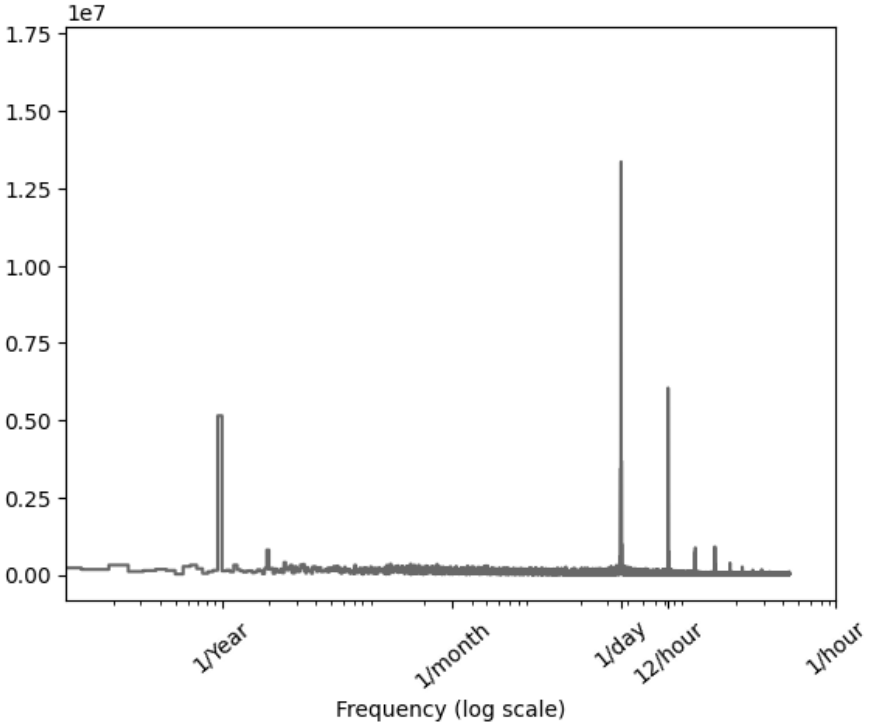

Figure 4.8 - Dominant Frequencies pf Power Values

Data preparation

Based on the previous analysis, the solar irradiance, temperature, and wind speed are the suitable features that can be used to predict the solar power, in addition to the daily frequency. In the context of machine learning, particularly when training neural networks, feature scaling is a crucial preprocessing step. This involves adjusting the range of the data to ensure consistency and to prevent certain features from dominating others due to their scale. Normalization is a commonly used feature scaling technique. It involves transforming the features such that they have a mean of 0 and a standard deviation of 1. Figure 4.9 shows the different features value after normalization step.

Based on the dominant daily frequency, I predict the solar power of the next hour based on the past 24-hourly observations. I apply a data windowing process to create windows of the dataset, where each window contains a consecutive sequence of data points. The input width of each window is 24 and the label width is 1. Each time step in the input contains the values of different features. I make the windowing process dynamic so that I can select which features to include in the input. The label, which is the expected output, is the actual power value of the 25-th time step. The windowing process is illustrated in Figure 4.10, that does not show the features axis of the data.

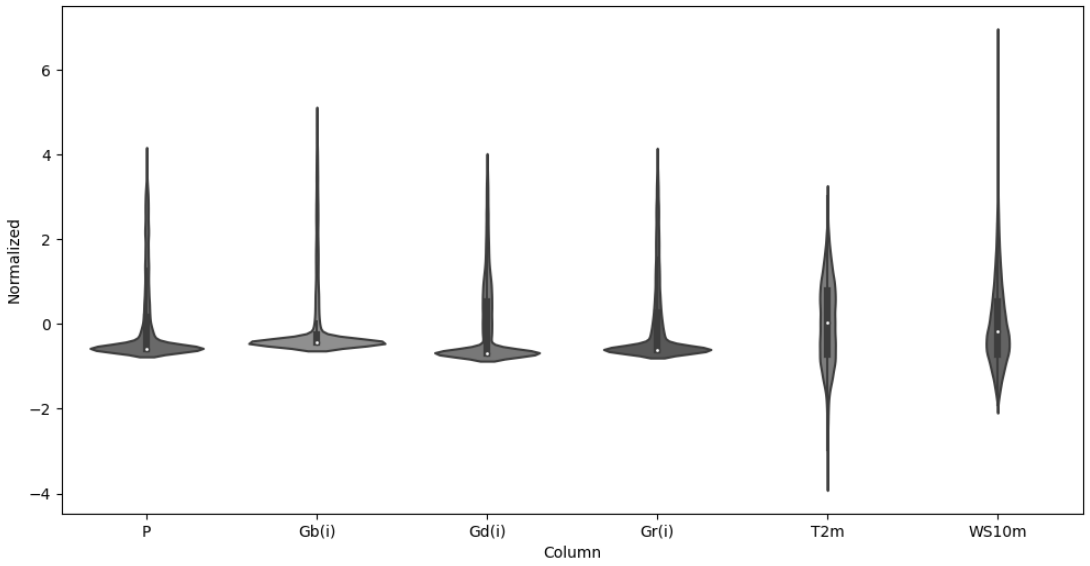

Figure 4.9 - Normalized Features

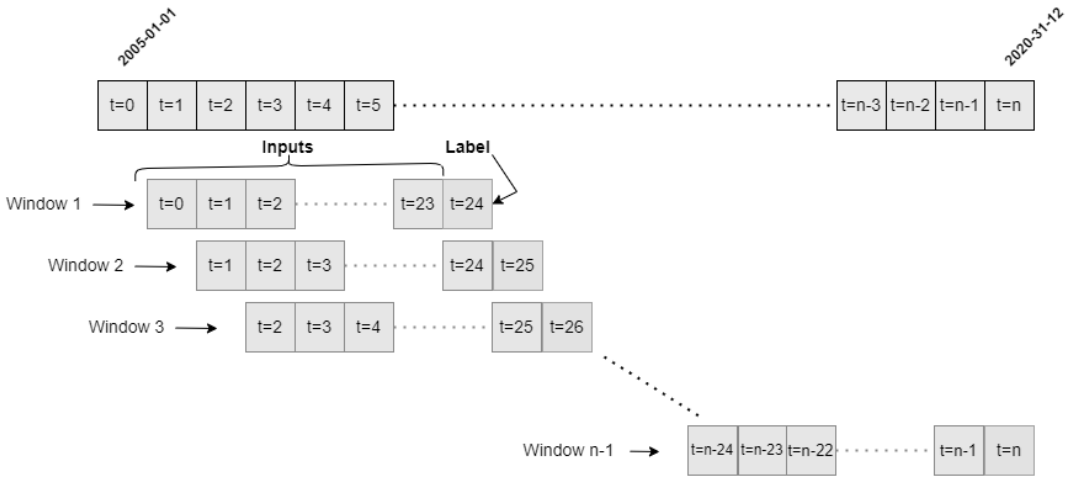

Figure 4.10 - Windowing Process

4.4.2 DL Model

Three distinct types of DL have been employed to forecast the solar power for the subsequent hour as follows:

1. DNN model, which comprises four layers: an input layer with 24 units, two hidden layers with 48 and 24 units respectively, and an output layer with a single output unit. ReLU activation function was used for all layers.

2. LSTM model, which consists of two layers: a recurrent layer housing the actual LSTM cells with 32 filters, and a fully connected layer that outputs a single continuous value.

3. The CNN with 32 filters (CNN32) model, which includes a single convolutional layer with 32 filters, followed by a fully connected layer consisting of 32 neurons. The output layer consists of a single neuron that contains the predicted solar power.

The three models utilize the windows of 24 hours of the features values from the windowing process to predict the value of the label (the power). The performance of the models was assessed by training them on various sets of input features, which are: 1) Beam (direct) irradiance Gb(i), 2) Diffuse irradiance Gd(i), 3) Reflected irradiance Gr(i), 4) air temperature T2m, 5) wind speed WS10m, 6) Beam (direct) irradiance and air temperature Gb(i)+T2m, 7) Diffuse irradiance and air temperature Gd(i)+T2m, 8) Reflected irradiance and air temperature Gr(i)+T2m, 9) all features. Each set of features represents a

different perspective of the data, and training the models on these diverse sets allows us to understand which features are most informative for the prediction task.

After training, the models' predictions were compared to the actual values in the validation and test subsets. Two metrics were used to quantify the performance of the models: the Mean Squared Error (MSE) and the Mean Absolute Error (MAE). The Mean Squared Error (MSE) is calculated as follows:

$$\mathbf{MSE} = \frac{\mathbf{1}}{\boldsymbol{n}}\sum_{\boldsymbol{i=1}}^{\boldsymbol{n}}(\boldsymbol{y_i} - \widehat{\boldsymbol{y}_i})^{\mathbf{2}} \tag{4.16}$$

where n is the number of observations, y_i is the actual value of the $i-th$ observation and $\widehat{y_i}$ is the predicted value of the $i-th$ observation. The MSE measures the average of the squares of the errors, that is, the average squared difference between the estimated values and the actual value. The Mean Absolute Error (MAE) is calculated as follows:

$$\mathbf{MAE} = \frac{\mathbf{1}}{\boldsymbol{n}}\sum_{\boldsymbol{i=1}}^{\boldsymbol{n}}(\boldsymbol{y_i} - \widehat{\boldsymbol{y}_i}) \tag{4.17}$$

The MAE measures the average of the absolute differences between the predicted and actual values. It provides a linear score, meaning all individual differences are weighted equally. By collecting these metrics for the validation and test subsets, I can objectively evaluate and compare the performance of the models trained on different feature sets.

The MAE and MSE for validation and test subsets for different input groups using the aforementioned models are presented in Figure 4.11, Figure 4.12, and Figure 4.13. I observe that, DNN model has the highest error values (MAE≈0.8, MSE≈1.0) for all features sets. However, only for all features set, MSE of DNN model is about 0.3. LSTM model has the same value for MAE and MSE and it approximately equals 0.3. Only for WS10m, LSTM model performs better than the other features sets and the error values for both MAE and MSE equals 0.32. The CNN32 model demonstrated the lowest error values and performed almost equally well for all input groups, where MAE is between 0.16 and 0.18, and MSE is between

0.13 and 0.14. Therefore, the CNN neural network was deemed the most suitable for solar power prediction in this research. The performance of the CNN32 is observed to be approximately uniform across all feature sets, making the selection of a specific feature set for prediction non-trivial. The prediction of solar power output necessitates the provision of the preceding 24-hour data of input

features to the model. This data can be acquired via sensor devices. Given the cost-effectiveness and ease of deployment of thermal sensors in comparison to wind or irradiance sensors, particularly in the context of small Internet of Things (IoT) devices, temperature was chosen as the primary feature to be input into the CNN models for the prediction of solar power output.

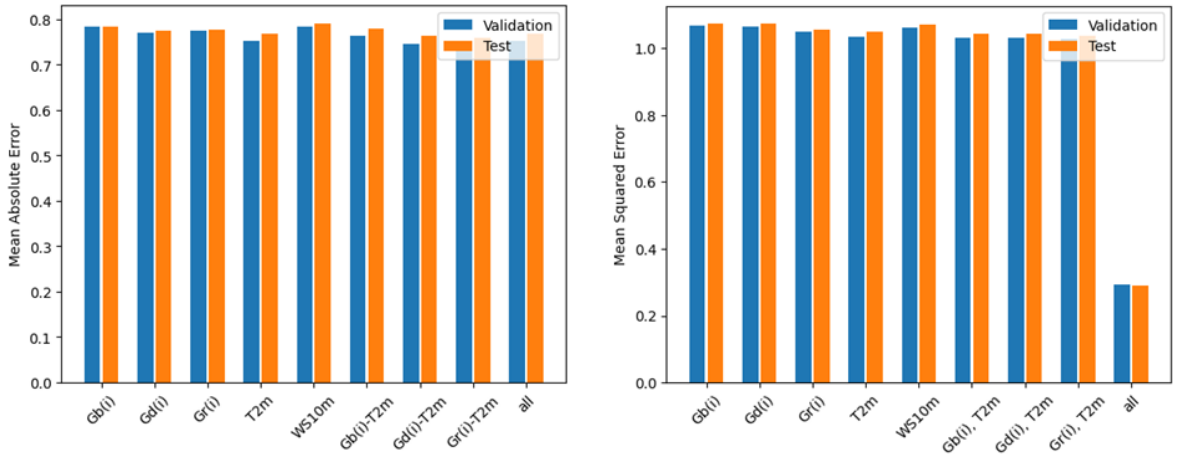

Figure 4.11 MSE for DNN Model with Different Features as Input

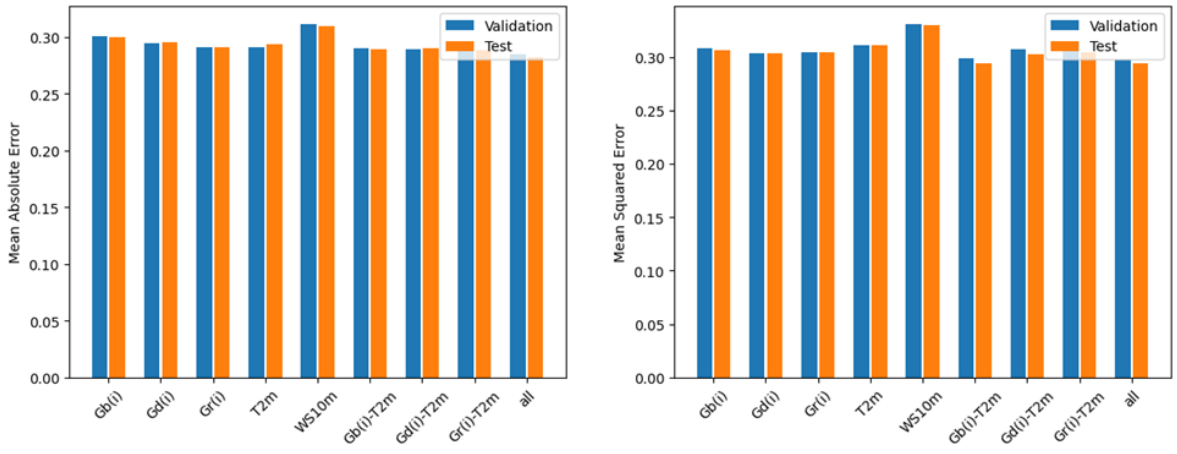

Figure 4.12 MAE and MSE for LSTM Model with Different Features as Input

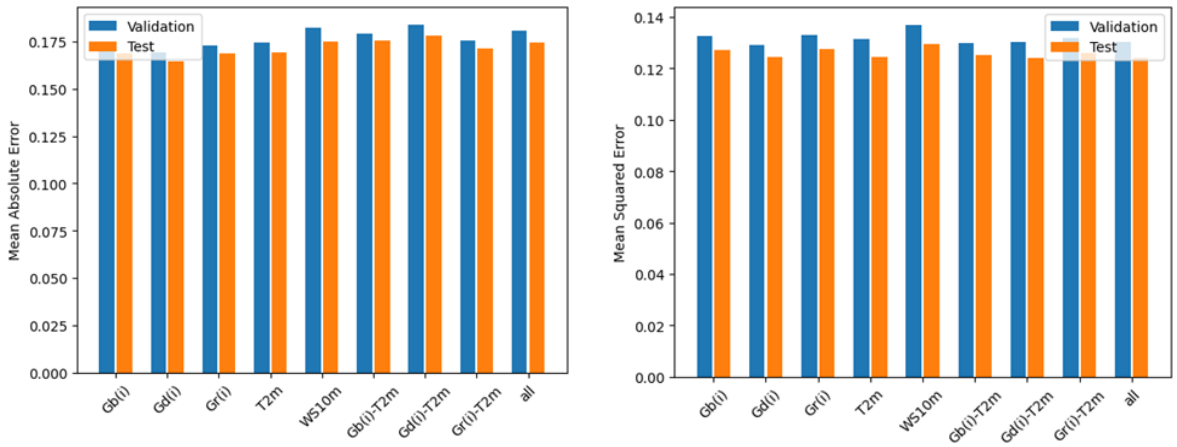

Figure 4.13 MAE and MSE for CNN Model with Different Features as Input

Model Performance to Complexity Comparison

In the context of deploying a neural network model on an Internet of Things (IoT) device, the model's size becomes a pivotal consideration due to the typically constrained storage capacity of such devices. Consequently, it is crucial to strike an optimal balance between the model's accuracy and its size. The size of DL models is contingent upon the number of hidden layers and neurons within each layer. Therefore, while a complex model structure may augment its size, it does not necessarily guarantee an enhancement in its accuracy. **CNN32** model has 32 filters in the convolutional layer followerd by a fully connected layer with 32 neruos. Thus, the size of CNN32 model approximately equals 10 KB which consider large for deployment in IoT devices.

An exhaustive investigation was undertaken to ascertain the trade-off between the accuracy and size of CNN models. A multitude of CNN models were trained exclusively using the temperature feature, each comprising a single convolutional layer succeeded by a fully connected layer. The quantity of filters in the convolutional layer and neurons in the fully connected layer are enumerated in Table 4.3, in conjunction with the sizes of the models. To juxtapose these diverse CNN models, the MAE and MSE for validation and test subsets were collected. Figure 4.14 and Figure 4.15 delineate the results of the training and testing phases. It is observed that even the CNN1 model outperforms the (LSTM model with 32 cells, thereby bolstering the credibility of my choice to utilize CNN. Additionally, it is noted that the error escalates with a reduction in model complexity, which is an anticipated outcome. However, excluding the CNN1 model, the disparity in MAE and MSE values between different models is not substantial.

Table 4.3 - Number of Filters and Neurons in CNN Models with their Size

Name	Filters number	Neurons	Size (kB)
CNN32	32	32	10.209
CNN16	16	16	4.913
CNN8	8	8	2.457
CNN4	4	4	1.277
CNN3	3	3	0.987
CNN2	2	2	0.699
CNN1	1	1	0.413

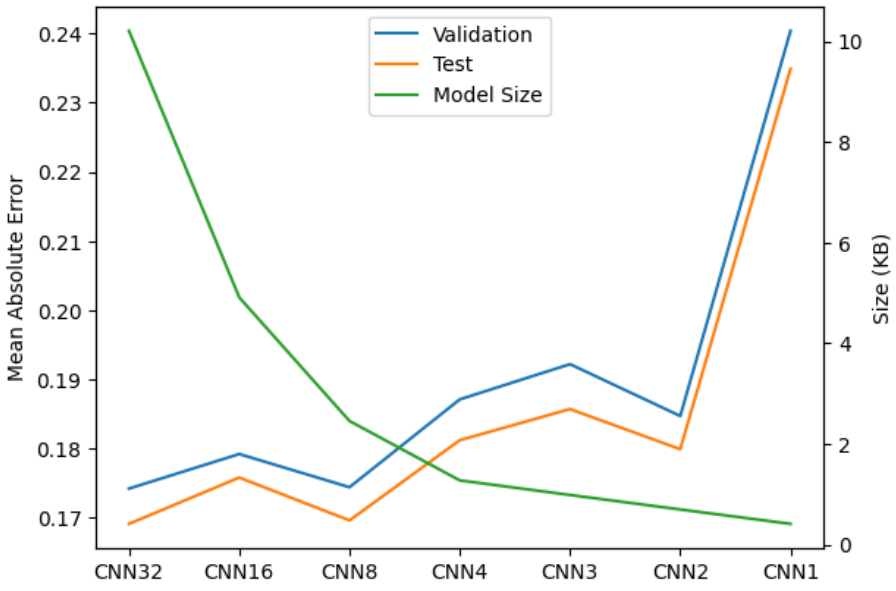

Figure 4.14 – Validation and Test MAE Versus Model Size for Different CNN Models

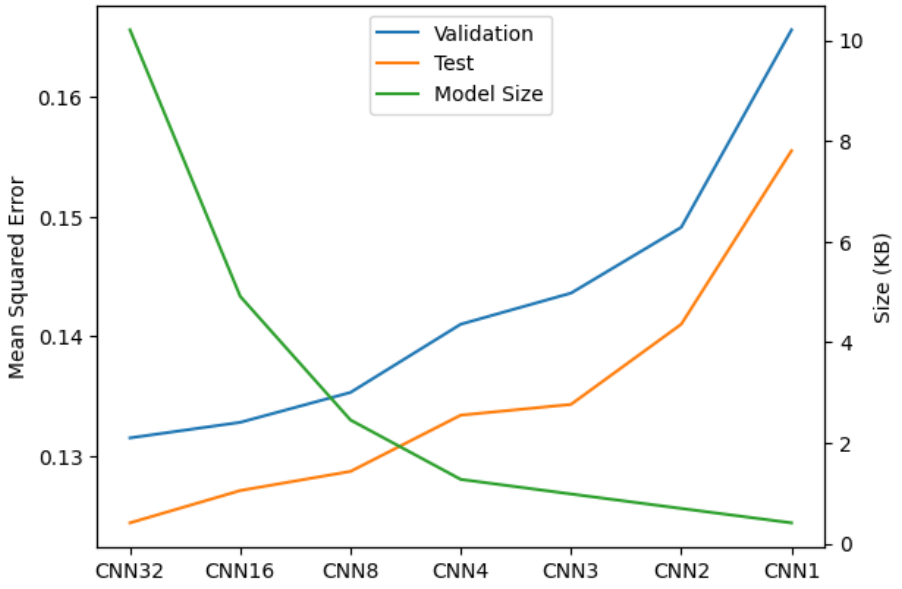

Figure 4.15 - Validation and Test MSE Versus Model Size for Different CNN Models

In the domain of model precision and complexity, Figures 14 and 15 demonstrate the compromise between these two parameters. These figures depict the model's complexity in relation to MAE and MSE. Both figures substantiate that the ideal balance is attained using the CNN4 or CNN8 models. A more detailed scrutiny of Figure 13 indicates that the CNN2 model exhibits similar performance to the CNN4 model when the model's complexity is halved relative to the CNN4 model. Therefore, I advocate for the use of CNN2, CNN3, and CNN4 models as the most effective solutions to alleviate the conundrum between model complexity and its accuracy. The finial selection of the best suitable model depends on the IoT device capability.

Model Prediction Analysis

In the predictive analysis, the CNN2 model was utilized to forecast solar power generation over a specific timeframe. An analysis of the predicted versus actual solar power values is presented in Figure 15. It is observed that the model predicts non-zero power values during periods where the actual power is zero. Two instances are highlighted in Figure 4.16 in yellow boxes. The model predicted a power value of 9.8 at 9 pm on the evening of February 14, 2005, while the actual value is zero due to the absence of sunlight. Similarly, the predicted value at 2 am on the morning of February 16, 2005, was 5.0. This discrepancy can be attributed to the model's inability to account for periods of nighttime when solar power is inherently zero. To address this prediction error, I propose integrating an additional statistical model that would determine whether the solar power should be zero based on parameters such as hour, day, and month. This approach aligns with the use of hybrid models in solar power prediction,

which have been found, Table 4.3 in my analysis, to be effective in balancing model stability with accuracy.

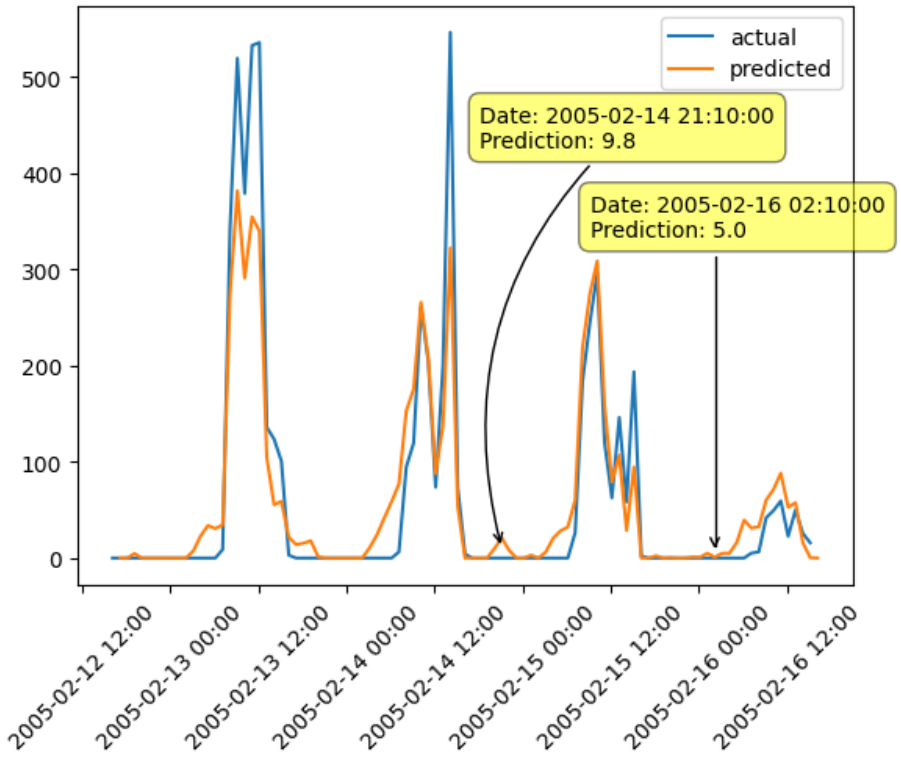

Figure 4.16 - CNN2 Model Prediction Results vs Actual Values over a Specific Timeframe

4.4.3 Hybrid Prediction Algorithm

For the used dataset, I want to classify the power values into two classes: class 1, indicating that the power value is zero, and class 2, indicating a non-zero power value. I extracted the hour, day, month values to construct the input of the classification model. Two statistical classification models, namely logistic regression and decision tree (Random Forest), were trained to predict the power class based on the hour, day, month values. The accuracy of the two classification models on the train and test subsets is shown in Table 4.4. Based on the accuracy results, the developed random forest model, with test accuracy equals to 0.992 is chosen to be used as a classifier. Logistic Regression model performs well during the training phase, but its test accuracy is very low ≈ 0.41.

Table 4.4 - Train and test accuracy of Logistic Regression and Random Forest classifiers

Classification Model	**Train Accuracy (%)**	**Test Accuracy (%)**
Logistic Regression	0.992	0.41
Random Forest	0.993	0.992

A hybrid algorithm, Figure 4.17, is constructed by integrating the developed Random Forest classifier with CNN2 model. The classifier is initially employed to predict the class of the power, given the values of the hour, day, and month of the time slot. If the classifier yields a class of 1, a zero value is returned as the power value. Conversely, if the classifier yields a class of 2, the CNN2 model is invoked to predict the solar power using the past 24 hourly-values of temperature and harvested solar power. This approach significantly reduces the computational and energy costs associated with invoking the CNN2 model during nighttime when the power value is zero. Furthermore, the hybrid model effectively eliminates noise in the final output (predicted power). Figure 4.18 presents a comparison between the predicted and actual values of solar power using the hybrid algorithm for the same time period as depicted in Figure 4.16. It is observed that the actual and predicted values are both zeros during nighttime, and the noise in the prediction is removed.

To calculate the reduction in prediction error between the CNN2 model alone and the hybrid algorithm, I applied the hybrid algorithm on the validation and test subsets and calculated MAE and MSE values. The results, Table 4.5 shows that the error reduction is about 7% for MAE and 3.5% for MSE.

Table 4.5 - Error Reduction Using Hybrid Algorithm in Comparison with CNN2 Model

Model	**MAE**		**MSE**	
	Validation	**Test**	**Validation**	**Test**
CNN2	0.1847	0.1799	0.1491	0.1410

Hybrid Algorithm	0.1747	0.1742	0.1366	0.1362
Error Reduction	6.5%	3.2%	8.4%	3.5%

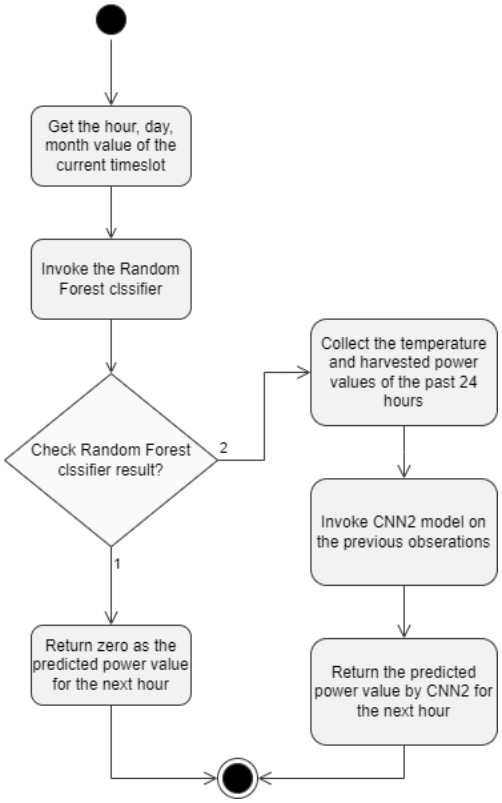

Figure 4.17 - Hybrid Prediction Algorithm

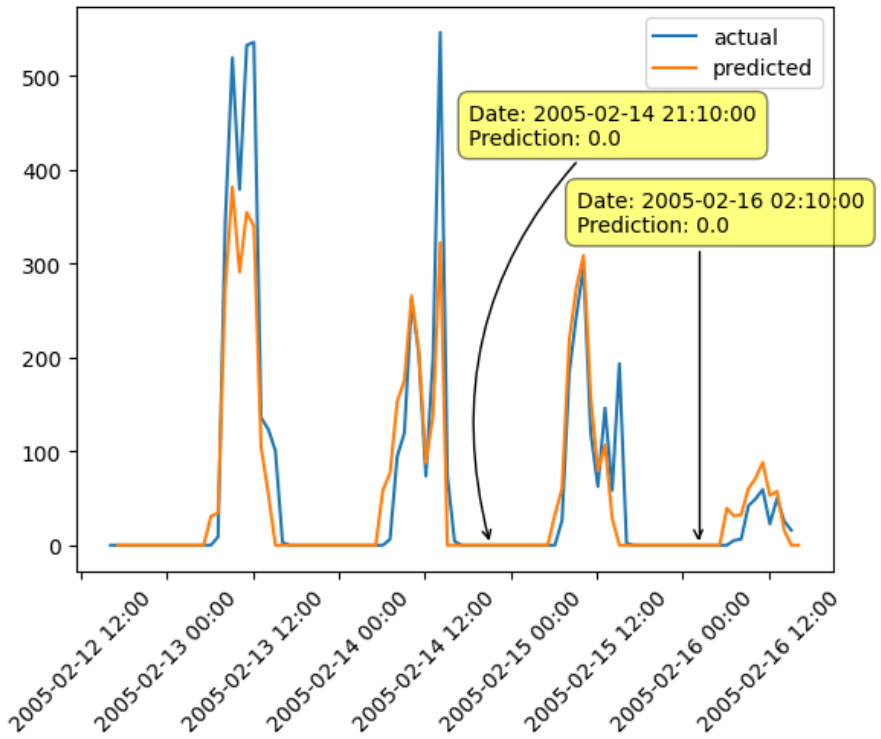

Figure 4.18 - Hybrid Algorithm Prediction vs Actual Values over a Specific Timeframe

Conclusion

I conducted a thorough analysis of photovoltaic energy forecasts using multiple models and approaches. I focused on the common approaches to solar energy forecasting over the short term, including physical, statistical, adaptive, and hybrid approaches, and their advantages and disadvantages. The analysis showed that using machine learning techniques alone or in combination with statistical techniques produces models that are more accurate and have less error than other approaches.

I studied the effectiveness of deep learning techniques in solar energy forecasting, including Deep Neural Networks (DNN), Recurrent Neural Networks (RNN), Long Short-Term Memory (LSTM), and Convolutional Neural Networks (CNN). In order to improve the CNN model's precision and effectiveness, I suggested a hybrid approach that combines a Random Forest classifier with a CNN model. The results showed that the hybrid approach reduced errors by about 7% when compared to the CNN model used alone. In addition, I performed a thorough model analysis to optimize the CNN model size while maintaining its performance, making it appropriate for Internet of Things (IoT) device deployment.

5 WSN'S QUALITY OF SERVICE

5.1 Quality of Service in Wireless Sensor Networks

Quality of Service (QoS) can be scientifically articulated as a collection of service criteria that must be met during the transmission of a packet from its origin to its endpoint. This concept is synonymous with the networking QoS facet, which necessitates the underlying network to offer a suite of service attributes. These attributes include parameters such as jitter, latency, bandwidth, and packet loss, which are essential for assessing the quality of the service provided. Figure 5.1 illustrates the two main QoS perspectives: Network QoS and Application QoS [103]. According to this paradigm, the network must offer the necessary service quality for the application and users. The network layer then maximizes network resource usage while supplying the necessary QoS level; additionally, the network assesses application requirements and implements a variety of network QoS techniques.

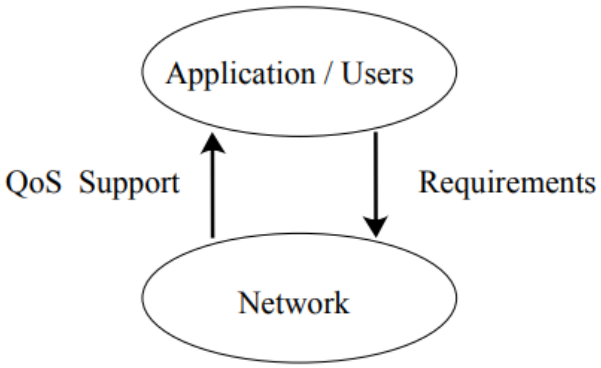

Figure 5.1 - QoS Model

A wireless IoT device is placed in an environment to keep an eye on a physical phenomenon, gather information, run light processes and transmit processed or raw data to a specific location. A large number of IoT device can be deployed in the environment in WSN network that play a central role in achieving the goal of smart environments. WSNs face communication difficulties due to a variety of factors, including low bandwidth, high node density, low energy devices, small power transceivers' capacity to sense, hardware constraints, and computing power [104]. WSNs should have a simplified architecture to reduce the impact of communication. As a result, most WSNs are built using a single

hop topology since multi-hop architecture, Figure 5.2, places a lot of demands on the bandwidth and routing protocol [105].

Strict QoS requirements for emerging WSNs include availability, integrity, timeliness, and high reliability. A WSN's capacity to meet these QoS demands is what defines its competence. Particularly in situations involving real-time situations, the speed and degree of reliability of data transferred between sensors and the control station are critical. The randomness of the communication channel, collisions, congestion, and interference all have an impact on how reliable WSNs are. The following are some of the main factors that must be addressed to enable efficient communication:

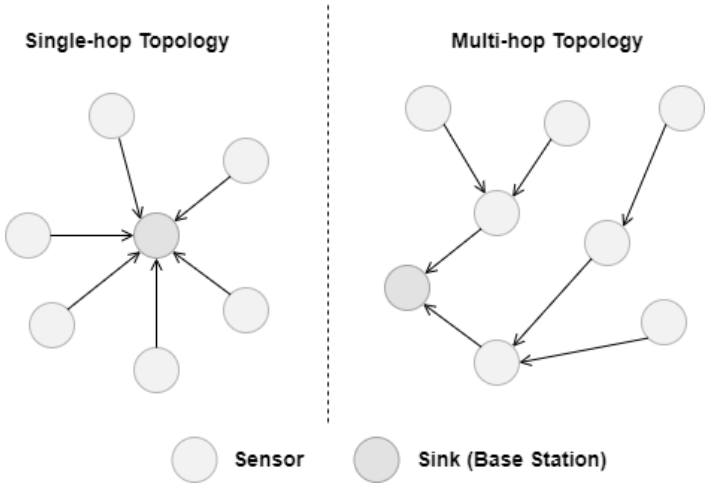

Figure 5.2 - Single-hop vs Multi-hop WSN Network Topology

1. Data transmission rate (known as bandwidth) is a constraint. Sensor bandwidth is extremely limited, thus the network must either discard packets or queue them up in memory if the load exceeds the available bandwidth.

2. Network Dynamics: Node mobility, node status, wireless link failures, and node failures can all lead to changes in network dynamics. This frequently makes QoS support more complicated.

3. Resource Constraints: Energy, memory, processing power, buffer capacity, and other resources are severely limited in wireless sensor networks. WSN QoS methods should be created without using computationally demanding algorithms that deplete certain nodes.

4. Buffer Size Limitation: The size of the buffer is crucial for holding data before sending it to the following node. Long sessions and data buffering are necessary for multi-hop routing of QoS data.

The buffer size makes a difference in the delay that packets experience when traveling over various paths.

5. Data Redundancy: One feature of wireless sensor networks is their high level of data redundancy. In multimedia WSNs, aggregation and data fusion techniques may make QoS design more difficult.

Sensor nodes are grouped into clusters in a sort of network called a Clustered Single-hop WSN, Figure 5.3. Each node in a single-hop network connects with the cluster head or base station directly, eliminating the need for data to travel via any other nodes. This type of network is often used in environments where the sensor nodes are densely and randomly deployed [106].

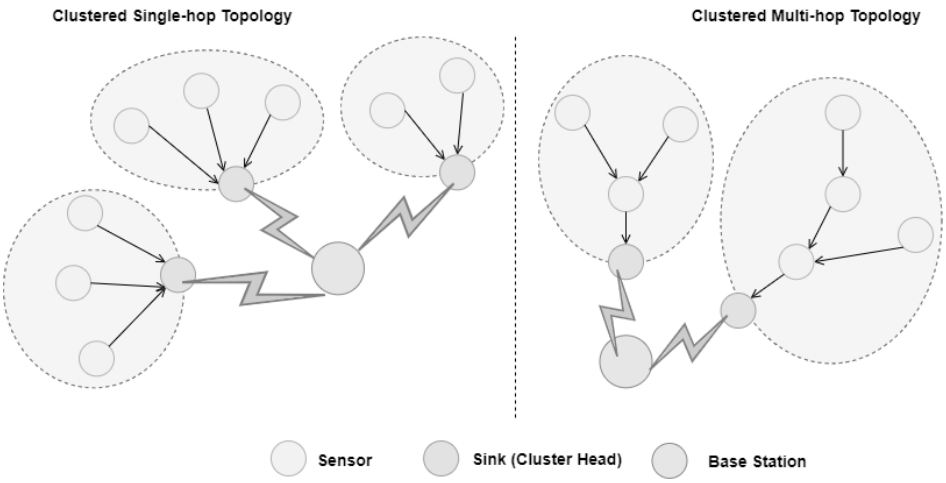

Figure 5.3 - Clustered Single-hop vs Multi-hop WSN Network Topology

5.2 QoS of Clustered Single-hop WSN

In a Clustered Single-hop WSN, the QoS requirements of the link between the sensor nodes and the cluster head are crucial for efficient and reliable data transmission. These requirements ensure that the network can support the necessary services while maintaining a high level of performance. These prerequisites guarantee that the network can uphold the necessary services while preserving superior performance. The additional link, which connects the cluster heads and the base station, does not pose a bottleneck issue. This is because both the cluster heads and the base station are robust nodes equipped with high energy and computational capabilities. Thus, I focused on the QoS requirements of the link between sensors and cluster heads. The following are some of these requirements:

1. Latency: The delay in data transmission should be minimized. Timely delivery of information is essential for real-time applications like health monitoring and catastrophe management.

2. Reliability: The link should ensure a high packet delivery ratio. Data transmitted by the sensor nodes should reach the cluster head without being lost in the network.

3. Bandwidth: The link should have sufficient bandwidth to support the data rate of the sensor nodes. This is especially important in applications that generate a large amount of data, such as multimedia surveillance systems.

4. Energy Efficiency: Since sensor nodes are typically battery-powered, the link should be energy-efficient to prolong the network lifetime.

5. Duty Cycle: It is important to optimize the duty cycle. The operational longevity of the sensor nodes can be increased with careful management of the duty cycle, which can help balance energy consumption and data transmission requirements.

5.3 Related Works

The authors [107] survey some strategies and techniques that can be used to improve QoS in WSNs, such as data compression, sensing rate adjustment, channel selection, and signal power modification. Choosing an optimal power transmission can serve as a strategy to extend both the lifespan of an individual node and the network as a whole. The minimum transmit power, which would meet the desired Bit Error Rate (BER) threshold, can be determined numerically. The use of multi-channel communications can lead to a substantial increase in the throughput of wireless networks. This is in contrast to single-channel communications, as the employment of multiple channels can mitigate the impact of interference.

To balance the communication quality and power consumption of sensor nodes using fuzzy logic, the authors [108] propose a method that adjusts the data rate and transmission power based on the error count and error interval, which reflect the environmental interference and noise. They analyze the relationship between power consumption, data rate, and transmission power, and show how to calculate the receiver sensitivity and SNR for different data rates for Texas Instruments CC1310 device. Their method is compared with a control group with fixed data rate and transmission power. The results show that the proposed method can achieve a low Packet Error Rate (PER) of around 1% and a low

power consumption of around 19.49 μA. They also estimate the battery life of the sensor nodes with the proposed method, which is more than 6.8 years.

A centralized metaheuristic algorithm that assigns minimum transmission power to each sensor node for every transmission link along with a scheduling slot while satisfying the Signal to Interference plus Noise Ratio (SINR) constraint is proposed [109]. The authors formulate the optimization problem with two objective functions: (1) minimizing the transmission power for each communication link and (2) minimizing the required number of scheduling slots. They also define the constraints and the parameters of the problem, such as the sensing range, the communication range, the interference range, the transmission power, the receiver interference, and the SINR.

The authors [110] review different hardware-based and software-based metrics to estimate the quality of wireless links in IoT networks, such as Received Signal Strength (RSSI), Link Quality Indication (LQI), Signal to Noise Ratio (SNR), Packet-Delivery Ratio (PDR), and (Requested Number of Packets) RNP. It also defines five classes of link quality based on PDR and RSSI values. They apply two machine learning algorithms, K-Nearest Neighbour (KNN) and LSTM, to classify and predict the link quality based on a real dataset collected from a testbed IoT network deployed at Grenoble, France. It compares the performance of the two algorithms and discusses their advantages and limitations. They conclude that, by predicting the link quality, the QoS can be improved especially in the case of critical application.

The authors [111] propose a link quality estimator (LQE) that uses PDR and RSSI as metrics to measure the quality of a wireless link in IoT networks. The LQE can adapt to different network conditions and traffic patterns. The authors also propose a link quality predictor (LQP) that uses machine learning techniques to forecast the future link quality based on historical data. The LQP can help to optimize routing decisions and improve network performance.

The transmission rate is dependent on the sampling frequency. Therefore, determining the optimal sampling frequencies lays the foundation for the best use of wireless bandwidth and prolongs the battery life of sensor networks [107]. The sampling frequency is the rate at which samples are taken. It directly affects the transmission rate, which in turn impacts the duty cycle. A higher sampling frequency can lead to a higher transmission rate, which may require a higher duty cycle to handle the increased data.

A new adaptive duty cycle scheme that enhances the S-MAC protocol with a priority queue where packet size is the parameter to adjust the duty cycle is proposed [112]. The idea is to give higher priority

to smaller packets and lower priority to larger packets, and to dynamically change the listen period of each node according to the network conditions. The results show that the proposed schema outperforms the default MAC and S-MAC protocol in all metrics.

The authors [113] use a continuous-time Markov chain and a Markov decision process (MDP) model to balance energy availability and QoS requirements. The adaptive duty cycling works by adjusting the duty cycle based on the state of the system, which includes the current battery level, the harvesting rate, and the QoS metrics. The system state transitions are modeled as a continuous-time Markov chain, and the optimal duty cycle is determined by solving the MDP. The authors conclude that their adaptive duty cycling scheme can effectively manage the energy resources in a wireless sensor network and meet the QoS requirements. They also show that their algorithm outperforms a random approach in terms of energy efficiency and QoS.

Table 5.1 Presented Work for QoS in WSN

Work	Main Focus	Key Techniques/Strategies	Results
[108]	Balance communication quality and power consumption	Fuzzy logic to adjust data rate and transmission power	Achieved low PER and power consumption, extended battery life
[109]	Assign minimum transmission power and scheduling slot	Centralized metaheuristic algorithm	Satisfies SINR constraint
[110]	Estimate and predict link quality in IoT networks	quality in IoT networks Hardware-based and software-based metrics, machine learning algorithms	Improved QoS in critical applications

[111]	Measure and forecast link quality in IoT networks	LQE and LQP using machine learning techniques	Optimized routing decisions, improved network performance
[112]	Enhance S-MAC protocol with adaptive duty cycle scheme	Priority queue where packet size is the parameter to adjust the duty cycle	Outperforms default MAC and S-MAC protocol in all metrics
[113]	Balance energy availability and QoS requirements	Continuous-time Markov chain and MDP model for adaptive duty cycling	Effectively manages energy resources, meets QoS requirements, outperforms a random approach

In conclusion, QoS in WSNs is a complex field that requires careful consideration of various factors such as latency, reliability, bandwidth, energy efficiency, and duty cycle. The use of techniques such as optimal power transmission, multi-channel communications, and machine learning for link quality estimation and prediction can significantly improve QoS. Nonetheless, there are still hurdles to overcome, especially when it comes to balancing the needs of data transmission with the limitations of energy and resource availability. As a result, this thesis is centered on developing a method that can adaptively adjust the power transmission and duty cycle based on available energy, without sacrificing the QoS requirements.

System Model

The system under consideration, Figure 5.4, is an Internet of Things (IoT) device that is a node within a Wireless Sensor Network (WSN). This IoT device is equipped with a battery and two energy harvesters: a solar panel and a mechanical vibration source. The sensing region (a cluster in a clustered WSN) contains N IoT devices and one sink node that is located in the sensing region and has unlimited energy and computational resources. I consider the sink node as a cluster head, as in clustering, low power nodes are utilized for sensing, whereas high power nodes can be employed to process detected data and interact with other nodes. That's, achieving greater scalability, longevity, and energy efficiency can

be accomplished with the clustering technique [105]. In this way, the IoT devices communicate with the sink node using a single-hop transmission to avoid multi-hop architecture that requires high demands on the bandwidth and routing protocol [105].

The IoT device operates in three distinct states: active A, idle I and sleep S.

- **Active State**: In the active state, the device collects data using its sensors and transmits them to the sink node (Base Station). The energy consumption in this state E_A is primarily due to sensing, data processing, and communication activities.

- **Idel State**: In the idle state, the device is not transmitting or receiving any data but is ready to do so, essentially functioning in a standby mode. The energy consumption in this state E_I is lower than the active state $E_I < E_A$.

- **Sleep State**: The sleep state is a power-saving state where the device is not active. The energy consumption in this state E_S is minimal $E_S \ll E_I < E_A$.

The device transitions between these states based on the duty cycles D_A, D_I and D_S, which are defined as the portion of time the device is in active, idle or sleep state per hour. The duty cycles and transmission power P_t of the device can be adapted depending on the available energy and Quality of Service (QoS) requirements. The goal of the system model is to optimize the battery load without compromising the QoS requirements. This involves a trade-off between energy efficiency (to prolong the battery life) and QoS (to ensure reliable and timely data transmission).

I assume that, the IoT device is able to generate and process L_0 bits per seconds. Let donate $T_{tr,0}$ as the time required to transmit L_0 bits to the sink node, and $T_{proc,0}$ is the time required to process L_0 bits, where $T_{proc,0} = 1\ s$ in the studied case. Thus, the total data, which is generated and transmitted by the IoT device in an hour (hourly time slot $t \in T$, where T is the total life time of the battery), during

$$\boldsymbol{L_{total,t} = L_0 * \frac{D_{A,t}}{T_{tr,0} + T_{proc,0}}} \tag{5.1}$$

the active state can be calculated using the duty cycle D_A as follows:

where $D_{A,t}$ is the duty cycle at time slot t.

5.4 Channel Model

The channel model depends on the environment where the wireless signal propagates from the sender to the receiver. The reduction in power density of the electromagnetic wave as it propagates through space is called the path loss. Therefore, the received signal quality is affected by the path loss and the noise in the propagation environment. I consider the widely-used Log-Distance path loss model to predict the path loss, which can be used for a wide range of environments [114]. It is formally expressed as:

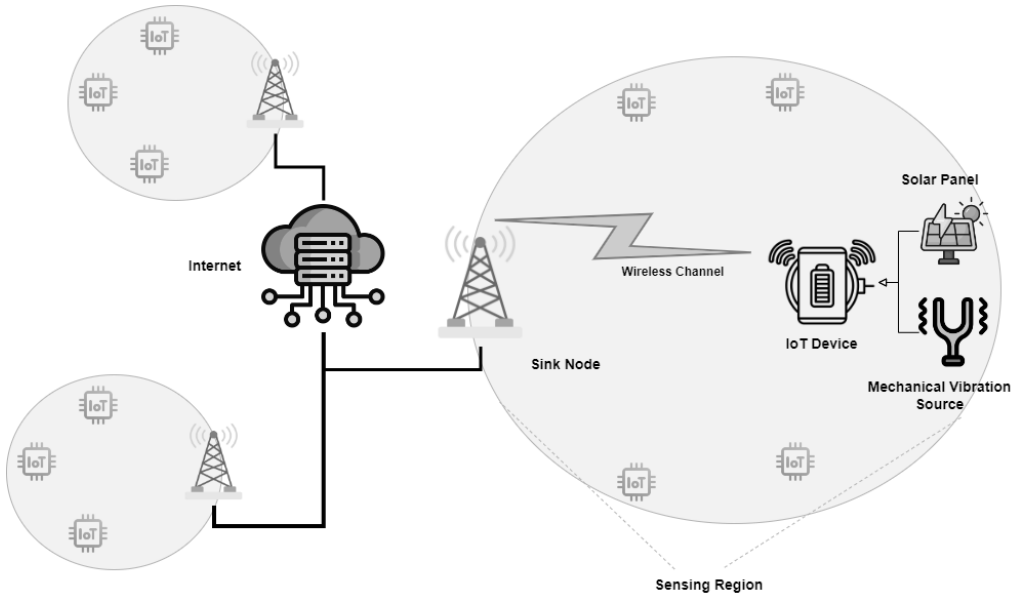

Figure 5.4 - System Model

$$\boldsymbol{PL = PL_0 + 10n \log_{10}\left(\frac{d}{d_0}\right)} \tag{5.2}$$

where PL_0 is the path loss at the reference distance d_0, d is the distance between transmitter and receiver, and n is the path loss exponent that is a key factor in determining how the signal strength decreases with distance. The value of n depends on the propagation environment and can be used to model different types of environments. For instance: In a free space environment (like an open outdoor area), n is typically around 2. In an environment with obstacles present (like an urban area with buildings), n can range from 2.7 to 3.5. In a dense urban or indoor environment, n can be even higher, sometimes exceeding 4. Table 5.2 shows the different values for n and the environments. Therefore, adjusting the value of n allows us to model and predict the path loss and subsequently the quality of

wireless communication in various environments. This is crucial in designing and optimizing wireless networks such as those involving IoT devices.

Table 5.2 - Path loss exponent values [114]

Path loss exponent (n)	Environment
2	Free space
2.7 to 3.5	Urban area cellular radio
3 to 5	Shadow urban cellular radio
1.6 to 1.8	Inside a building – line-of-sight
4 to 6	Obstructed in building
2 to 3	Obstructed in factory

Signal to Noise Ratio (SNR) is one of the most used factors to estimate the channel quality [108], [109], [110]. Mathematically, SNR at time slot t is donated as follows:

$$\boldsymbol{SNR_t = \frac{P_t G}{N_0}} \tag{5.3}$$

where $\boldsymbol{P_t}$ is the transmission power of the IoT device, G is the channel gain and $\boldsymbol{N_0}$ is the noise power. The channel gain G is expressed as:

$$\boldsymbol{G = \frac{\rho}{PL}} \tag{5.4}$$

where ρ is the small-scale fading term and PL is the path loss. According to the Shannon–Hartley theorem, the transmission rate at time slot t is given by:

$$\boldsymbol{R_t = B \log_2(1 + SNR_t)} \tag{5.5}$$

where B is the bandwidth. By boosting the transmission power $\boldsymbol{P_t}$, I can improve the signal quality. This increase in power results in a higher SNR and, consequently, a higher transmission rate $\boldsymbol{R}$.

5.5 Energy Consumption Model

The energy consumption of the device is dependent on the chosen duty cycle and transmission power. I assume that E_I is constant and E_S is negligible comparing with E_A and E_I. E_A primarily depends on the selected transmission power.

Let $\{Pt_1, Pt_2, \dots, Pt_N\}$ are predefined transmission power levels that can used by the transmitter. The time required to transmit L bits depend on the actual data transmission R and is equal to L/R. Thus, using (5.1) and (5.3). I can donate the transmission time as follows:

$$\boldsymbol{T_{tr} = \frac{L_{total,t}}{B \log_2\left(1 + \frac{P_{t,i}G)}{N_0}\right)}, 1 \le i \le N} \tag{5.6}$$

where $\boldsymbol{P_{t,i}}$ is the transmission power level of the transmitter at time slot t. Consequently, the processing time and the total active time are given, respectively, by:

$$T_{proc} = T_{proc,0} * \frac{L_{total,t}}{L_0} \tag{5.7}$$

$$T_{active} = T_{proc} + T_{tr}\text{ , where } T_{active} \le D_{A,t} \tag{5.8}$$

Let's denote the required power consumption for the processing phase during the active state as P_{proc}. Therefore, I have: $E_A = T_{proc} * P_{proc} + T_{tr} * \ P_t$. The total energy consumption, E_{total} at time slot t, can be calculated as:

$$\boldsymbol{E_{total,t} = T_{proc} * P_{proc} + T_{tr} * \ P_{t,i} + E_I} \tag{5.9}$$

By substituting (5.1), (5.6) and (5.7) into (5.9), I can express the total energy consumption in terms of the transmission power $\boldsymbol{P_{t,i}}$ and the duty cycle $D_{A,t}$:

$$E_{total,t} = \frac{D_{A,t}}{\frac{L_0}{B\log_2\left(1+\frac{P_{t,i}G)}{N_0}\right)}+1}\left[P_{proc} + \frac{L_0}{B\log_2\left(1+\frac{P_{t,i}G)}{N_0}\right)}P_{t,i}\right] + E_I \tag{5.10}$$

5.6 Battery Model

To maintain a minimum battery capacity, I define SoC_{min} as the minimum state of charge that should be maintained. I propose an efficient hourly mechanism that monitors the battery's state of charge, using Coulomb Counting Method, and chooses how to use the predicted harvesting energy from the two harvesters. I define S_e and S_c as the outputs of source of energy and source of charging. At the beginning of each hour, I predict the harvested solar energy E_s^{pred} and mechanical energy E_m^{pred} for the next hour. I monitor SoC and set the charging source to the source with larger predicted value if the SoC lower than the allowed minimum SoC_{min}, and the source of energy to the other source. If the SoC is larger than the minimum, then the priority is to enhance the QoS and I set the source of energy to the source with the larger predicted value. Then, I set S_e and S_c as follows:

$$\boldsymbol{S_e = \begin{cases} E_s \ if \ \begin{cases} SoC > SoC_{min} \ and \ E_s^{pred} > E_m^{pred} \\ SoC \le SoC_{min} \ and \ E_s^{pred} \le E_m^{pred} \end{cases} \\ E_m \ if \ \begin{cases} SoC > SoC_{min} \ and \ E_s^{pred} \le E_m^{pred} \\ SoC \le SoC_{min} \ and \ E_s^{pred} > E_m^{pred} \end{cases} \end{cases}} \tag{5.11}$$

$$S_c = \begin{cases} E_s \ \ if \ \begin{cases} SoC > SoC_{min} \ and \ E_s^{pred} \leq E_m^{pred} \\ SoC \leq SoC_{min} \ and \ E_s^{pred} > E_m^{pred} \end{cases} \\ E_m \ \ if \ \begin{cases} SoC > SoC_{min} \ and \ E_s^{pred} > E_m^{pred} \\ SoC \leq SoC_{min} \ and \ E_s^{pred} \leq E_m^{pred} \end{cases} \end{cases} \quad (5.12)$$

Based on the previous method, the total energy consumption by the sensing, processing and transmission of the IoT device could be covered by the suitable source of harvested energy S_e. Thus, the battery load could be minimized to cover the remaining required energy that cannot be covered by S_e. Thus, I can donate the battery load at time slot t as:

$$BL_t = \begin{cases} E_{total,t} - S_{e,t} & if \ E_{total,t} > S_{e,t} \\ 0 & \text{otherwise} \end{cases} \quad (5.13)$$

where $S_{e,t}$ is the source of energy at time slot t. The state of charge of the battery at time slot t depends on the total energy consumption and the generated energy of both harvesters at the previous time slot $t-1$. Thus, I can rewrite the SoC equation (5.5) as:

$$SoC_t = SoC_{t-1} + \frac{1}{Q_{current}}\left[S_{c,t-1} - BL_{t-1}\right] * 100\% \quad (5.14)$$

where Q_{max} is the battery capacity that follows the Capacity Fade Estimation method and $S_{c,t-1}$ is the output of source of charging at time slot $t-1$.

5.7 QoS Model

My goal is to enhance energy efficiency and extend battery life using harvesters, without sacrificing the QoS requirements. The duration of a device's active state, which directly influences the volume of data generated and transmitted, is determined by the duty cycle. Therefore, selecting the optimal duty cycle for a given time slot is crucial. I aim to leverage harvested energy to extend the active state duration whenever feasible. Moreover, the ability to adjust the transmission power enables us to improve signal quality by boosting the SNR.

Let's denote the minimum duty cycle that satisfies the application layer's requirement as $D_{A,min}$. If $D_{A,min}$ is small, it indicates that the application does not demand a large amount of collected data. Conversely, a large $D_{A,min}$ is suitable for scenarios where the application needs to gather as much data as possible from the sensing region. let's denote the minimum SNR that satisfies the network layer's

requirement as SNR_{min}. If SNR_{min} is small, it indicates that the application can tolerate a higher level of noise in the signal, which might be the case for applications with less stringent data quality requirements. Conversely, a large SNR_{min} is suitable for scenarios where the application requires a high-quality signal with minimal noise interference, such as in precision sensing applications.

Based on (5.3) and (5.5), SNR_{min} can be achieved by changing the transmission power to a certain level. Let's donate the minimum transmission power that achieves SNR_{min} as $P_{t,min} \in \{Pt_1, Pt_2, \dots, Pt_N\}$, the minimum achievable transmission rate using $P_{t,min}$ as R_{min}. I can represent the minimum QoS requirements at time slot t as follows:

$$\begin{cases} \boldsymbol{P_{t,i} \geq P_{t,min}} \\ \boldsymbol{D_{A,t} \geq D_{A,min}} \end{cases} \tag{5.15}$$

However, the duty cycle and the SNR can significantly impact both the Packet Delivery Rate (PDR) and the Bit Error Rate (BER) metrics, which are given by:

$$PDR = \frac{Number\ of\ packets\ suuessfully\ received}{Total\ number\ of\ packets\ sent} \tag{5.16}$$

$$BER = \frac{Number\ of\ bit\ errors}{Total\ number\ of\ bits\ transfered} \tag{5.17}$$

The PDR can be influenced by the duty cycle. A longer active state duration, facilitated by a larger duty cycle, can potentially increase the PDR as more data is generated and transmitted. However, this is contingent on the quality of the transmission, which is where the SNR comes into play. A higher SNR, indicating a stronger signal relative to the background noise, can enhance the quality of the transmission and thus improve the PDR. On the other hand, the BER is also affected by these parameters. A higher duty cycle can lead to more bits being transferred, potentially increasing the chance of bit errors, especially in noisy environments. However, a higher SNR can help mitigate this by reducing the likelihood of bit errors, thereby lowering the BER.

To quantify the QoS requirements, represented in (5.14), I define the QoS enhancement function that can measure how much I improve the QoS by setting Pt_i and $D_{A,t}$ above the threshold values $P_{t,min}$ and $D_{A,min}$ at time slot t by:

$$\boldsymbol{QoS_t = \alpha\big(P_{t,i} - P_{t,min}\big) + (1-\alpha)\big(D_{A,t} - D_{A,min}\big)} \tag{5.18}$$

where α is a weighting factor in [0,1] range that determines the relative importance of transmission power and data cycles in determining QoS. If α is set to 1, the QoS is determined solely by the transmission power. This means that the system prioritizes strategies that adjust the transmission power to improve QoS. This could potentially allow for more data to be transmitted at a given time, but it might also consume more energy and thus reduce the time the device can remain in an active state. On the other hand, when α is set to 0, the QoS is determined solely by the duty cycle percentage. This means that the system prioritizes strategies that adjust the duty cycle. This could potentially extend the time the device can remain in an active state and thus increase the amount of data collected over time. However, it might also limit the rate at which data can be transmitted at any given moment. Therefore, adjusting α allows us to balance between collecting more data at a faster rate (by prioritizing transmission power) and collecting data over a longer period (by prioritizing duty cycles). The optimal value of α would depend on the specific requirements of IoT application.

5.8 Problem Formulation

The objective is to maximize the QoS while minimizing the battery load to prolong its life time T. Mathematically, I can represent it as:

$$\max_{\alpha, P_{t,i}, D_{A,t}} QoS_t \qquad (5.19)$$

$$\min_{E_{total,t}, S_{e,t}} BL_t$$

s.t.

$C1$: $P_{t,min} \leq P_{t,i} \leq P_{t,N}, \forall t \leq T, 1 \leq i \leq N$

$C2$: $D_{A,min} \leq D_{A,t} \leq 3600 - D_I, \forall t \leq T$

$C3$: $SoC_{min} \leq SoC_t \leq 100, \forall t \leq T$

$C4$: $0 \leq \alpha \leq 1$

I notice that (5.19) is a multi-objective optimization problem, each objective is optimized independently. The solution to this problem will provide a set of Pareto optimal solutions, where no solution can be found that would increase the value of one objective without decreasing the value of another objective. $C1$ constraint defines the limits of the transmission power, where selection $\boldsymbol{P_{t,i}}$ to the level

that does not meet the QoS requirements is forbidden and the maximum selectable level is $\boldsymbol{P_{t,N}}$. Similarly, in $C2$ constrain, $D_{A,t}$ value cannot be lesser than $D_{A,min}$. The upper bound in $C2$ comes from the fact that the device is in idle state for D_I each hour. Thus, $D_{A,t}$ is bounded by the total duration of one hour minus D_I. $C3$ constraint restricts the battery state of the charge to not be lower than the minimum allowed state SoC_{min}. Finally, $C4$ constraint is the weight factor α, introduced in (5.18).

The multi-objective optimization problem can be reformulated as a single-objective optimization problem by combining the two objectives into one using a weighted sum approach. I define the profit function at time slot t as:

$$\boldsymbol{Profit_t = w_1 * QoS_t - w_2 * BL_t} \tag{5.20}$$

where $\boldsymbol{w_1}$ and $\boldsymbol{w_2}$ are the weights assigned to QoS and BL, respectively and $\boldsymbol{w_1 + w_2 = 1}$. When $\boldsymbol{w_1}$ is closer to 1, more weight is given to maximizing the QoS function. This means the optimization problem will prioritize strategies that improve QoS, even if it might lead to higher energy consumption. On the other hand, when $\boldsymbol{w_2}$ is closer to 1, more weight is given to minimizing the battery load (energy saving). This means the optimization problem will prioritize strategies that reduce energy consumption, even if it might lead to a lower QoS. Therefore, by adjusting the value of $\boldsymbol{w_1}$ and $\boldsymbol{w_2}$, I can control whether the system prioritizes energy saving or QoS improvement. This allows for flexibility in managing the performance of the IoT device based on the specific needs and constraints of its operating environment.

Thus, the weighted factors $\boldsymbol{w_1}$, $\boldsymbol{w_2}$, and α are use case-related factors that can be investigated to examine the system behavior for different applications, while $P_{t,i}$ and $D_{A,t}$ are the factors that directly effect the system for specific use case. I reformulate (35) using (36) as follow:

$$\max_{\boldsymbol{P_{t,i}, D_{A,t}}} \boldsymbol{Profit_t} \tag{5.21}$$

s.t.

$C1$: $\boldsymbol{P_{t,min} \leq P_{t,i} \leq P_{t,N}}, \forall t \leq T, 1 \leq i \leq N$

$C2$: $D_{A,min} \leq D_{A,t} \leq 3600 - D_I, \forall t \leq T$

$C3$: $SoC_{min} \leq \boldsymbol{SoC_t} \leq 100, \forall t \leq T$

$C4: 0 \leq \alpha \leq 1$

$C5: 0 \leq \boldsymbol{w_1} \leq 1, 0 \leq \boldsymbol{w_2} \leq 1, \boldsymbol{w_1} + \boldsymbol{w_2} = 1$

5.9 Proposed Energy Management Algorithm

In the following, I propose an energy management algorithm that adapts the duty cycle $\boldsymbol{D_{A,t}}$ and transmission power $\boldsymbol{P_{t,i}}$ of the device based on the expected energy of the harvesters at each time slot t. Figure 5.5 shows the proposed algorithm diagram. The selected $\boldsymbol{P_{t,i}}$ and $\boldsymbol{D_{A,t}}$ should achieve the maximum value of the proposed profit function (5.20) in the optimization problem. The algorithm assumes certain conditions or constraints that are defined in the problem formulation and uses grid search technique to find the optimal $\boldsymbol{P_{t,i}}$ and $\boldsymbol{D_{A,t}}$ values at each hour.

5.9.1 Assumptions

I assume that the communication channel between the IoT device and the sink node follows the Log-Distance model (5.2) in a specific environment. The value path loss exponent n is determined based on Table 5.2, and the distance d between IoT device and sink node is known. For small-scale fading term, I consider a Rayleigh distribution.

Regarding energy consumption model, I assume that the energy consumption at the idle state $E_{\boldsymbol{I}}$ is constant and at the sleep state E_S is negligible. The energy consumption $E_{t,i}$, for each predefined transmission power level $P_{t,i}$, is also predefined. The algorithm uses the proposed hybrid prediction algorithm to predict the harvested solar energy E_s^{pred}. For the prediction of the harvested piezoelectric energy E_m^{pred}, the generated electrical energy of the piezoelectric harvester is stored in a lookup table over 24 hours/ 7 days a week as shown in Table 5.3. I assume that, the device is aware of the minimum accepted signal quality SNR_{min} and the minimum duty cycle $D_{A,min}$.

Table 5.3 PZT harvested Energy Lookup Table

Hour	Weekday Energy [mJ]	Weekend Energy [mJ]
0	0.54	0.27
1	0.54	0.27
2	0.54	0.27
3	0.54	0.27
4	0.54	0.27
5	0.54	0.27
6	0.54	0.27
7	1.62	0.27
8	1.62	0.27
9	1.62	0.27
10	0.54	0.27
11	0.54	0.27
12	0.54	0.27
13	0.54	0.27
14	0.54	0.27
15	0.54	0.27
16	0.54	0.27
17	1.62	0.27
18	1.62	0.27
19	1.62	0.27
20	0.54	0.27
21	0.54	0.27
22	0.54	0.27
23	0.54	0.27

5.9.2 Steps

In the initial step, the algorithm begins by setting energy consumption, data processing, battery load, QoS and Profit function constants:

- The path loss exponent n and the distance between transmitter and receiver d.

- the path loss PL_0 at the reference distance d_0.
- The bandwidth B and the noise power N_0.
- The transmission power levels $\{P_{t,1}, P_{t,2}, \dots, P_{t,N}\}$ and their corresponded energy consumption levels $\{E_{t,1}, E_{t,2}, \dots, E_{t,N}\}$.
- The energy consumption at the idle state E_I.
- The energy consumption of data processing and the generated data length per second L_0.
- The battery capacity Q_{original}, degradation rate and the minimum state of charge SoC_{min}.
- The QoS constants: α, SNR_{min} and $D_{A,min}$.
- The Profit function constants: w_1 and w_2.

The algorithm also defines the initial values for the different variables, such as the current battery capacity Q_{current}, the current state of charge SoC_t and the full and partial battery life cycle counters.

In the next steps, based on the initial values, the algorithm calculates the path loss and determines the minimum transmission power level $P_{t,min}$ that achieves the minimum signal quality requirement SNR_{min}. After that, the algorithm initializes a timer that triggers the following steps at the start of each hour:

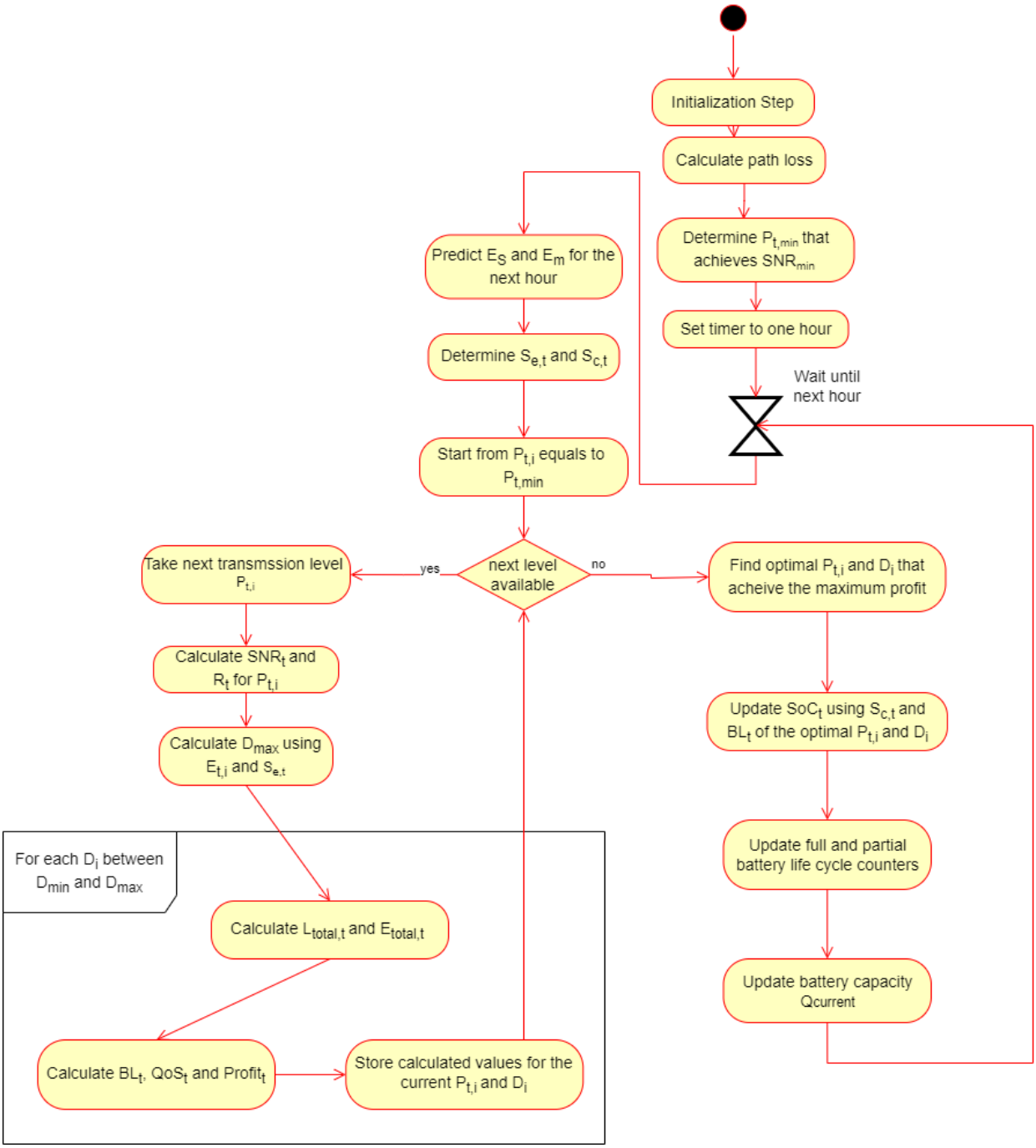

Figure 5.5 Proposed Energy Management Algorithm

1. Using the proposed hybrid prediction algorithm and the collected values from the temperature sensor and the previously harvested power, the algorithm gets the predicted energy of the solar harvester for the next hour.

2. Using the lookup table, the algorithm gets the predicted energy of the mechanical harvester for the next hour.

3. Using (5.11) and (5.12), the algorithm determines the source of energy $\boldsymbol{S_{e,t}}$ and the source of charge $S_{c,t}$ for the next hour t.

4. For each level $P_{t,i}$ starting from $P_{t,min}$:

    a. Calculate the achieved signal quality and the achieved data transmission rate for the current level $P_{t,i}$.

    b. Calculate the maximum duty cycle $D_{A,max}$ that can be covered by the source of energy $\boldsymbol{S_{e,t}}$.

    c. For each duty cycle level D_i between $D_{A,min}$ and $D_{A,max}$:

        i. Calculate the achieved data length and the energy consumption of current $P_{t,i}$ and D_i.

        ii. Calculate the battery load, the value of QoS and profit functions.

        iii. Store the calculated values for comparison.

5. After scanning all possible values transmission power and duty cycle, the algorithm compares the collected values of profit function and select $P_{t,i}$ and D_i that achieve the maximum profit value.

6. Next, the algorithm updates the battery's state of charge based on the current source of charge and the battery load of the selected $P_{t,i}$ and D_i.

7. Finally, the full and partial counters are updated, and the current battery capacity is calculated based on the proposed Capacity Fade Estimation method.

6 IMPLEMENTATION AND VALIDATION

In this Chapter, a series of simulation experiments are conducted to evaluate the effectiveness of the proposed algorithm. These experiments involve running the algorithm with a diverse range of values for all variables in the optimization problem. A grid search technique explores how these variables impact the algorithm's performance. Furthermore, various simulation scenarios are created to compare the algorithm's performance, which utilizes two energy harvesters, against other scenarios where either one or no energy harvesters are used. This comparative analysis highlights the proposed algorithm's advantages in different energy harvesting contexts.

6.1 Simulation Setup

To begin, I establish the values for various parameters required by the proposed algorithm. These parameters, along with their corresponding values, are outlined in Table 6.1 which provides a list of the device's power levels and energy consumption. The active-duty cycle $D_{A,t}$ has a range of values. It starts from $D^*_{A,min}$= 0.1 and goes up to $1 - D^*_I = 0.9$, where the increment between each value in this range is 0.1. The values of path loss exponent n are listed in Table 2. The values of the weight factors $w1$, $w2$ and α are in the range $\{0, 0.1, 0.2, \dots, 1\}$.

Table 6.1 Simulation Parameters' values

$\boldsymbol{B}$	$10\ KHz$	$\boldsymbol{D_I}$	360 s
$\boldsymbol{N_0}$	$-140\ dB$	$\boldsymbol{L_0}$	$5\ KB$
$\boldsymbol{PL_0}$	0	$\boldsymbol{T_{proc,0}}$	$1\ s$
$\boldsymbol{d_0}$	1	$\boldsymbol{E_{idel}}$	0.735 µJ
$\boldsymbol{degradation\_rate}$	20% after 500 cycles	$\boldsymbol{Q}_{orginal}$	$2\ W$
$\boldsymbol{\rho}$	0.5	$\boldsymbol{d}$	$1500\ m$

$\boldsymbol{SNR_{min}}$	10 dB	$\boldsymbol{SoC_{min}}$	40 %
$\boldsymbol{D_{A,min}}$	360 s	$\boldsymbol{E_{proc}}$	0.049 μJ

Table 6.2 Transmission power and energy consumption levels of the device

$\boldsymbol{Pt_i}$ $(\boldsymbol{mW})$	15.30	17.35	19.22	21.35	23.60	25.36	27.13	29.20
$\boldsymbol{E_i}$ $(\boldsymbol{\mu J})$	0.735	0.84	0.93	1.02	1.125	1.215	1.305	1.395

Table 6.3 Values of the path loss exponent

$\boldsymbol{n}$	2.8	3	3.05	3.1	3.15	3.2	3.21	3.22	3.23	3.24	3.25	3.26	3.27	3.28	3.29

6.2 Simulation Scenarios

1. **Without harvesters**: In this run, I run the algorithm without the harvested energy, which means that the device will uses the its battery as the only energy source. Thus, the algorithm sets the power transmission and duty cycle to the levels that meet the minimum QoS requirement without improving the QoS. The simulation stops when the battery capacity reaches the zero value.

2. **With solar energy harvester**: In this run, I run the algorithm with the solar energy harvester. Thus, the algorithm tries to enhance the QoS when it is possible using the solar energy. The simulation stops when the battery capacity reaches the zero value.

3. **With mechanical energy harvester**: In this run, I run the algorithm with the mechanical energy harvester. Thus, the algorithm tries to enhance the QoS when it is possible using the mechanical energy. The simulation stops when the battery capacity reaches the zero value.

4. **With Solar and mechanical energy harvesters**: In this run, I run the algorithm with the solar and mechanical energy harvesters for a period of 15 years. Thus, the algorithm uses one harvester to enhance the QoS and the other to charge the device battery.

6.3 Results

Impact of path loss (n)

In Figure 2, I plot the maximum SNR for each value of n, considering all possible combinations of $w1$, $w2$ and α. I observe that the scenario involving two harvesters yields the highest SNR values across all scenarios. This is because it adaptively selects the source of energy to enhance the QoS. When comparing the solar-only and mechanical-only scenarios, the former provides superior signal quality. Nevertheless, both these scenarios exceed SNR_{min} up to a certain n value. As expected, the no-harvester scenario archives the lowest SNR values, but it stills larger than SNR_{min}. However, for n values greater than 3.295, the highest transmission power level of the device cannot achieve SNR_{min} for all scenarios.

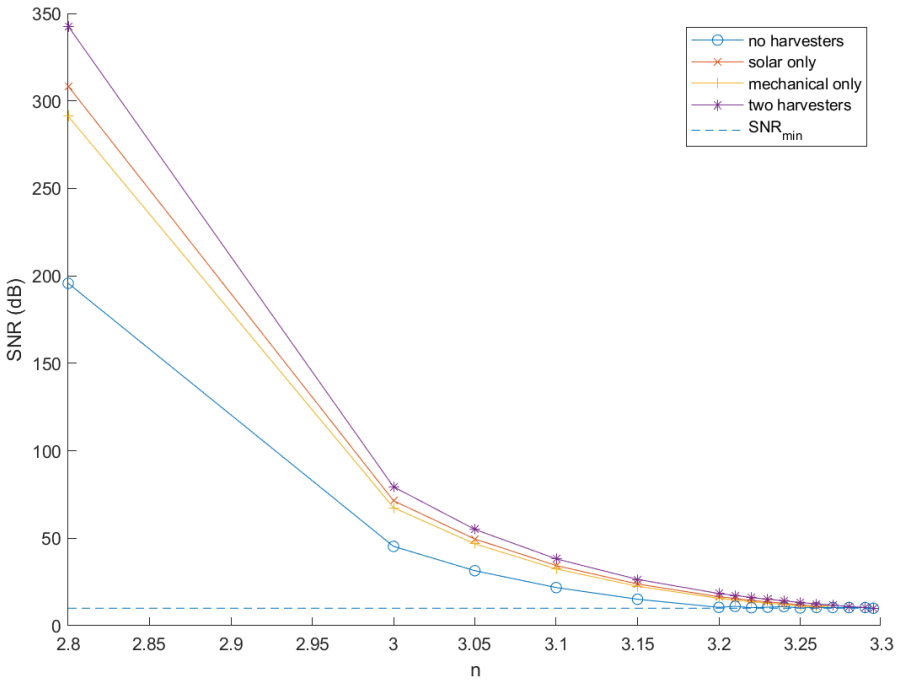

Figure 6.1 - SNR for different scenarios and n values

In Figure 6.2, I illustrate heat maps that represent the frequency of transmission power level selection for each value of n. This takes into account all possible combinations of $w1$, $w2$, and α for all scenarios. In the scenario without a harvester, the algorithm consistently selects the same level for each n value. This indicates that the algorithm is choosing the minimum level that satisfies the SNR requirement. In contrast, for other scenarios, the algorithm not only selects the minimum level that meets the SNR requirement but also the highest level to improve signal quality. Interestingly, in the scenario with two harvesters, the algorithm tends to select the highest level more frequently compared to the scenarios with only solar or mechanical harvesters due to the higher power availability. As n increases the algorithm selects the higher level to achieve the SNR requirement.

The variation in frequency ranges across different scenarios is attributed to the algorithm's termination once the battery capacity depletes completely. This explains why the scenario without a harvester exhibits the lowest maximum frequency, approximately 6000 time slots. Conversely, the scenario with two harvesters displays the highest maximum frequency, around 140 thousand time slots.

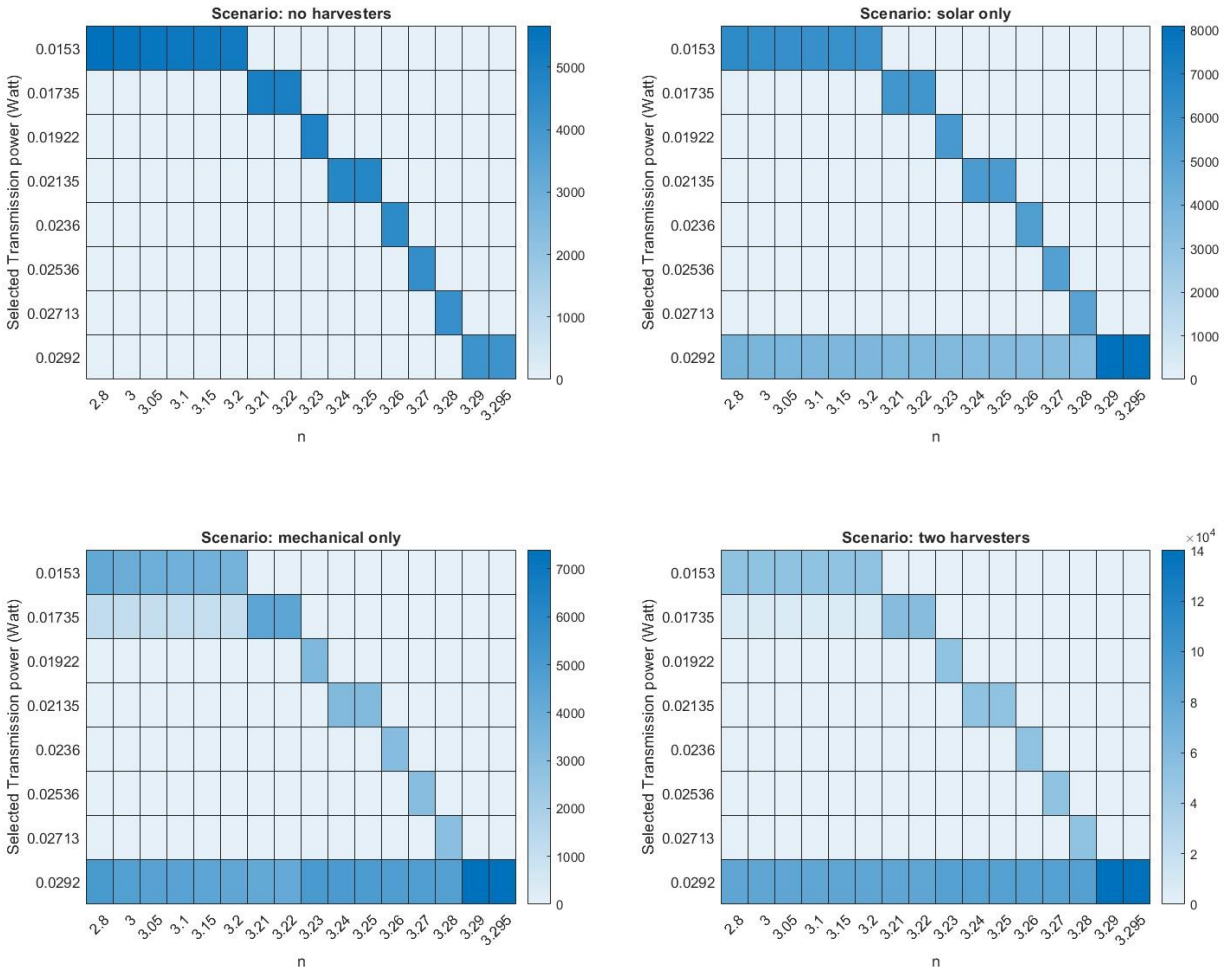

Figure 6.2 - Frequency of transmission power level selection for each value of n, across different energy harvesting scenarios

Impact of factor α

As observed earlier, the number of time slots varies across different scenarios. To understand the influence of the factor α on the QoS function, I have graphed the total transmission power and the total duty cycle (in seconds) for the initial 6000 hours across all four scenarios, with n set to 3.23. In Figure 6.3, I have plotted the total transmission power for various α values. It's evident that when α is zero, the total transmission power reaches its minimum for all scenarios, and it progressively increases as α increases. As for the total duty cycle, it is at its minimum when α is one, as depicted in Figure 6.4. This is anticipated since the factor α is designed to balance the trade-off between the transmission power and the duty cycle.

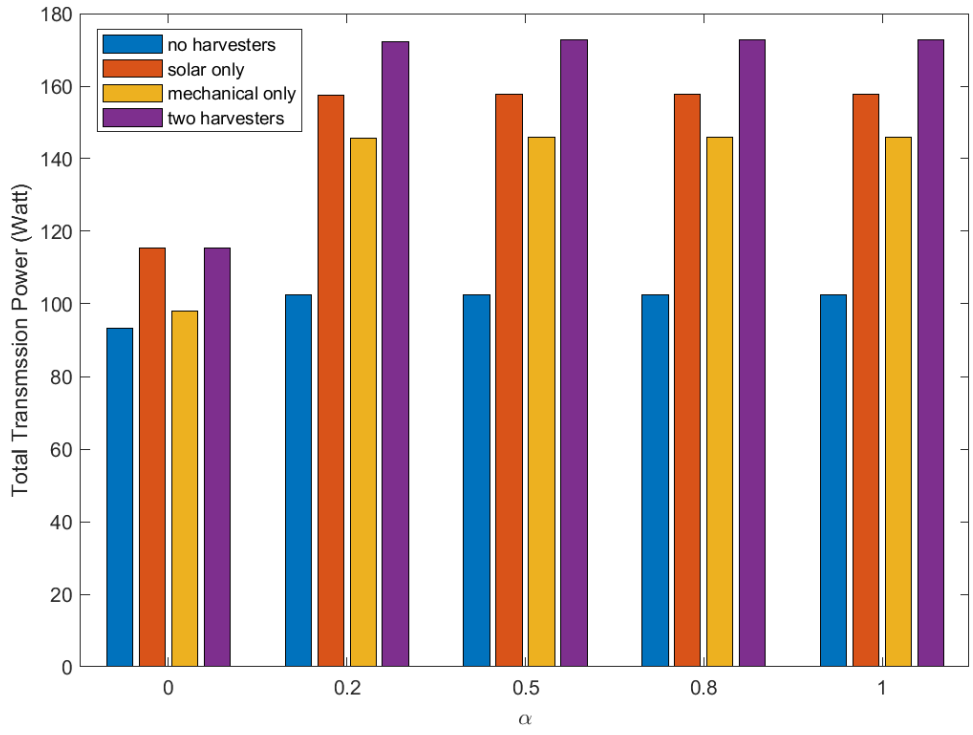

Figure 6.3 - Total transmission power for various α values

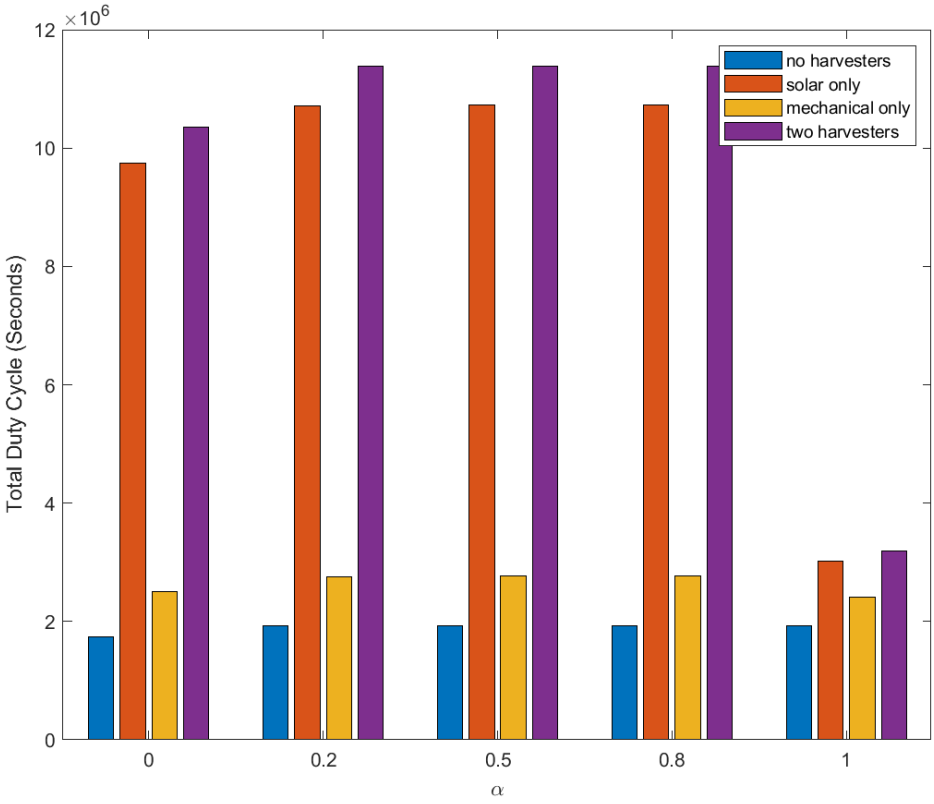

Figure 6.4 - Total duty cycle for various α values

Impact of $w1$ and $w2$

As depicted in Figure 6.5, the value of the Profit function escalates as w1 increases in both the two-harvesters and solar-only scenarios. The two-harvesters scenario slightly outperforms the solar-only scenario. Conversely, the mechanical-only and no-harvesters scenarios yield a profit value close to zero for all w1 values, indicating that they are not conducive to boosting the system's profit. Figure 6.6 plots the QoS function. It's evident that the two-harvesters scenario delivers the highest QoS values among all scenarios, and these values increase as w1 increases. The solar-only scenario follows a similar trend, albeit with slightly lower QoS values than the two-harvesters scenario. The no-harvester and mechanical-only scenarios, on the other hand, yield QoS values near zero, implying that they do not contribute to the enhancement of the system's QoS.

As illustrated in Figure 6.7, while not enhancing the QoS, the no-harvester and mechanical-only scenarios impose the greatest strain on the device's battery. Conversely, the two-harvesters scenario exerts the least load on the battery, followed by the solar-only scenario.

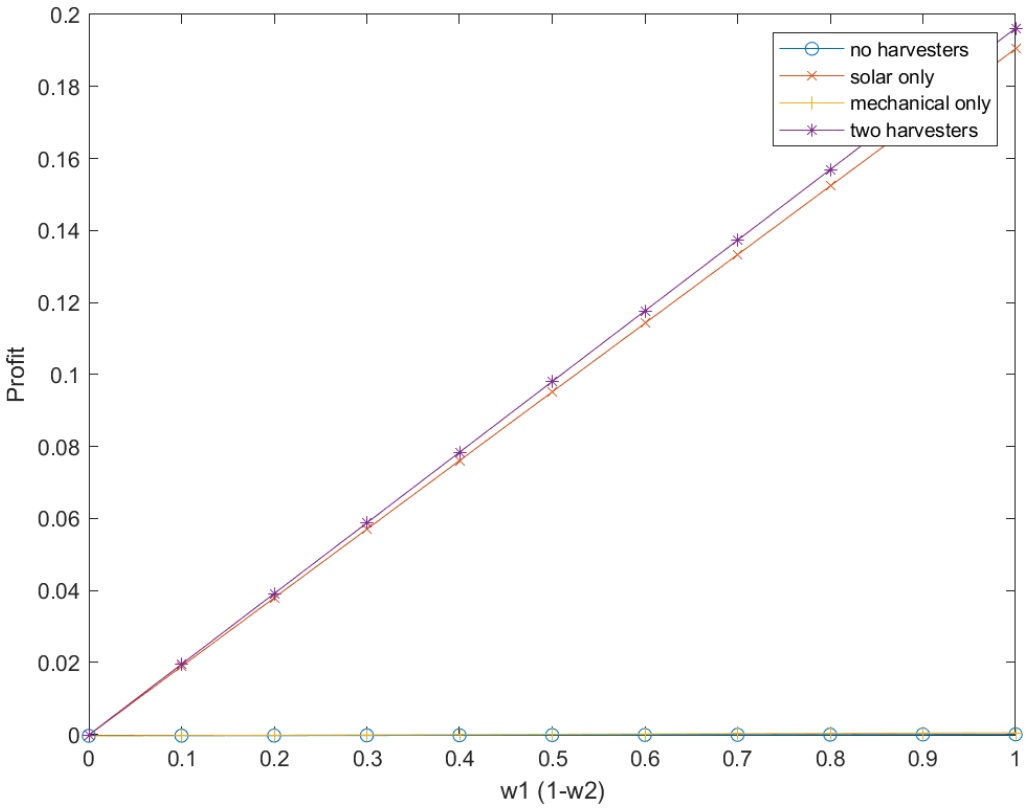

Figure 6.5 - Profit for various w1 values

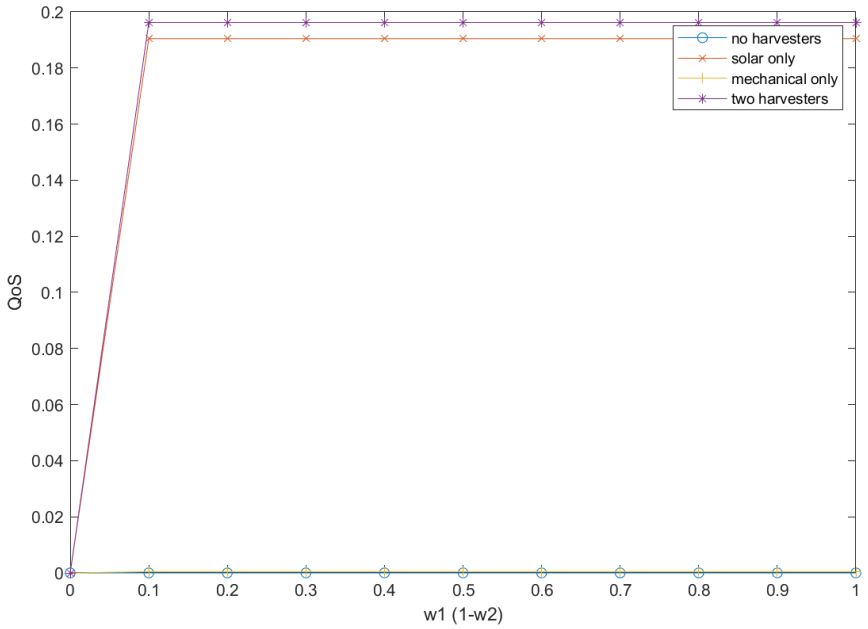

Figure 6.6 - QoS for various w1 values

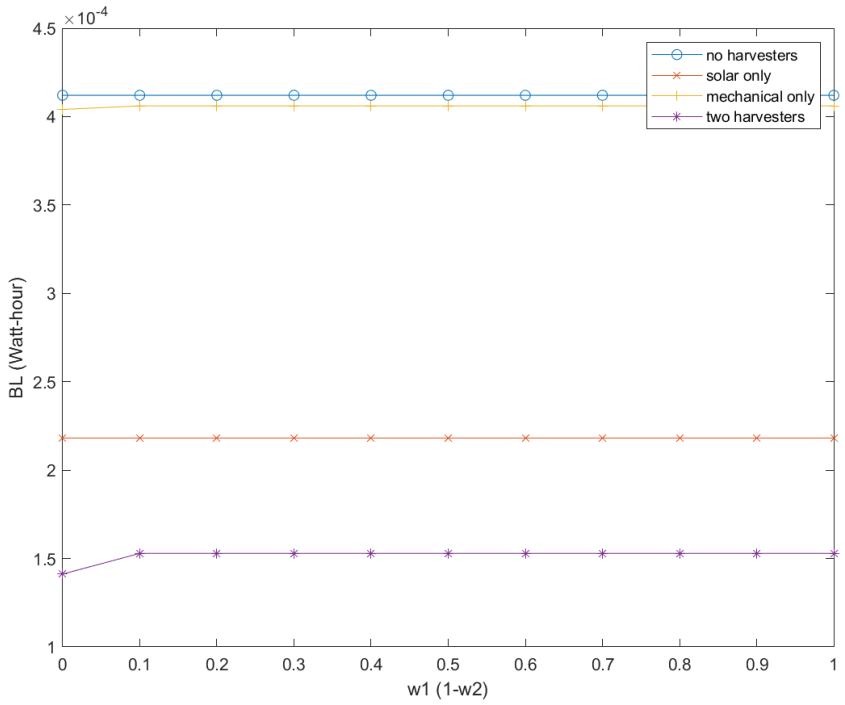

Figure 6.7 - Battery load for various w1 values

Impact on device battery

To evaluate the effect of the four scenarios on battery life, I charted the State of Charge (SoC) for each scenario. As depicted in Figure 6.8:

- The no-harvester scenario depletes the battery to a zero state of charge in approximately 5000 hours (around 208 days).
- The mechanical-only scenario exhausts the battery after about 8300 hours (roughly 345 days).
- The solar-only scenario drains the battery after about 9100 hours (approximately 380 days).

In contrast, the battery SoC in the two-harvesters scenario fluctuates between 90% and 100%, indicating more efficient energy usage after approximately 15 years, as shown in Figure 6.9.

Despite the promising State of Charge (SoC) results in the two-harvesters scenario, it's crucial to examine the effects of charging and discharging on the battery lifespan. Figure 6.10 illustrates the battery capacity over time, following the capacity fade estimation method.

In my simulation setup, I have defined the degradation rate to be 20% after 500 cycles. Consequently, the battery capacity, initially at a maximum of 2 Watt-hours, will decrease to 1.6 Watt-hours after 500 cycles.

The battery capacity drops to 80% of its maximum capacity in the different scenarios as follows:

- Mechanical-only scenario: after 32640 hours (approximately 3.72 years).
- Solar-only scenario: after 48800 hours (around 5.56 years).
- Two-harvesters scenario: after 66000 hours (about 7.52 years).

Figure 6.11 presents similar values, where we've plotted the full cycles of the proposed combined algorithm of Coulomb Counting and battery life cycle counter for the different scenarios.

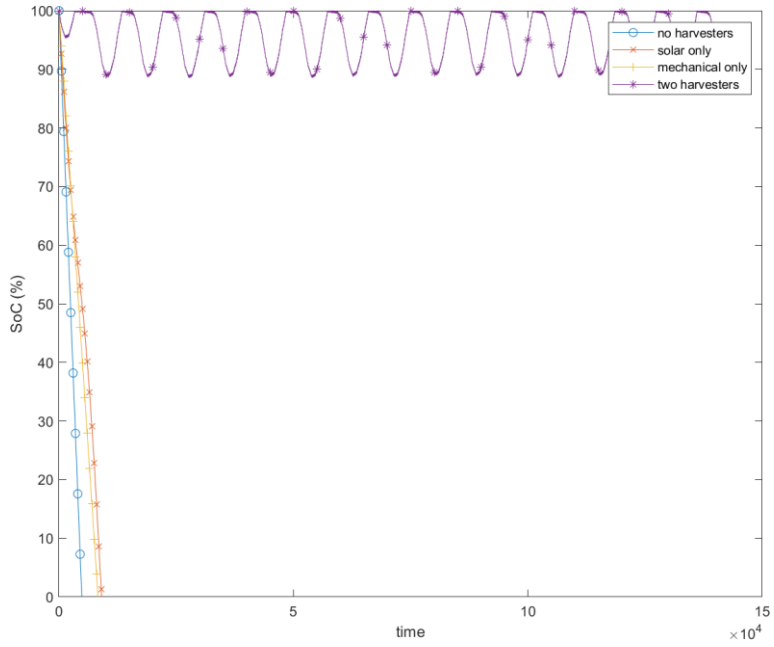

Figure 6.8 - SoC for different scenarios

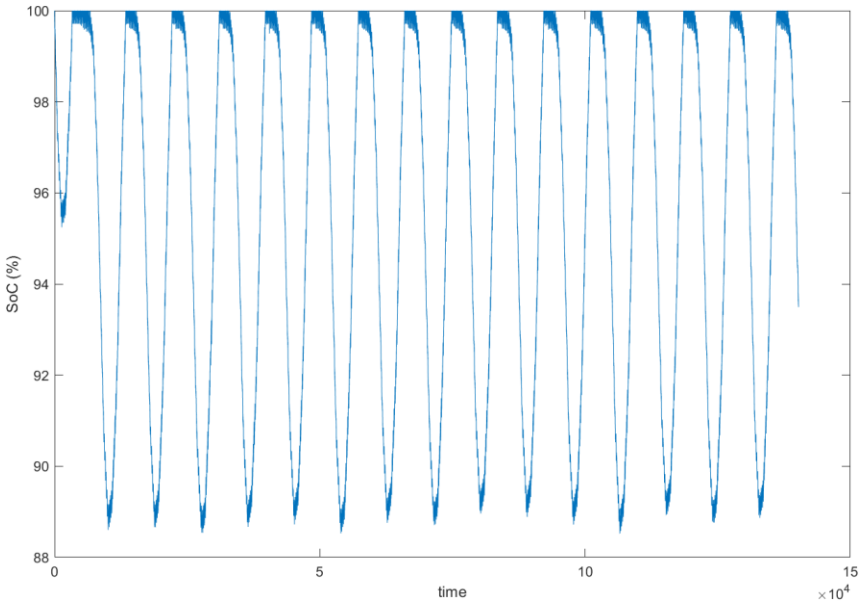

Figure 6.9 - SoC for two-harvesters scenario

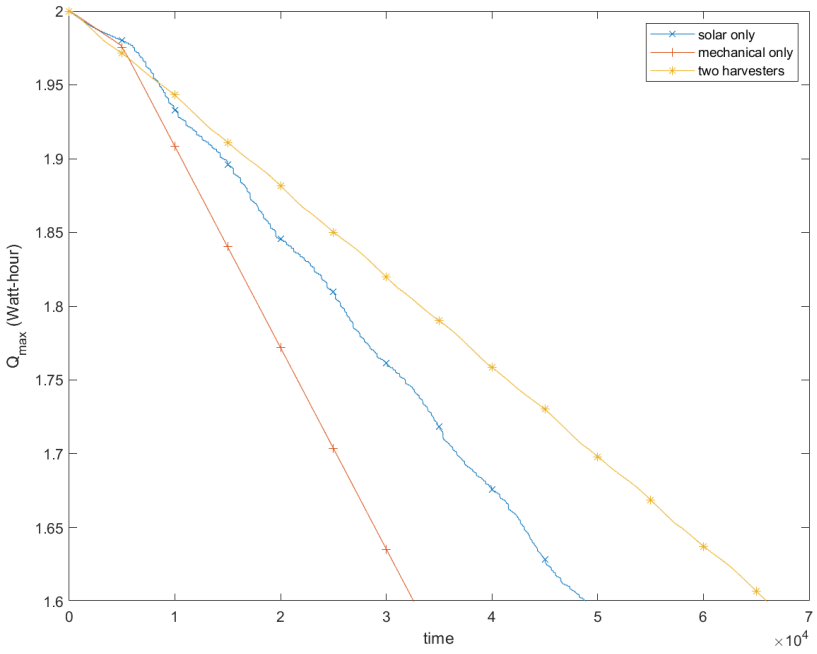

Figure 6.10 - Battery capacity for different scenarios

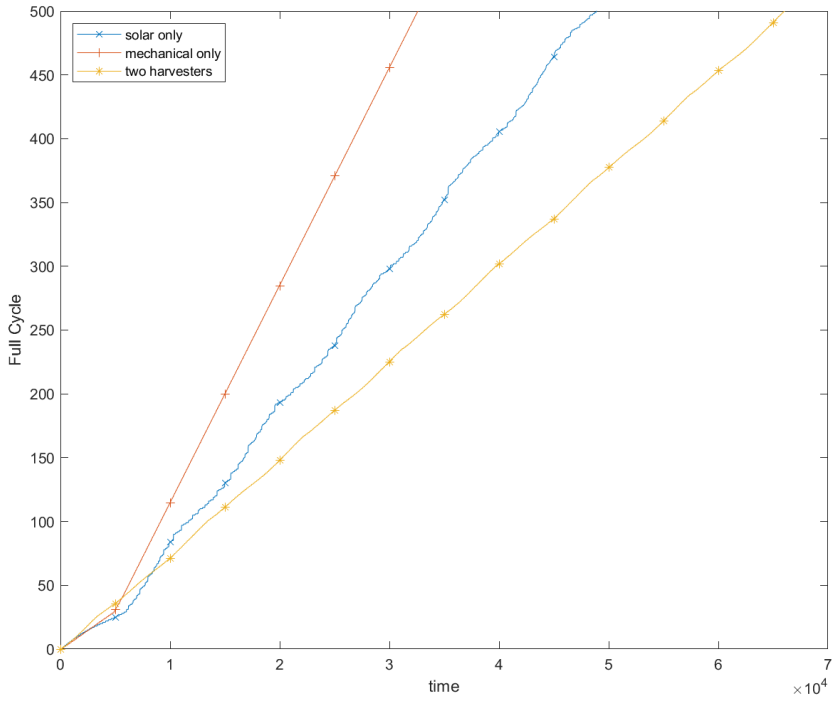

Figure 6.11 - Full cycle for different scenarios

7 EXPERIMENTS

In this chapter, the implementation results of the proposed Energy Management System (EMS) and adaptive Quality of Service (QoS) algorithm in an actual Wireless Sensor Network (WSN) node within a real-world environment are presented and discussed. This includes an examination of how available harvested energy influences the battery's State of Charge (SoC), duty cycle, and transmission power. Section 1 details the circuit design and setup of the WSN. Section 2 introduces the laboratory setup and the measurement tools used. In Section 3, trials are conducted both with and without the proposed EMS and adaptive QoS algorithm to observe their impacts. Finally, Section 4 presents the results, discussions, and performance evaluations of the algorithm, providing an in-depth analysis.

7.1 Laboratory

7.1.1 WSN

The experiment conduct on a clustered single-hop Wireless Sensor Network (WSN) utilizing three ESP32S NodeMCU devices which have 32-bit LX6 microprocessor [115]. Among these nodes, one serve as the sink which is equipped with an unlimited energy source. The second node is a standard node powered by a battery. The third node operates using the proposed EMS with a combination of two energy harvesters (Photovoltaic (PV) and Piezoelectric (PZT)) along with a battery as shown in Figure Figure 7.1.

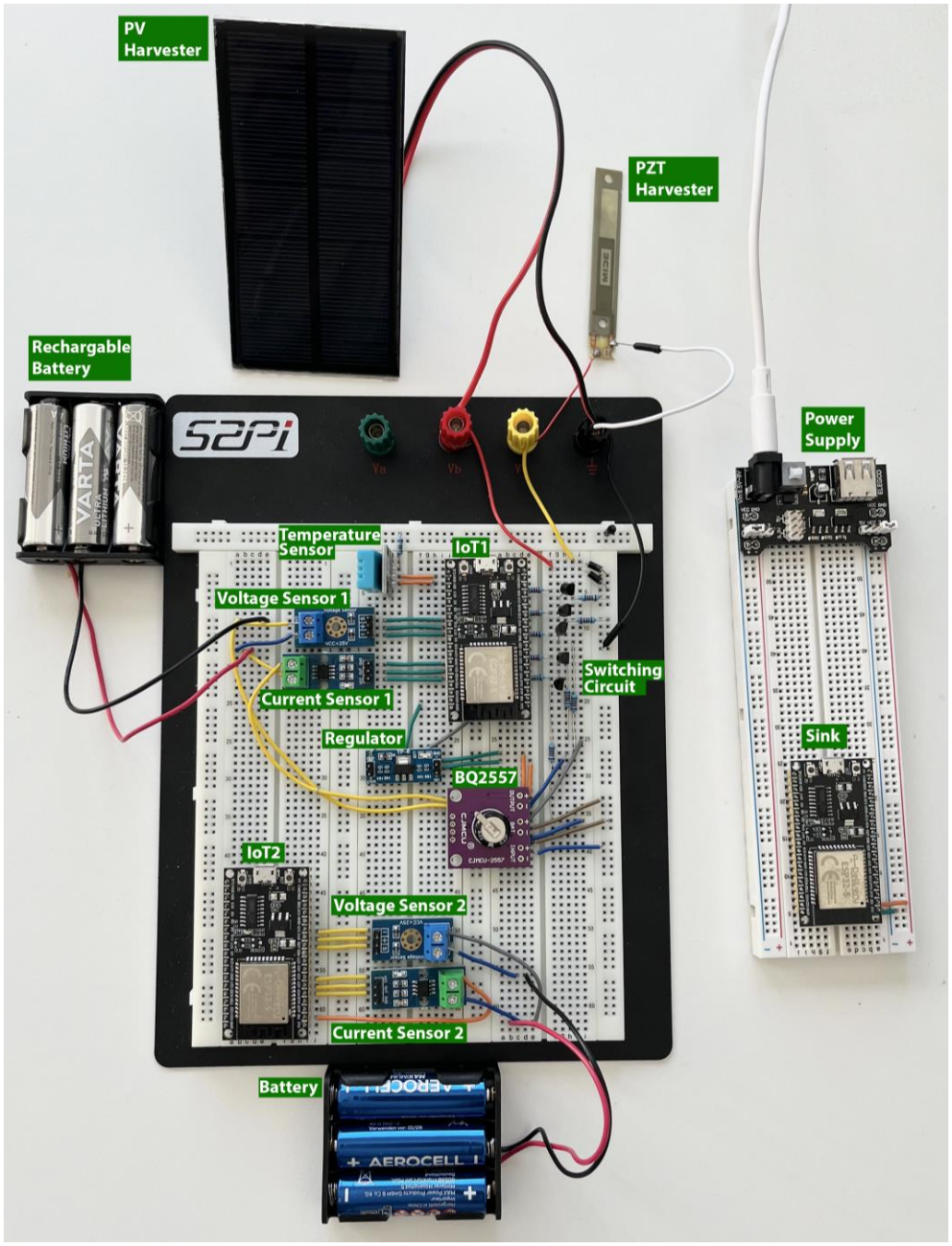

Figure 7.1 WSN setup

7.1.2 Vibration Part

The vibration part consists of PZT, function generator, and vibration generator connected as shown in Figure 7.2. PZT is S129-H5FR-1803YB which is a piezoelectric energy harvesting moule with dimensions of 71 mm x 10.3 mm x 0.74 mm, output power of 4.5mW, output voltage 28.2Vm and weight of 23.375 g. The function generator is designed to replicate the vibration acceleration signals observed from passing trains on a railway [116]. These signals are inputs to a vibration generator, which mimics real-world vibrations. A PZT harvester, attached to this generator, then produces electrical energy. This setup provides accurate laboratory measurements, an essential solution given the practical challenges of conducting such experiments on an actual railway. This approach ensures realistic data collection for energy harvesting research without the need for on-site railway testing.

Figure 7.2 Vibration Harvesting Part

7.1.3 EMS Circuit

The EMS circuit consists of switching circuit, voltage regulator, sensors, and a buck boost converter. The switching circuit is designed using Metal Oxide Semiconductor Field Effect Transistor (MOSFET) type P which are used as switches as shown in Figure 7.3. The control signal form microcontroller with open and close the transistors to behalf as switches to choose the energy source of the IoT device.

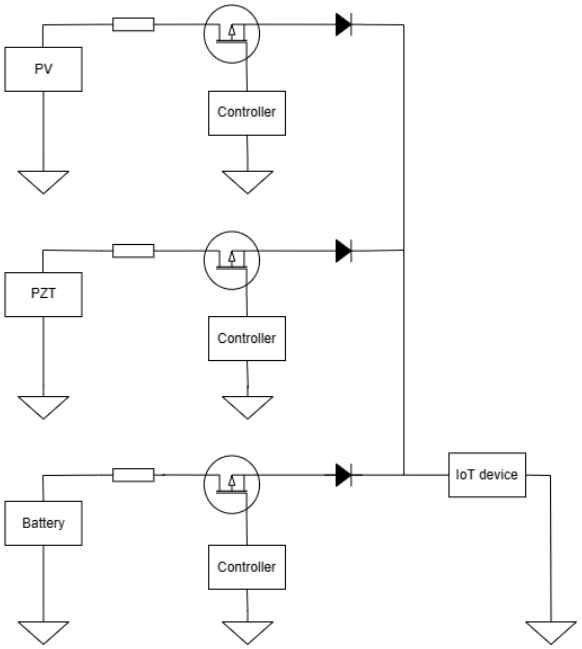

Figure 7.3 Switching Circuit

The chosen voltage regulator AMS1117 will guarantee delivering a fixed 3.3V to the IoT device as shown in. The output voltage is observed by choosing the values of the resistors in the equation:

$$V_{OUT} = V_{REF}\left(1 + \frac{R_2}{R_1}\right) + I_{ADJ}R_2 \tag{7.1}$$

Where:

- V_{OUT} is the output voltage
- V_{REF} is reference voltage between the output and the adjust terminal and equals 1.25V.
- I_{ADJ} is normally the specified minimum load current of 10mA.
- R_2 and R_1 are the resistors defines the value of output voltage.

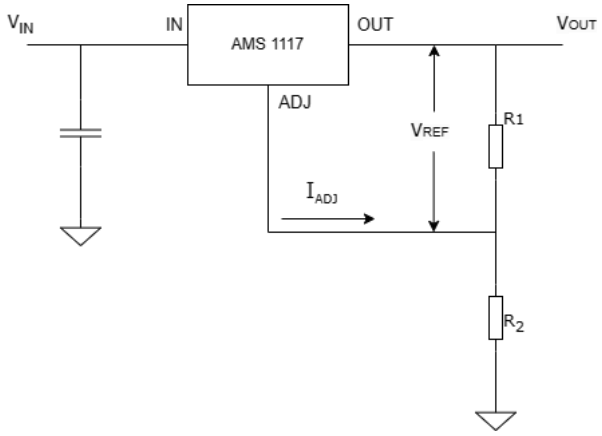

Figure 7.4 Voltage Regulator Circuit

The Buck-Boost converter utilized in this setup is the BQ25570, an ultra-low power operation Integrated Circuit (IC) from Texas Instruments. It is compatible with both Photovoltaic (PV) and Piezoelectric (PZT) harvesters and offers the capability to implement a Maximum Power Point Tracking (MPPT) algorithm.

The sensors employed in this setup include temperature, voltage, and current sensors. The temperature sensor will supply real-time temperature data to the Photovoltaic (PV) prediction algorithm and the Energy Management System (EMS) for battery protection. The voltage and current sensors are tasked with monitoring the battery's status and the energy flow. This monitoring is crucial for calculating the battery's state of charge and assessing its degradation.

7.1.4 Photovoltaic

The PV harvester is Polycrystalline Silicon solar panel with dimensions of 11*6 cm, maximum output power of 1W and working current of 0.25A.

Measurements Tools:

The measurement tools utilized in this setup include a 100MHz Bandwidth Oscilloscope for capturing and storing signal data for further analysis and visualization, along with a Digital Multimeter for reading instantaneous values.

The experiment bench is shown in Figure 7.5

Figure 7.5 Experiment bench

7.2 Setup

To implement the proposed EMS and QoS algorithm on the IoT device (ESP32S), a Software (SW) has been developed that encompasses the components illustrated in Figure 7.6. Upon initiation, this program establishes the necessary matrices, including logging temperature and harvested solar power values for the preceding 24 hours. Additionally, it sets constant values, such as the distance to the sink node and the minimum required Signal-to-Interference-plus-Noise Ratio (SINR).

Following initialization, the program commences an hourly timer. With each hour, the timer activates the subsequent procedure:

1. **Power prediction**: The SW employs the proposed hybrid model to forecast solar power for the upcoming hour based on the current month, day, hour, recorded temperature, and harvested solar energy. Additionally, it utilizes the lookup table to predict the mechanical power.

2. **Energy Management**: The SW initiates the proposed energy management algorithm upon obtaining the predicted values. It determines the optimal transmission power and duty cycle for the current time slot and configures the device to utilize them.

3. **Monitoring**: At the conclusion of the current time slot, the program logs various metrics, such as the battery's State of Charge (SoC), life cycle counters, and the actual harvested power.

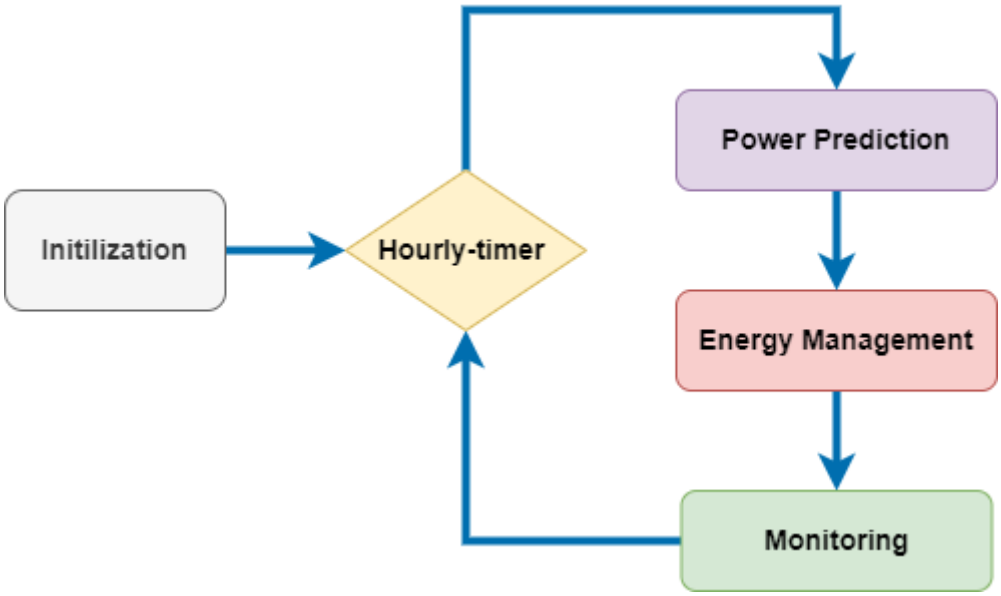

Figure 7.6 Implemented program blocks

7.3 Scenarios:

I examine two distinct scenarios involving two separate devices. In the first scenario, the device relies solely on the battery for energy. Conversely, in the second scenario, the device utilizes both solar and mechanical energy harvesters. Both devices operate for a duration of one week, specifically from the 15th to the 21st of September, 2023.

The proposed hybrid model for solar power prediction necessitates data from the preceding 24 hours, including temperature and actual harvested solar power. Consequently, the device in the two-harvester scenario commences in a passive mode for the initial 24 hours, solely recording the requisite values prior to the operation of the battery-only device. Moreover, I used the collected data to run the simulation for the same period.

7.4 Results

7.4.1 Power Predictions

Initially, I generate a plot of the actual versus predicted solar power, as depicted in Figure 7.7. It is evident from the plot that the predicted values align closely with the actual harvested power. Utilizing these observed values, I computed various metrics, the results of which are presented in Table 1. It is noteworthy that my proposed hybrid model achieved a remarkably low prediction error, with a Root Mean Square Error (RMSE) of 0.077 and a coefficient of determination ($\boldsymbol{R^2}$), of 0.958, where an optimal $\boldsymbol{R^2}$ value is 1.

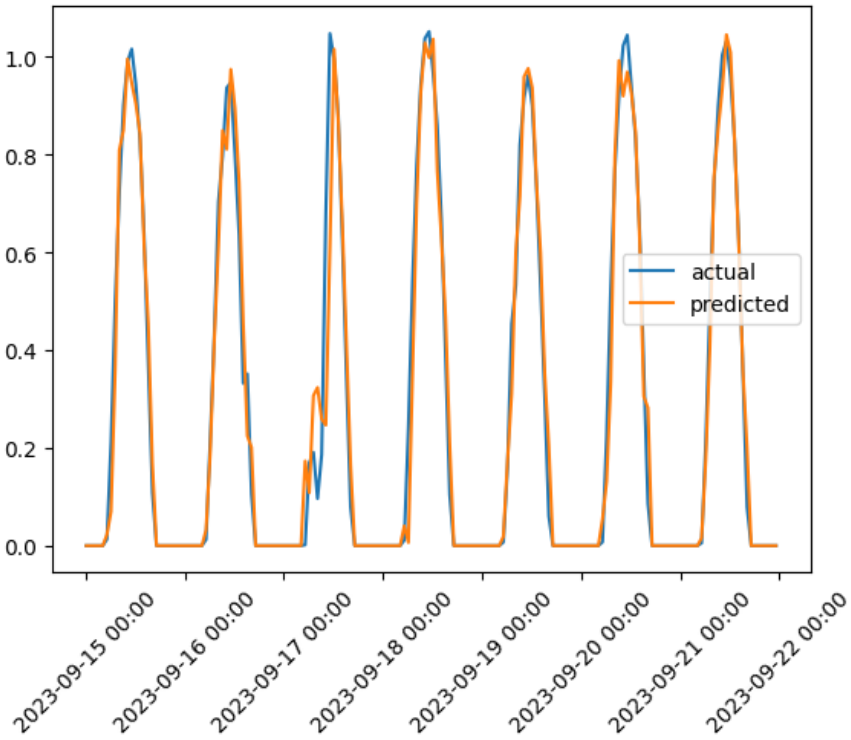

Figure 7.7 - Actual and predicted solar power

Table 7.1 - Prediction Metrics

Mean Squared Error (MSE)	**Mean Absolute Error (MAE)**	**Root Squared Error (RMSE)**	**R-squared (R^2)**

0.0059	0.03	0.077	0.958

7.4.2 Transmission Power

Throughout the entire experiment, I recorded the power level selected at each time slot for both devices, in addition to the simulation. The results are illustrated in Figure 7.8, which represents the frequency of each selected level for the different scenarios and the cumulative transmission power for the entire duration. It is observable that the battery scenario consistently utilizes the lowest level across all time slots. In contrast, the two-harvester and simulation scenarios predominantly select the highest level, approximately 70% of the time slots, specifically 67% for the two-harvester scenario and 73% for the simulation. This is further corroborated by the total transmission power, where the discrepancy between the two-harvester and simulation scenarios is approximately 2.5%.

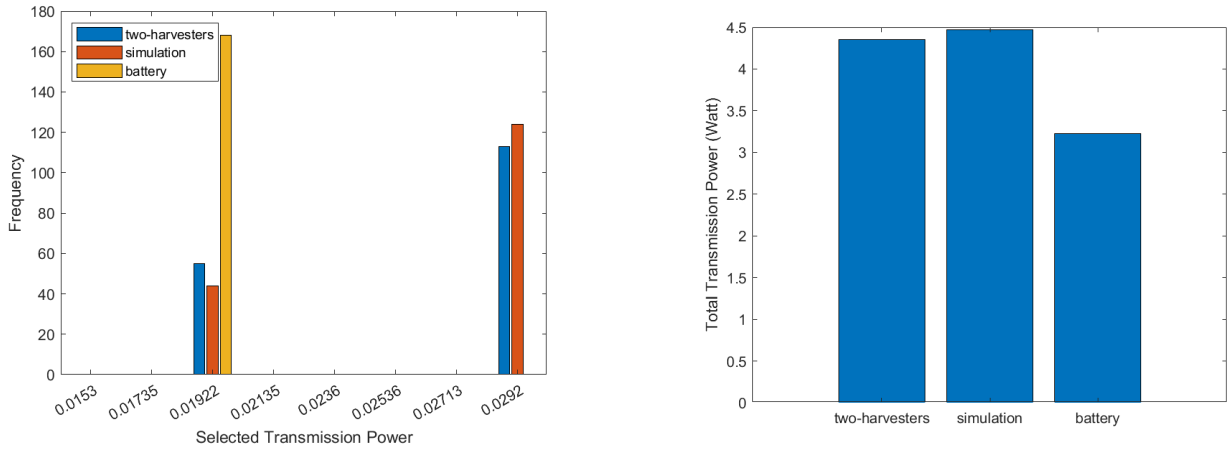

Figure 7.8 - Selected and total transmission power

7.4.3 Duty Cycle

As anticipated, the battery scenario consistently opts for the lowest duty cycle level across all time slots, as depicted in Figure 7.9. Conversely, the two-harvester and simulation scenarios select elevated levels contingent on the available energy. It is observable that the two-harvester scenario selects the highest level more frequently than the simulation, resulting in an increased total duty cycle duration. Quantitatively, the total duty cycle duration of the two-harvester scenario surpasses the simulation by approximately 2.3%.

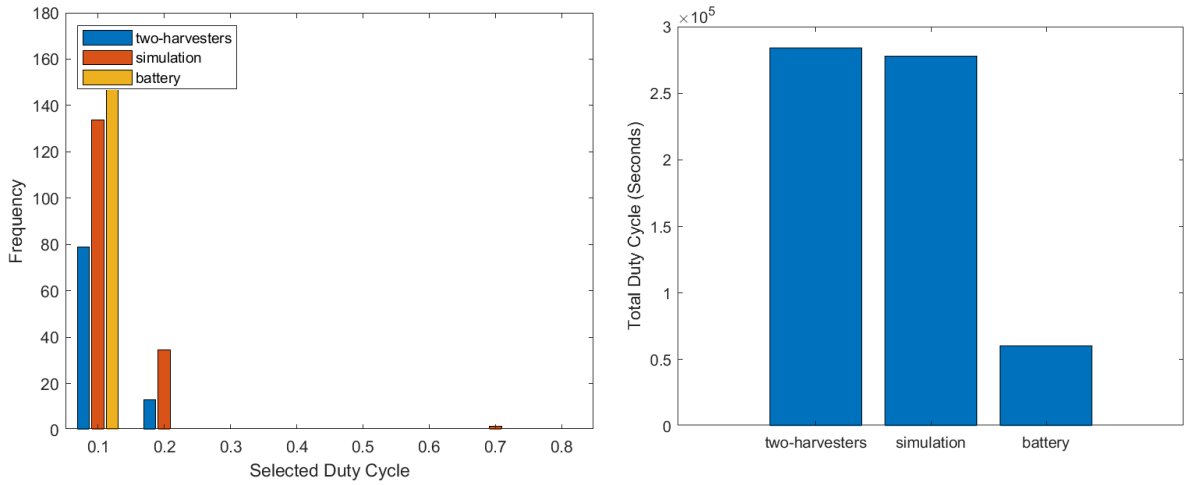

Figure 7.9 - Selected and total duty cycle

7.4.4 Battery Metrics

I have graphed the battery's SOC for the three scenarios, as illustrated in Figure 7.10. It is discernible that the battery scenario depleted approximately 3.5% of the battery by the conclusion of the experiment, while the two-harvester scenario utilized roughly 0.6%, a figure that aligns closely with the simulation results. However, the two-harvester scenario employs one of the harvesters to recharge the battery, which consequently reduces the battery's life cycle.

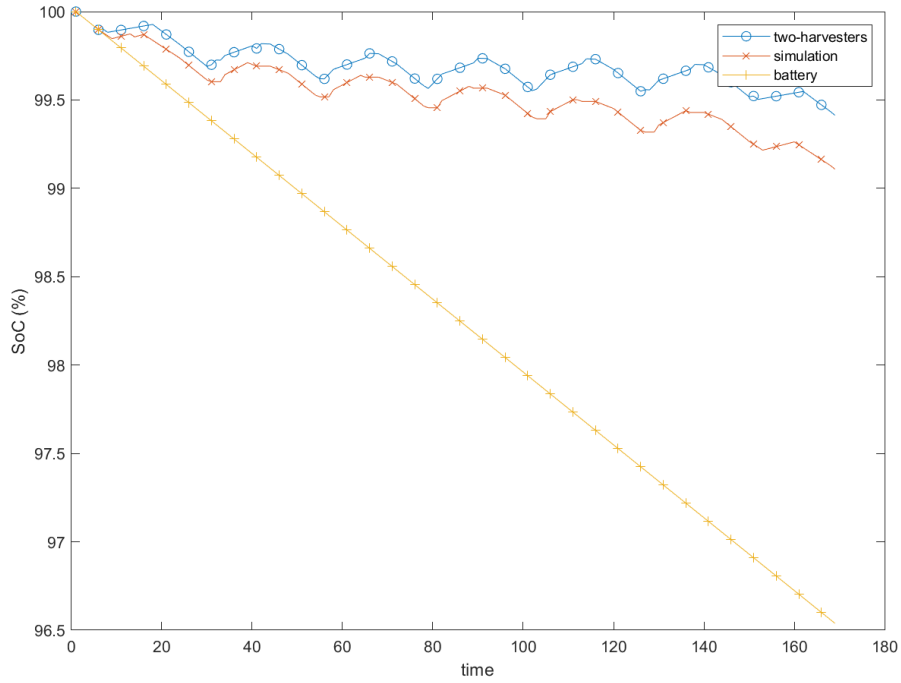

Figure 7.10 - SoC for the three scenarios

Figure 7.11 presents the full cycle metric and battery capacity, indicating that after approximately 140 hours, the device in the two-harvester scenario exhausts one full cycle. This is comparable to the simulation scenario, which reaches this point after about 150 hours. Contently this decreases the maximum battery capacity by 0.04% of its original capacity.

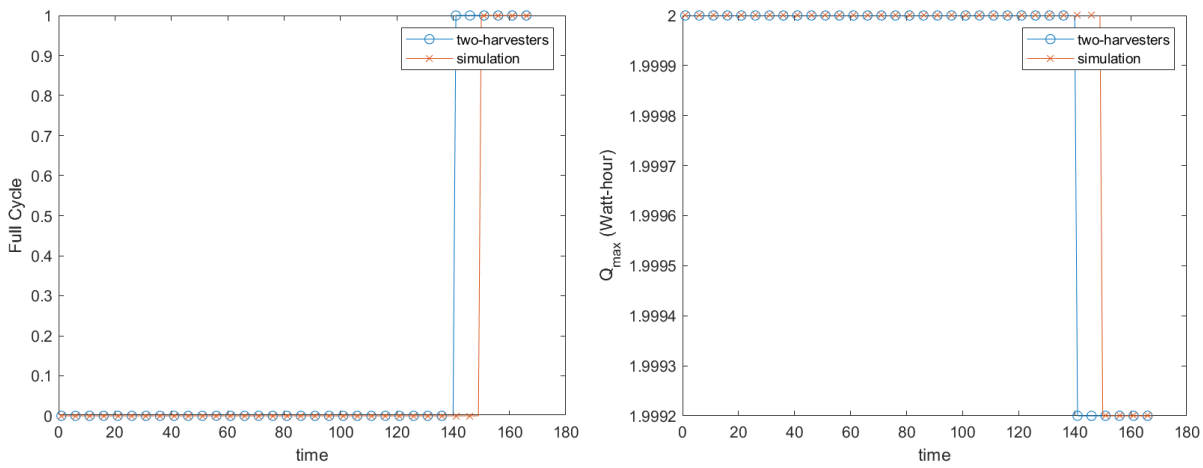

Figure 7.11 - Full cycle and battery capacity

8 CONCLUSION AND FUTURE WORK

The dissertation's goals require exploring various aspects of telecommunications, electrical engineering and computer science, focusing on WSN quality of service (QoS), energy harvesting systems, energy management systems, circuit design, machine learning, modeling, prediction algorithms, and optimization. Each chapter thoroughly describes a particular problem and introduces a novel solution as a contribution to the field.

In Chapter 2, I introduce the primary focus of my study: energy harvesting for Wireless Sensor Networks (WSN). The chapter begins with a detailed overview of the fundamentals of WSN, highlighting their diverse applications and the architecture of WSN nodes. Then I discuss energy management systems techniques in WSN, dividing them into two principal categories: Energy Consumption and Energy Provision. Further in the chapter, I concentrate on energy storage resources for WSN nodes; particular emphasis is put on batteries and supercapacitors. Through comprehensive comparisons among different types, I conclude this segment with a summary, highlighting the batteries and supercapacitor as some of the most efficient energy resources for WSN nodes. Then, I explore energy harvesting techniques as a viable alternative for energy storage devices in WSN nodes. I present a comparative analysis of these techniques, resulting in a summary that identifies Photovoltaic (PV) and Piezoelectric (PZT) harvesters as having the highest energy density. However, I also highlight the challenges associated with energy harvesting for WSN nodes, mainly due to their intermittent nature. In the final section of the chapter, I address the potential of multi-input energy harvesting systems to overcome these challenges. Here, I review various techniques utilized in multi-input energy harvesting systems, comparing them in order to provide insights into their effectiveness and practicality for application in WSN. This comprehensive examination highlights these systems' potential to enhance the efficiency and reliability of energy provision in WSN networks.

In Chapter 3, I deal with Energy Management System (EMS) fundamental requirements for IoT devices. To address these requirements, I propose an EMS architecture, drawing on insights from the comprehensive review in Chapter 2. This includes an in-depth exploration of piezoelectric and photovoltaic energy harvesting theories and an introduction to electrical and mathematical modeling. I explain in detail the sizing of Piezoelectric (PZT) and Photovoltaic (PV) harvesters tailored for this specific application. Furthermore, I introduce novel energy-combining techniques utilizing a multi-input buck-boost converter. This approach allows for selecting an energy source based on the predicted

output power. I also present advanced battery management system techniques, including State of Charge (SoC) estimation, capacity fade estimation, health monitoring, and protection mechanisms. A significant contribution of this chapter is the proposal of a new energy combining technique, employing a multi-input buck-boost converter. Besides that, I introduce a novel algorithm designed to calculate battery degradation. The chapter is concluded with a comprehensive discussion on the design of the dynamic behavior of the EMS and its energy flow. This section emphasizes how the EMS is suitably structured to adapt to varying conditions and requirements, underlining the adaptability and robustness of the proposed system.

Chapter 4 explores the motivation behind studying PV energy prediction, explicitly focusing on short-term forecasting methods. I classify these methods in this chapter and provide a comprehensive state-of-the-art overview. This overview encompasses physical methods, statistical methods (including regression and time series-based approaches), hybrid methods, and adaptive methods. The chapter deals with methods that employ Neural Networks and Support Vector Machines. I conclude this section by summarizing the advantages and disadvantages of each method, discussing the challenges they encounter, and presenting a comparative table of their prediction errors. It is noted that the physical method exhibits the highest possible error (45%), while the hybrid method demonstrates the lowest prediction error (3%). The chapter then shifts its focus to deep learning for short-term prediction. I begin by establishing the rationale for choosing deep learning techniques and proceed to examine various methods in this domain, including Deep Neural Networks (DNN), Recurrent Neural Networks (RNN), Long Short-Term Memory (LSTM) networks, and Convolutional Neural Networks (CNN). A review of the current state-of-the-art applications of these techniques for short-term forecasting is provided, along with a comparative analysis of their effectiveness. Furthermore, the chapter presents an in-depth dataset analysis that includes historical data from a solar panel equipped with temperature, wind, and irradiation sensors. To choose the proper model for the data set, DNN, CNN, and LSTM models are developed and compared based on their Mean Absolute Error (MAE) and Mean Squared Error (MSE). This analysis reveals that the CNN model features the lowest prediction errors for the chosen dataset. Subsequently, I describe the development of a novel prediction algorithm using CNN. I focus on the trade-off between model complexity and performance, which is particularly important as the model is intended for use in an embedded device with limited size and computing power. I compare the impact of the number of filters and model size on both the MAE and MSE. This comparison leads to the conclusion that the ideal balance is achieved with the CNN4 or CNN8 models. To further enhance the accuracy of the developed model, I combine the statistical method with the CNN model to mitigate noise and reduce prediction errors. This integration results in a significant error reduction of

approximately 7% in MAE and 3.5% in MSE, illustrating the efficacy of this hybrid approach in improving the accuracy of PV energy prediction.

In Chapter 5, I conduct a comprehensive analysis of the QoS requirements and challenges in WSN, with a focus on critical factors such as latency, reliability, bandwidth, energy efficiency, and duty cycle, which are essential for effective communication in WSN. The chapter deals with various strategies to enhance QoS, including techniques like data compression, power transmission optimization, and machine learning. This explains the motivation behind developing a method that adaptively adjusts power transmission and duty cycle based on available energy to maintain high QoS standards. To achieve this objective, the chapter begins with designing a system model to optimize battery load while preserving the QoS. This model balances the need for energy efficiency to prolong battery life against the necessity of reliable data transmission. I introduce an equation to quantify the total data transmitted by an IoT device in an hour, considering its active state and duty cycles. Following this, I propose a channel model that considers the path loss exponent n for different environmental conditions. I also introduce an energy consumption model incorporating elements like the duty cycle and transmission power. Additionally, I present a detailed battery model, which includes aspects such as the battery's state of charge, degradation, and the energy it receives from harvesters. The chapter then moves on to introduce a QoS model, defining a QoS enhancement function that includes variables such as duty cycle and transmission power. Subsequently, I formulate the multi-objective optimization problem to maximize transmission power and duty cycle while minimizing energy consumption. The main contribution of this chapter is the development of an adaptive QoS algorithm energy awareness. This algorithm is designed to adapt the device's duty cycle and transmission power based on the anticipated energy input from the harvesters in each time slot. This approach aligns to efficiently manage energy while maintaining robust QoS standards in WSN, thereby addressing one of the critical challenges in WSN.

Chapter 6 outlines the simulation setup for an IoT device, incorporating real-world parameters like transmission power, energy consumption, and path loss values. In this chapter, I describe a series of simulation experiments conducted to evaluate the effectiveness of the proposed algorithm. These experiments involve running the algorithm across various values for all variables in the optimization problem, using a grid search technique to determine the impact of these variables on performance. I compare the performance of the proposed algorithm, which employs dual energy harvesters, with scenarios using either a single energy harvester or none. The results show that the Signal to Noise Ratio (SNR) across the different scenarios and for various path loss values reaches its maximum with the proposed EMS, outperforming traditional energy harvesting setups and battery-only configurations. I

observe the same results in the analysis of transmission power values. To study the impact of the proposed algorithm on the battery SoC and SoH, I perform the simulation over 15 years. The data demonstrates a significant enhancement in QoS achieved with the proposed QoS adaptive algorithm and EMS compared to traditional methods, which show a notable drop in QoS over time. The findings indicate that a battery alone powers the IoT device for 5000 hours; a mechanical harvester extends this time to 8300 hours; and a solar harvester to 9100 hours. However, under the proposed EMS, the battery's SoC remains above 90%, indicating a sustainable operation for the battery's SoH; the results indicate that with mechanical harvesters, the battery capacity drops below 80% of its maximum after 32640 hours, and with solar harvesters after 48800 hours. In contrast, with the implementation of the proposed EMS, this reduction in capacity occurs much later, after 66000 hours. This confirms the efficacy of the proposed system in not only extending the battery life but also in significantly enhancing the QoS of the IoT device.

In Chapter 7, I describe my implementation of the adaptive QoS algorithm and proposed EMS on an IoT device, specifically the ESP32S NodeMCU. The setup begins with a WSN consisting of three nodes in a clustered single-hop topology. One node is equipped with the adaptive QoS algorithm and the proposed EMS, another one operates traditionally using only a battery, and the third one serves as the sink node with an unlimited energy source. The implementation of vibration experiments is detailed next, using a vibration generator and function generator to simulate real-world vibrations akin to those on train railways. The chapter then introduces the PZT harvester and the PV harvester. Attention is paid to the EMS circuits, including switching circuits, the voltage regulator AMS1117, and the buck-boost converter, where BQ25570 is used. The sensors used for current, voltage, and temperature measurements and the employed measurement tools are mentioned. The setup of the experiments is described, highlighting how the proposed QoS algorithm and EMS are implemented on the IoT device ESP32S NodeMCU. Two experimental scenarios matching practical applications are mentioned. The first scenario involves a device relying on battery power, while the second one utilizes PV and PZT energy harvesters. These experiments were conducted over a week. The chapter then discusses the observed results, focusing on the IoT device's transmission power and duty cycle with the proposed EMS and adaptive QoS algorithms implemented, compared to the battery-powered IoT device. It assesses the accuracy of measured results against simulation data, using metrics like Mean Squared Error (MSE), Mean Absolute Error (MAE), Root Squared Error (RMSE), and R squared (R^2). The results reveal a discrepancy of approximately 2.5% for transmission power and 2.3% for duty cycle between experiments and simulation scenarios. Finally, the chapter compares the SoC for the IoT device with the implemented proposed EMS and adaptive QoS algorithm against the battery-powered IoT device. During the week-long experiment, the SoC of the battery-powered IoT device dropped to 96.5%. In

comparison, the SoC for the device with the implemented EMS and adaptive QoS algorithm remained above 99.5%, demonstrating the effectiveness of the proposed system in maintaining energy efficiency.

8.1 Main Contributions

I summarize the main contributions as follows:

- A novel energy management system EMS design for communication devices, with special emphasis on IoT applications.
- A novel energy combining technique, employing a multi-input buck-boost converter, choosing the predicted data's energy source base.
- A novel algorithm for battery degradation calculation.
- A novel hybrid energy prediction algorithm using CNN and statistical methods.
- A novel adaptive QoS algorithm for WSN devices energy awareness.

8.2 Fulfillment of Dissertation Goals

Here, all the dissertation goals defined in Chapter 1 are presented again and demonstrate how these objectives have been successfully achieved.

Objective 1: To design a novel Energy Management System (EMS) that combines the energy from two harvesters, Photovoltaic and Piezoelectric, to extend the life span of WSN node batteries. The achievement of this objective is described in chapter 3 where a novel design of the EMS is introduced. EMS combine the energy from PV and PZT harvesters to charge the battery. Chapter 6 shows that the life span of WSN node battery will drop by 20% in case of using PZT in 3.7 years, for PV in 5.5 years, and for the proposed EMS in 7.5 years.

Objective 2: To study various solar energy forecasting methods, including physical, statistical, adaptive, and hybrid models, focusing on their effectiveness and accuracy, mainly through machine learning and deep learning techniques. The achievement of this objective is described in chapter 4, where I summarize the advantages and disadvantages of each method, discussing the challenges they encounter, and presenting a comparative table of their prediction errors. Then I present the developed

models for deep learning methods DNN, CNN, and LSTM and compare them based on their Mean Absolute Error (MAE) and Mean Squared Error (MSE).

Objective 3: To develop and validate a novel hybrid forecasting algorithm that integrates a Random Forest classifier with a Convolutional Neural Network (CNN) model, aiming to enhance the precision and efficiency of solar energy predictions, focusing on optimizing the model for potential deployment in Wireless Sensor Network node. The achievement of this objective is described in Chapter 4, where I propose a novel prediction algorithm using CNN. Then, I optimize the model to be used in embedded devices by trading between the size and accuracy. Furthermore, I combine a statistical method with the CNN model to mitigate noise and reduce prediction errors, which enhance the accuracy. I achieved a significant reduction of approximately 7% in MAE and 3.5% in MSE, illustrating the efficacy of this hybrid approach in improving the accuracy of PV energy prediction.

Objective 4: To develop an algorithm and a framework that ensures high Quality of Service QoS while efficiently using the battery to extend the operational life and lifespan of the wireless sensor node. And validate the proposed algorithm with actual data using realistic Energy Management System (EMS) hardware and Wireless Sensor Network. The achievement of this objective is described in Chapter 5, where I present the designed algorithm to adapt the device's duty cycle and transmission power based on the anticipated energy input from the harvesters in each time slot. I start by creating models for data transmission, channel, energy consumption, and detailed battery models. Then, I define the QoS enhancement, including transmission power and duty of cycle. After that, I formulate a Multi-objective optimization problem to maximize transmission power and duty cycle while minimizing energy consumption, and I solve it using the grid search technique. In Chapter 6, I examine the algorithm with real data for transition power and path loss (collected for 15 years), and I prove the efficiency of the algorithm by comparing different scenarios. In Chapter 7, I describe the experiments using WSN mode up of three ESP32S NodeMCU (performed for one week); the results match the simulation results very well, differing just by 2.5% to 3%.

8.3 Future Work

Future research building on this dissertation could expand in several directions. One key area is the investigation of cross-layer design strategies. This approach would consider the interactions between network layers, such as physical, MAC, and network layers to optimize overall network performance. Additionally, exploring energy efficiency and Quality of Service (QoS) in multi-hop Wireless Sensor

Networks (WSN) would be valuable, mainly because the current research focuses on single-hop architectures.

Incorporating more QoS factors, particularly security, is another significant challenge for future work. The extra energy available from efficient energy management could enhance network security. This aspect becomes increasingly essential as IoT networks expand and integrate into critical infrastructure and services.

Future research should investigate more efficient energy harvesting methods to further enhance the sustainability of communication devices, with special emphasis on IoT applications. This could include combining energy from unlimited energy harvesters and considering their simultaneous use. Such advancements would push the boundaries of energy harvesting and management, leading to more robust and long-lasting IoT devices capable of operating in diverse and challenging environments.

Another important research direction is to enhance the accuracy of the prediction algorithm for photovoltaic (PV) systems. This involves refining the algorithm to ensure higher precision in energy predictions, which is crucial for effective energy management in future communication networks.

References

[1] V. Potdar, A. Sharif, and E. Chang, “Wireless Sensor Networks: A Survey,” in *2009 International Conference on Advanced Information Networking and Applications Workshops*, May 2009, pp. 636–641. doi: 10.1109/WAINA.2009.192.

[2] S. Shankar, G. Deepika, G. Devi, S. Ramesh, S. Srivastava, and S. S. Kumar, “Development of Efficient Wireless Sensor Network for IoT Applications,” in *2023 3rd International Conference on Pervasive Computing and Social Networking (ICPCSN)*, Salem, India: IEEE, Jun. 2023, pp. 1419–1424. doi: 10.1109/ICPCSN58827.2023.00237.

[3] A. Othman and D. Maga, “Relation Between Security and Energy Consumption in Wireless Sensor Network (WSN),” in *2018 New Trends in Signal Processing (NTSP)*, Liptovský Mikuláš, Slovakia: IEEE, Oct. 2018, pp. 1–8. doi: 10.23919/NTSP.2018.8524094.

[4] S. Yoo and T. Kim, “Industrial Wireless Sensor Networks: Protocols and Applications,” *Sensors*, vol. 20, no. 20, Art. no. 20, Jan. 2020, doi: 10.3390/s20205809.

[5] M. Pejanovi and G. Dimi, “A survey of military applications of wireless sensor networks,” 2012.

[6] V. R. Adama, “Wireless Sensor Network Architecture for Smart Buildings”.

[7] P. N. Mosana and T. Muchenje, “An Intelligent ZigBee Algorithm for Healthcare Monitoring System using Wireless Sensor Networks,” in *2022 International Conference on Computational Science and Computational Intelligence (CSCI)*, Las Vegas, NV, USA: IEEE, Dec. 2022, pp. 1700–1704. doi: 10.1109/CSCI58124.2022.00302.

[8] G. M. E. Rahman, K. A. Wahid, and A. Dinh, “IoT enabled Low power and Wide range WSN platform for environment monitoring application,” in *2020 IEEE Region 10 Symposium (TENSYMP)*, Dhaka, Bangladesh: IEEE, 2020, pp. 908–911. doi: 10.1109/TENSYMP50017.2020.9230959.

[9] E. Vlasceanu, M. Dima, D. Popescu, and L. Ichim, “Sensor and Communication Considerations in UAV-WSN Based System for Precision Agriculture,” in *2019 IEEE International Conference on Cybernetics and Intelligent Systems (CIS) and IEEE Conference on Robotics, Automation and Mechatronics (RAM)*, Bangkok, Thailand: IEEE, Nov. 2019, pp. 281–286. doi: 10.1109/CIS-RAM47153.2019.9095823.

[10] J. A. Khan, H. K. Qureshi, and A. Iqbal, “Energy management in Wireless Sensor Networks: A survey,” *Comput. Electr. Eng.*, vol. 41, pp. 159–176, Jan. 2015, doi: 10.1016/j.compeleceng.2014.06.009.

[11] F. Wang *et al.*, “To Reduce Delay, Energy Consumption and Collision through Optimization Duty-Cycle and Size of Forwarding Node Set in WSNs,” *IEEE Access*, vol. 7, pp. 55983–56015, 2019, doi: 10.1109/ACCESS.2019.2913885.

[12] E. Taqieddin, F. Awad, and H. Ahmad, “Location-Aware and Mobility-Based Performance Optimization for Wireless Sensor Networks”.

[13] J. Zhang, Z. Lin, P.-W. Tsai, and L. Xu, “Entropy-driven data aggregation method for energy-efficient wireless sensor networks,” *Inf. Fusion*, vol. 56, pp. 103–113, Apr. 2020, doi: 10.1016/j.inffus.2019.10.008.

[14] F. K. Shaikh and S. Zeadally, “Energy harvesting in wireless sensor networks: A comprehensive review,” *Renew. Sustain. Energy Rev.*, vol. 55, pp. 1041–1054, Mar. 2016, doi: 10.1016/j.rser.2015.11.010.

[15] A. Othman, “Energy storage system options in Intelligent Wireless Sensor Network,” in *2017 International Conference on Military Technologies (ICMT)*, Brno, Czech Republic: IEEE, May 2017, pp. 772–778. doi: 10.1109/MILTECHS.2017.7988860.

[16] T. S. Aina, O. O. Akinte, and B. Iyaomolere, “Wireless Charging System and Mobile sensors: A Comprehensive Review,” vol. 5, no. 2.

[17] N. A. Pantazis, S. A. Nikolidakis, and D. D. Vergados, “Energy-Efficient Routing Protocols in Wireless Sensor Networks: A Survey,” *IEEE Commun. Surv. Tutor.*, vol. 15, no. 2, pp. 551–591, 2013, doi: 10.1109/SURV.2012.062612.00084.

[18] T. Ying, X. Gao, W. Hu, F. Wu, and D. Noreus, “Studies on rechargeable NiMH batteries,” *Int. J. Hydrog. Energy*, vol. 31, no. 4, pp. 525–530, Mar. 2006, doi: 10.1016/j.ijhydene.2005.04.018.

[19] X. Luo, J. Wang, M. Dooner, and J. Clarke, “Overview of current development in electrical energy storage technologies and the application potential in power system operation,” *Appl. Energy*, vol. 137, pp. 511–536, Jan. 2015, doi: 10.1016/j.apenergy.2014.09.081.

[20] H. Chen, T. N. Cong, W. Yang, C. Tan, Y. Li, and Y. Ding, “Progress in electrical energy storage system: A critical review,” *Prog. Nat. Sci.*, vol. 19, no. 3, pp. 291–312, Mar. 2009, doi: 10.1016/j.pnsc.2008.07.014.

[21] L. G. H. Staaf, P. Lundgren, and P. Enoksson, “Present and future supercapacitor carbon electrode materials for improved energy storage used in intelligent wireless sensor systems,” *Nano Energy*, vol. 9, pp. 128–141, Oct. 2014, doi: 10.1016/j.nanoen.2014.06.028.

[22] A. R. Dehghani-Sanij, E. Tharumalingam, M. B. Dusseault, and R. Fraser, “Study of energy storage systems and environmental challenges of batteries,” *Renew. Sustain. Energy Rev.*, vol. 104, pp. 192–208, Apr. 2019, doi: 10.1016/j.rser.2019.01.023.

[23] A. Kansal, J. Hsu, S. Zahedi, and M. B. Srivastava, “Power management in energy harvesting sensor networks,” *ACM Trans. Embed. Comput. Syst.*, vol. 6, no. 4, p. 32, Sep. 2007, doi: 10.1145/1274858.1274870.

[24] A. Othman, “Modeling of piezoelectric energy harvesting system embedded in soldier’s boot using Matlab/Simulink,” in *2017 International Conference on Military Technologies (ICMT)*, May 2017, pp. 787–792. doi: 10.1109/MILTECHS.2017.7988862.

[25] S. Bradai, G. Bouattour, S. Naifar, and O. Kanoun, “Electromagnetic Energy Harvester for Battery-Free IoT Solutions,” in *2020 IEEE 6th World Forum on Internet of Things (WF-IoT)*, Jun. 2020, pp. 1–5. doi: 10.1109/WF-IoT48130.2020.9221051.

[26] A. Othman and D. Maga, “Indoor Photovoltaic Energy Harvester with Rechargeable Battery for Wireless Sensor Node,” in *2018 18th International Conference on Mechatronics - Mechatronika (ME)*, Dec. 2018, pp. 1–6. Accessed: Dec. 13, 2023. [Online]. Available: https://ieeexplore.ieee.org/document/8624684

[27] A. M. Abdal-Kadhim and K. S. Leong, “Application of thermal energy harvesting from low-level heat sources in powering up WSN node,” in *2017 2nd International Conference on Frontiers of Sensors Technologies (ICFST)*, Apr. 2017, pp. 131–135. doi: 10.1109/ICFST.2017.8210489.

[28] M. Amokrane, A. Baysse, B. Nogarede, and M. Rguiti, “Pyroelectric power harvesting using a lead-lanthanum-zirconate-titanate (7/60/40 PLZT) pyroelectric cell,” in *2013 IEEE 11th International Workshop of Electronics, Control, Measurement, Signals and their application to Mechatronics*, Jun. 2013, pp. 1–6. doi: 10.1109/ECMSM.2013.6648972.

[29] M. Kurvey and A. Kunte, “RF Energy Harvesting System,” in *2018 International Conference on Smart City and Emerging Technology (ICSCET)*, Jan. 2018, pp. 1–4. doi: 10.1109/ICSCET.2018.8537306.

[30] S. Roundy, P. K. Wright, and J. Rabaey, “A study of low level vibrations as a power source for wireless sensor nodes,” *Comput. Commun.*, vol. 26, no. 11, pp. 1131–1144, Jul. 2003, doi: 10.1016/S0140-3664(02)00248-7.

[31] A. Jushi, A. Pegatoquet, and T. N. Le, “Wind Energy Harvesting for Autonomous Wireless Sensor Networks,” in *2016 Euromicro Conference on Digital System Design (DSD)*, Aug. 2016, pp. 301–308. doi: 10.1109/DSD.2016.43.

[32] Y. Gao, L. Liu, J. Cho, and S. Choi, “Flexible and Scalable Biochemical Energy Harvesting: A Yarn-Based Biobattery,” in *2019 IEEE 32nd International Conference on Micro Electro Mechanical Systems (MEMS)*, Jan. 2019, pp. 966–969. doi: 10.1109/MEMSYS.2019.8870873.

[33] S. Salem, K. Fraňa, I. Nová, and J. Erhart, “Acoustic Energy Harvesting Using Piezo-Electric Materials,” in *2020 International Youth Conference on Radio Electronics, Electrical and Power Engineering (REEPE)*, Mar. 2020, pp. 1–6. doi: 10.1109/REEPE49198.2020.9059190.

[34] G. Yang, B. H. Stark, S. J. Hollis, and S. G. Burrow, “Challenges for Energy Harvesting Systems Under Intermittent Excitation,” *IEEE J. Emerg. Sel. Top. Circuits Syst.*, vol. 4, no. 3, pp. 364–374, Sep. 2014, doi: 10.1109/JETCAS.2014.2337172.

[35] “JRC Photovoltaic Geographical Information System (PVGIS) - European Commission.” Accessed: Feb. 05, 2024. [Online]. Available: https://re.jrc.ec.europa.eu/pvg_tools/en/#DR

[36] “Chicago North Bridge | Real Vibrations.” Accessed: Feb. 05, 2024. [Online]. Available: https://realvibrations.nipslab.org/node/550

[37] J. Estrada-López, A. Abuellil, Z. Zeng, and E. Sánchez-Sinencio, “Multiple Input Energy Harvesting Systems for Autonomous IoT End-Nodes,” *J. Low Power Electron. Appl.*, vol. 8, no. 1, p. 6, Mar. 2018, doi: 10.3390/jlpea8010006.

[38] A. Othman, J. Hrad, J. Hajek, and D. Maga, “Control Strategies of Hybrid Energy Harvesting—A Survey,” *Sustainability*, vol. 14, no. 24, Art. no. 24, Jan. 2022, doi: 10.3390/su142416670.

[39] M. R. Elhebeary, M. A. A. Ibrahim, M. M. Aboudina, and A. N. Mohieldin, “Dual-Source Self-Start High-Efficiency Microscale Smart Energy Harvesting System for IoT,” *IEEE Trans. Ind. Electron.*, vol. 65, no. 1, pp. 342–351, Jan. 2018, doi: 10.1109/TIE.2017.2714119.

[40] C. Vanhecke *et al.*, “Multisource and Battery-Free Energy Harvesting Architecture for Aeronautics Applications,” *IEEE Trans. Power Electron.*, vol. 30, no. 6, pp. 3215–3227, Jun. 2015, doi: 10.1109/TPEL.2014.2331365.

[41] F. Deng, X. Yue, X. Fan, S. Guan, Y. Xu, and J. Chen, “Multisource Energy Harvesting System for a Wireless Sensor Network Node in the Field Environment,” *IEEE Internet Things J.*, vol. 6, no. 1, pp. 918–927, Feb. 2019, doi: 10.1109/JIOT.2018.2865431.

[42] M. Ferrari, V. Ferrari, M. Guizzetti, D. Marioli, and A. Taroni, “Piezoelectric multifrequency energy converter for power harvesting in autonomous microsystems,” *Sens. Actuators Phys.*, vol. 142, no. 1, pp. 329–335, Mar. 2008, doi: 10.1016/j.sna.2007.07.004.

[43] D. Carli, D. Brunelli, L. Benini, and M. Ruggeri, “An effective multi-source energy harvester for low power applications,” in *2011 Design, Automation & Test in Europe*, Grenoble: IEEE, Mar. 2011, pp. 1–6. doi: 10.1109/DATE.2011.5763142.

[44] Y. K. Tan and S. K. Panda, “Energy Harvesting From Hybrid Indoor Ambient Light and Thermal Energy Sources for Enhanced Performance of Wireless Sensor Nodes,” *IEEE Trans. Ind. Electron.*, vol. 58, no. 9, pp. 4424–4435, Sep. 2011, doi: 10.1109/TIE.2010.2102321.

[45] A. Othman, D. Maga, and J. Hrad, “Multi-input Energy Harvesting System with Battery Management Support for WSN Applications,” in *2022 20th International Conference on Mechatronics - Mechatronika (ME)*, Dec. 2022, pp. 1–4. doi: 10.1109/ME54704.2022.9983095.

[46] J. Amanor-Boadu, M. A. Abouzied, S. Carreon-Bautista, R. Ribeiro, X. Liu, and E. Sanchez-Sinencio, “A switched mode Li-ion battery charger with multiple energy harvesting systems simultaneously used as input sources,” in *2014 IEEE 57th International Midwest Symposium on Circuits and Systems (MWSCAS)*, College Station, TX, USA: IEEE, Aug. 2014, pp. 330–333. doi: 10.1109/MWSCAS.2014.6908419.

[47] R. V. C. Adrivan, R. K. G. Conde, A. B. Caberos, and C. T. C. Doloriel, “An Energy Combiner for Multi-Source Energy Harvesting with Charge Control,” in *2019 19th International Symposium on Communications and Information Technologies (ISCIT)*, Ho Chi Minh City, Vietnam: IEEE, Sep. 2019, pp. 371–376. doi: 10.1109/ISCIT.2019.8905138.

[48] F. Caricchi, F. Crescimbini, A. D. Napoli, O. Honorati, and E. Santini, “Testing of a new DC/DC converter topology for integrated wind-photovoltaic generating systems,” in *1993 Fifth European Conference on Power Electronics and Applications*, Sep. 1993, pp. 83–88 vol.8. Accessed: Dec. 12, 2023. [Online]. Available: https://ieeexplore.ieee.org/abstract/document/264746

[49] Yaow-Ming Chen, Yuan-Chuan Liu, and Feng-Yu Wu, “Multi-input DC/DC converter based on the multiwinding transformer for renewable energy applications,” *IEEE Trans. Ind. Appl.*, vol. 38, no. 4, pp. 1096–1104, Jul. 2002, doi: 10.1109/TIA.2002.800776.

[50] H. Matsuo, K. Kobayashi, Y. Sekine, M. Asano, and Lin Wenzhong, “Novel solar cell power supply system using the multiple-input DC-DC converter,” in *INTELEC - Twentieth International Telecommunications Energy Conference (Cat. No.98CH36263)*, San Francisco, CA, USA: IEEE, 1999, pp. 797–802. doi: 10.1109/INTLEC.1998.793656.

[51] R. Redl, L. Balogh, and D. W. Edwards, “Optimum ZVS full-bridge DC/DC converter with PWM phase-shift control: analysis, design considerations, and experimental results,” in *Proceedings of 1994 IEEE Applied Power Electronics Conference and Exposition - ASPEC’94*, Feb. 1994, pp. 159–165 vol.1. doi: 10.1109/APEC.1994.316405.

[52] J. Colomer-Farrarons, P. Miribel-Catala, A. Saiz-Vela, and J. Samitier, “A Multiharvested Self-Powered System in a Low-Voltage Low-Power Technology,” *IEEE Trans. Ind. Electron.*, vol. 58, no. 9, pp. 4250–4263, Sep. 2011, doi: 10.1109/TIE.2010.2095395.

[53] C.-W. Liu, H.-H. Lee, P.-C. Liao, Y.-L. Chen, M.-J. Chung, and P.-H. Chen, “Dual-Source Energy-Harvesting Interface With Cycle-by-Cycle Source Tracking and Adaptive Peak-Inductor-Current

Control," *IEEE J. Solid-State Circuits*, vol. 53, no. 10, pp. 2741–2750, Oct. 2018, doi: 10.1109/JSSC.2018.2844358.

[54] J. J. Estrada-Lopez, A. Abuellil, A. Costilla-Reyes, M. Abouzied, S. Yoon, and E. Sanchez-Sinencio, "A Fully Integrated Maximum Power Tracking Combiner for Energy Harvesting IoT Applications," *IEEE Trans. Ind. Electron.*, vol. 67, no. 4, pp. 2744–2754, Apr. 2020, doi: 10.1109/TIE.2019.2907449.

[55] S. S. Amin and P. P. Mercier, "MISIMO: A Multi-Input Single-Inductor Multi-Output Energy Harvesting Platform in 28-nm FDSOI for Powering Net-Zero-Energy Systems," *IEEE J. Solid-State Circuits*, vol. 53, no. 12, pp. 3407–3419, Dec. 2018, doi: 10.1109/JSSC.2018.2865467.

[56] G. Chowdary, A. Singh, and S. Chatterjee, "An 18 nA, 87% Efficient Solar, Vibration and RF Energy-Harvesting Power Management System With a Single Shared Inductor," *IEEE J. Solid-State Circuits*, vol. 51, no. 10, pp. 2501–2513, Oct. 2016, doi: 10.1109/JSSC.2016.2585304.

[57] S. N. Soheli, G. Sarowar, Md. A. Hoque, and M. S. Hasan, "Design and Analysis of a DC -DC Buck Boost Converter to Achieve High Efficiency and Low Voltage Gain by using Buck Boost Topology into Buck Topology," in *2018 International Conference on Advancement in Electrical and Electronic Engineering (ICAEEE)*, Gazipur, Bangladesh: IEEE, Nov. 2018, pp. 1–4. doi: 10.1109/ICAEEE.2018.8643001.

[58] N. Kawai, Y. Kushino, and H. Koizumi, "MPPT controled piezoelectric energy harvesting circuit using synchronized switch harvesting on inductor," in *IECON 2015 - 41st Annual Conference of the IEEE Industrial Electronics Society*, Yokohama: IEEE, Nov. 2015, pp. 001121–001126. doi: 10.1109/IECON.2015.7392250.

[59] D. Singh and H. Singh, "Technical Survey and review on MPPT techniques to attain Maximum Power of Photovoltaic system," in *2019 5th International Conference on Signal Processing, Computing and Control (ISPCC)*, Solan, India: IEEE, Oct. 2019, pp. 265–268. doi: 10.1109/ISPCC48220.2019.8988382.

[60] V. Kostylev and A. Pavlovski, "Solar Power Forecasting Performance – Towards Industry Standards," 2011. Accessed: Nov. 21, 2023. [Online]. Available: https://www.semanticscholar.org/paper/Solar-Power-Forecasting-Performance-%E2%80%93-Towards-Kostylev-Pavlovski/692a76f7f0bf93cf69480ddced1ba42326ed77e0

[61] "Photovoltaic Power Forecasting: Models and Methods | IEEE Conference Publication | IEEE Xplore." Accessed: Nov. 24, 2023. [Online]. Available: https://ieeexplore.ieee.org/document/8582674

[62] A. Mellit, A. Massi Pavan, E. Ogliari, S. Leva, and V. Lughi, "Advanced Methods for Photovoltaic Output Power Forecasting: A Review," *Appl. Sci.*, vol. 10, no. 2, Art. no. 2, Jan. 2020, doi: 10.3390/app10020487.

[63] R. J. Zamora, E. G. Dutton, M. Trainer, S. A. McKeen, J. M. Wilczak, and Y.-T. Hou, "The Accuracy of Solar Irradiance Calculations Used in Mesoscale Numerical Weather Prediction," *Mon. Weather Rev.*, vol. 133, no. 4, pp. 783–792, Apr. 2005, doi: 10.1175/MWR2886.1.

[64] F. H. Gandoman, S. H. E. Abdel Aleem, N. Omar, A. Ahmadi, and F. Q. Alenezi, "Short-term solar power forecasting considering cloud coverage and ambient temperature variation effects," *Renew. Energy*, vol. 123, pp. 793–805, Aug. 2018, doi: 10.1016/j.renene.2018.02.102.

[65] B. Wolff, J. Kuehnert, E. Lorenz, O. Kramer, and D. Heinemann, “Comparing support vector regression for PV power forecasting to a physical modeling approach using measurement, numerical weather prediction, and cloud motion data,” *Sol. Energy*, vol. 135, pp. 197–208, Oct. 2016, doi: 10.1016/j.solener.2016.05.051.

[66] P. Bacher, H. Madsen, and H. A. Nielsen, “Online short-term solar power forecasting,” *Sol. Energy*, vol. 83, no. 10, pp. 1772–1783, Oct. 2009, doi: 10.1016/j.solener.2009.05.016.

[67] R. Ramakrishna and A. Scaglione, *A compressive sensing framework for the analysis of solar Photo-Voltaic power*. 2016, p. 312. doi: 10.1109/ACSSC.2016.7869048.

[68] L. Mora-López, I. Martínez-Marchena, M. Piliougine, and M. Sidrach-de-Cardona, “Binding Statistical and Machine Learning Models for Short-Term Forecasting of Global Solar Radiation,” in *Advances in Intelligent Data Analysis X*, J. Gama, E. Bradley, and J. Hollmén, Eds., in Lecture Notes in Computer Science. Berlin, Heidelberg: Springer, 2011, pp. 294–305. doi: 10.1007/978-3-642-24800-9_28.

[69] “Solar Harvested energy prediction algorithm for wireless sensors | IEEE Conference Publication | IEEE Xplore.” Accessed: Nov. 22, 2023. [Online]. Available: https://ieeexplore.ieee.org/document/6320497

[70] “Power management in energy harvesting sensor networks | ACM Transactions on Embedded Computing Systems.” Accessed: Nov. 22, 2023. [Online]. Available: https://dl.acm.org/doi/10.1145/1274858.1274870

[71] “Prediction and management in energy harvested wireless sensor nodes | IEEE Conference Publication | IEEE Xplore.” Accessed: Nov. 22, 2023. [Online]. Available: https://ieeexplore.ieee.org/document/5172412

[72] “Balanced energy allocation scheme for a solar-powered sensor system and its effects on network-wide performance - ScienceDirect.” Accessed: Nov. 22, 2023. [Online]. Available: https://www.sciencedirect.com/science/article/pii/S0022000010001236

[73] “Pro-Energy: A novel energy prediction model for solar and wind energy-harvesting wireless sensor networks | IEEE Conference Publication | IEEE Xplore.” Accessed: Nov. 22, 2023. [Online]. Available: https://ieeexplore.ieee.org/document/6502504

[74] “Forecasting sub-hourly solar irradiance for prediction of photovoltaic output - NASA/ADS.” Accessed: Nov. 19, 2023. [Online]. Available: https://ui.adsabs.harvard.edu/abs/1987pvsp.conf..171C/abstract

[75] A. H. Dehwah, S. Elmetennani, and C. Claudel, “UD-WCMA: An energy estimation and forecast scheme for solar powered wireless sensor networks,” *J. Netw. Comput. Appl.*, vol. 90, pp. 17–25, Jul. 2017, doi: 10.1016/j.jnca.2017.04.003.

[76] S. Eroshenko, A. Khalyasmaa, and D. Snegirev, “Machine learning techniques for short-term solar power stations operational mode planning,” *E3S Web Conf.*, vol. 51, p. 02004, 2018, doi: 10.1051/e3sconf/20185102004.

[77] V. P. Singh, V. Vijay, M. Siddhartha Bhatt, and D. K. Chaturvedi, “Generalized neural network methodology for short term solar power forecasting,” in *2013 13th International Conference on Environment and Electrical Engineering (EEEIC)*, Nov. 2013, pp. 58–62. doi: 10.1109/EEEIC-2.2013.6737883.

[78] C. Chen, S. Duan, T. Cai, and B. Liu, “Online 24-h solar power forecasting based on weather type classification using artificial neural network,” *Sol. Energy*, vol. 85, no. 11, pp. 2856–2870, Nov. 2011, doi: 10.1016/j.solener.2011.08.027.

[79] L.-L. Li, P. Cheng, H.-C. Lin, and H. Dong, “Short-term output power forecasting of photovoltaic systems based on the deep belief net,” *Adv. Mech. Eng.*, vol. 9, no. 9, p. 1687814017715983, Sep. 2017, doi: 10.1177/1687814017715983.

[80] Z. Zhen *et al.*, “SVM based cloud classification model using total sky images for PV power forecasting,” in *2015 IEEE Power & Energy Society Innovative Smart Grid Technologies Conference (ISGT)*, Feb. 2015, pp. 1–5. doi: 10.1109/ISGT.2015.7131784.

[81] Z. Liu and Z. Zhang, “Solar forecasting by K-Nearest Neighbors method with weather classification and physical model,” in *2016 North American Power Symposium (NAPS)*, Sep. 2016, pp. 1–6. doi: 10.1109/NAPS.2016.7747859.

[82] Y. M. Saint-Drenan, S. Bofinger, R. Fritz, S. Vogt, G. H. Good, and J. Dobschinski, “An empirical approach to parameterizing photovoltaic plants for power forecasting and simulation,” *Sol. Energy*, vol. 120, pp. 479–493, Oct. 2015, doi: 10.1016/j.solener.2015.07.024.

[83] Y.-K. Wu, C.-R. Chen, and H. Abdul Rahman, “A Novel Hybrid Model for Short-Term Forecasting in PV Power Generation,” *Int. J. Photoenergy*, vol. 2014, p. e569249, Jun. 2014, doi: 10.1155/2014/569249.

[84] G. Cervone, L. Clemente-Harding, S. Alessandrini, and L. Delle Monache, “Short-term photovoltaic power forecasting using Artificial Neural Networks and an Analog Ensemble,” *Renew. Energy*, vol. 108, pp. 274–286, Aug. 2017, doi: 10.1016/j.renene.2017.02.052.

[85] “Solar Energy Forecasting Using Machine Learning and Deep Learning Techniques | Archives of Computational Methods in Engineering.” Accessed: Nov. 27, 2023. [Online]. Available: https://link.springer.com/article/10.1007/s11831-023-09893-1

[86] Y. LeCun, Y. Bengio, and G. Hinton, “Deep learning,” *Nature*, vol. 521, no. 7553, Art. no. 7553, May 2015, doi: 10.1038/nature14539.

[87] Goodfellow, Ian, Bengio, Yoshua, and Courville, Aaron, *Deep Learning*. The MIT Press, 2016.

[88] J. L. Elman, “Finding structure in time,” *Cogn. Sci.*, vol. 14, no. 2, pp. 179–211, Apr. 1990, doi: 10.1016/0364-0213(90)90002-E.

[89] “(PDF) Untersuchungen zu dynamischen neuronalen Netzen.” Accessed: Nov. 15, 2023. [Online]. Available: https://www.researchgate.net/publication/243781690_Untersuchungen_zu_dynamischen_neuronalen_Netzen

[90] Y. Bengio, P. Simard, and P. Frasconi, “Learning long-term dependencies with gradient descent is difficult,” *IEEE Trans. Neural Netw.*, vol. 5, no. 2, pp. 157–166, Mar. 1994, doi: 10.1109/72.279181.

[91] S. Hochreiter and J. Schmidhuber, “Long Short-Term Memory,” *Neural Comput.*, vol. 9, no. 8, pp. 1735–1780, Nov. 1997, doi: 10.1162/neco.1997.9.8.1735.

[92] F. A. Gers, J. Schmidhuber, and F. Cummins, “Learning to forget: continual prediction with LSTM,” *Neural Comput.*, vol. 12, no. 10, pp. 2451–2471, Oct. 2000, doi: 10.1162/089976600300015015.

[93] Y. LeCun *et al.*, “Backpropagation Applied to Handwritten Zip Code Recognition,” *Neural Comput.*, vol. 1, no. 4, pp. 541–551, Dec. 1989, doi: 10.1162/neco.1989.1.4.541.

[94] “Energies | Free Full-Text | Day-Ahead Solar Irradiance Forecasting for Microgrids Using a Long Short-Term Memory Recurrent Neural Network: A Deep Learning Approach.” Accessed: Nov. 29, 2023. [Online]. Available: https://www.mdpi.com/1996-1073/12/10/1856

[95] H. Zhou, Q. Liu, K. Yan, and Y. Du, “Deep Learning Enhanced Solar Energy Forecasting with AI-Driven IoT,” *Wirel. Commun. Mob. Comput.*, vol. 2021, p. e9249387, Jun. 2021, doi: 10.1155/2021/9249387.

[96] J. Wang, L. Guo, C. Zhang, L. Song, J. Duan, and L. Duan, “Thermal power forecasting of solar power tower system by combining mechanism modeling and deep learning method,” *Energy*, vol. 208, p. 118403, Oct. 2020, doi: 10.1016/j.energy.2020.118403.

[97] D. Chandola, H. Gupta, V. Tikkiwal, and M. Bohra, “Multi-step ahead forecasting of global solar radiation for arid zones using deep learning,” *Procedia Comput. Sci.*, vol. 167, pp. 626–635, Jan. 2020, doi: 10.1016/j.procs.2020.03.329.

[98] S. Malakar *et al.*, “Designing a long short-term network for short-term forecasting of global horizontal irradiance,” *SN Appl. Sci.*, vol. 3, no. 4, p. 477, Mar. 2021, doi: 10.1007/s42452-021-04421-x.

[99] Y. Sun, V. Venugopal, and A. Brandt, “Short-term solar power forecast with deep learning: Exploring optimal input and output configuration,” *Sol. Energy*, vol. 188, pp. 730–741, Aug. 2019, doi: 10.1016/j.solener.2019.06.041.

[100] “Convolutional Neural Network for Short-term Solar Panel Output Prediction | IEEE Conference Publication | IEEE Xplore.” Accessed: Nov. 29, 2023. [Online]. Available: https://ieeexplore.ieee.org/document/8547400

[101] “Applied Sciences | Free Full-Text | Training and Testing of a Single-Layer LSTM Network for Near-Future Solar Forecasting.” Accessed: Nov. 29, 2023. [Online]. Available: https://www.mdpi.com/2076-3417/10/17/5873

[102] “Energies | Free Full-Text | Recurrent Neural Network-Based Hourly Prediction of Photovoltaic Power Output Using Meteorological Information.” Accessed: Nov. 29, 2023. [Online]. Available: https://www.mdpi.com/1996-1073/12/2/215

[103] A. Ganz, Z. Ganz, and K. Wongthavarawat, *Multimedia Wireless Networks: Technologies, Standards and Qos*. Upper Saddle River, NJ: Prentice Hall, 2003.

[104] I. Demirkol, C. Ersoy, and F. Alagoz, “MAC protocols for wireless sensor networks: a survey,” *IEEE Commun. Mag.*, vol. 44, no. 4, pp. 115–121, Apr. 2006, doi: 10.1109/MCOM.2006.1632658.

[105] V. K R, S. T., and M. Kumaraswamy, *QoS Routing Algorithms for Wireless Sensor Networks*. 2020. doi: 10.1007/978-981-15-2720-3.

[106] Y. Zhao, “Clustered Wireless Sensor Network Assisted the Design of Intelligent Art System,” *J. Sens.*, vol. 2022, p. e3216727, Jan. 2022, doi: 10.1155/2022/3216727.

[107] R. Clotet *et al.*, *QoS in Wireless Sensor Networks: A Survey*. 2009.

[108] C.-W. Hung, Y.-D. Zhuang, C.-H. Lee, C.-C. Wang, and H.-H. Yang, "Transmission Power Control in Wireless Sensor Networks Using Fuzzy Adaptive Data Rate," *Sensors*, vol. 22, no. 24, Art. no. 24, Jan. 2022, doi: 10.3390/s22249963.

[109] S. K. Mohanty and S. K. Udgata, "SATPAS: SINR-based adaptive transmission power assignment with scheduling in wireless sensor network," *Eng. Appl. Artif. Intell.*, vol. 103, p. 104313, Aug. 2021, doi: 10.1016/j.engappai.2021.104313.

[110] C. Boucetta, B. Nour, A. Cusin, and H. Moungla, "QoS in IoT Networks based on Link Quality Prediction," in *ICC 2021 - IEEE International Conference on Communications*, Montreal, QC, Canada: IEEE, Jun. 2021, pp. 1–6. doi: 10.1109/ICC42927.2021.9500396.

[111] "Estimating and predicting link quality in wireless IoT networks | Annals of Telecommunications." Accessed: Dec. 03, 2023. [Online]. Available: https://link.springer.com/article/10.1007/s12243-021-00835-1

[112] "(PDF) An enhanced adaptive duty cycle scheme for energy efficiency and QoS awareness in wireless sensor networks." Accessed: Dec. 05, 2023. [Online]. Available: https://www.researchgate.net/publication/361406417_An_enhanced_adaptive_duty_cycle_scheme_for_energy_efficiency_and_QoS_awareness_in_wireless_sensor_networks

[113] W. H. R. Chan *et al.*, "Adaptive Duty Cycling in Sensor Networks With Energy Harvesting Using Continuous-Time Markov Chain and Fluid Models," *IEEE J. Sel. Areas Commun.*, vol. 33, no. 12, pp. 2687–2700, Dec. 2015, doi: 10.1109/JSAC.2015.2478717.

[114] "Path loss exponent estimation in large wireless networks | IEEE Conference Publication | IEEE Xplore." Accessed: Dec. 02, 2023. [Online]. Available: https://ieeexplore.ieee.org/document/5044933

[115] *ESP32 Series data sheet*.

[116] "Train | Real Vibrations." Accessed: Jan. 14, 2024. [Online]. Available: https://realvibrations.nipslab.org/index.php/node/1093

List of Publications

All authors of every listed publication have contributed equally to the content of the corresponding publication unless it is mentioned otherwise. The papers are sorted based on date starting from the most recent ones.

Publications Related to the Topic of the Dissertation Thesis

Journal papers (with impact factor)

[1J] A. Othman, J. Hrad, J. Hajek, and D. Maga, “Control Strategies of Hybrid Energy Harvesting—A Survey,” *Sustainability*, vol. 14, no. 24, Art. no. 24, Jan. 2022, doi: 10.3390/su142416670. (Impact Factor: 3.9)

[2J] D. Maga, J. Hrad, J. Hajek, and A. Othman, “Application of Minimum Energy Effect to Numerical Reconstruction of Insolation Curves,” *Energies*, vol. 14, no. 17, p. 5313, Aug. 2021, doi: 10.3390/en14175313. (Impact Factor: 3.2)

Journal papers (without impact factor)

[3J] Othman, A. "The Energy Storage Systems and its applications in the telecommunications." *Svet digitalni ekonomiky* 1.1 (2016): 29-33.

Conference papers

[1C] A. Othman, D. Maga, and J. Hrad, “Multi-input Energy Harvesting System with Battery Management Support for WSN Applications,” in *2022 20th International Conference on Mechatronics - Mechatronika (ME)*, Dec. 2022, pp. 1–4. doi: 10.1109/ME54704.2022.9983095.

[2C] A. Othman and D. Maga, “Indoor Photovoltaic Energy Harvester with Rechargeable Battery for Wireless Sensor Node,” in *2018 18th International Conference on Mechatronics - Mechatronika (ME)*, Dec. 2018, pp. 1–6. Accessed: Dec. 13, 2023. [Online]. Available: https://ieeexplore.ieee.org/document/8624684

[3C] A. Othman and D. Maga, “Relation Between Security and Energy Consumption in Wireless Sensor Network (WSN),” in *2018 New Trends in Signal Processing (NTSP)*, Liptovský Mikuláš, Slovakia: IEEE, Oct. 2018, pp. 1–8. doi: 10.23919/NTSP.2018.8524094.

[4C] A. Othman, “Modeling of piezoelectric energy harvesting system embedded in soldier’s boot using Matlab/Simulink,” in *2017 International Conference on Military Technologies (ICMT)*, May 2017, pp. 787–792. doi: 10.1109/MILTECHS.2017.7988862.

[5C] A. Othman, “Energy storage system options in Intelligent Wireless Sensor Network,” in *2017 International Conference on Military Technologies (ICMT)*, Brno, Czech Republic: IEEE, May 2017, pp. 772–778. doi: 10.1109/MILTECHS.2017.7988860.

[6C] A. Othman, K. Belda, and P. Burget, “Physical modelling of energy consumption of industrial articulated robots,” in *2015 15th International Conference on Control, Automation and Systems (ICCAS)*, Busan, Korea (South): IEEE, Oct. 2015, pp. 784–789. doi: 10.1109/ICCAS.2015.7364727.

Publications Non-Related to the Topic of the Dissertation Thesis

[7C] A. Othman, K. Belda, and P. Burget, “Physical modelling of energy consumption of industrial articulated robots,” in *2015 15th International Conference on Control, Automation and Systems (ICCAS)*, Busan, Korea (South): IEEE, Oct. 2015, pp. 784–789. doi: 10.1109/ICCAS.2015.7364727.

Citations

This chapter contains publications that have cited the author's work as per Google Scholar, excluding any self-citations.

[1] Mishra, Kaushik, et al. "Analytical evaluation and experimental validation of energy harvesting using low frequency band of piezoelectric bimorph actuator." Smart Structures and Systems, An International Journal 26.3 (2020): 391-401.

[2] Venugopal, Mohankumar, and Govindanayakanapalya Venkatagiriyappa Jayaramaiah. "Simulation and performance analysis of self-powered piezoelectric energy harvesting system for low power applications." International Journal of Electrical and Computer Engineering (IJECE) 12.6 (2022): 5861-5871.

[3] Shafiq, Raghda RG, et al. "A power source for E-devices based on green energy." Energy Harvesting and Systems 0 (2023).

[4] Rao, Sudheshna, et al. "Design, Development and Analysis of Energy-Harvesting System." Journal of Vibration Engineering & Technologies (2023): 1-9.

[5] Deb, Anindita, Debika Debnath, and Joy Saha. "Design & Analysis of a PV-Piezoelectric based Off-grid Energy Harvester in Tripura." Journal of Physics: Conference Series. Vol. 2286. No. 1. IOP Publishing, 2022.

[6] Dwivedi, Aakriti, et al. "Evaluation of ambient energy harvesting technologies for low power devices." 2021 Second International Conference on Electronics and Sustainable Communication Systems (ICESC). IEEE, 2021.

[7] Patel, Harshil R., and Manish Patel. "Modelling of Piezoelectric Harvesting System." 2022 7th International Conference on Communication and Electronics Systems (ICCES). IEEE, 2022.

[8] Hegde, Hariprasad, Ugra Mohan Roy, and Mrinal Kumar. "Design of Piezoelectric Based Power Generation System for Electric Vehicle." International Journal of Recent Technology and Engineering (IJRTE) 9.4 (2020).

[9] Franka, Grazhdani, Anackova Maja, and Jovanova Jovana. "627. ENERGY HARVESTING USING PIEZOELECTRIC CERAMICS INCORPORATED IN A SHOE-SOLE." Mechanical Engineering–Scientific Journal 38.1 (2020): 29-36.

[10] Gaspar, Gabriel, et al. "IoT-ready temperature probe for smart monitoring of forest roads." Applied Sciences 12.2 (2022): 743.

[11] Shore, Andrew, et al. "Indoor light energy harvesting for battery‐powered sensors using small photovoltaic modules." Energy Science & Engineering 9.11 (2021): 2036-2043.

[12] Ďuďák, Juraj, et al. "A Low-Power Data Logger with Simple File System for Long-Term Environmental Monitoring in Remote Areas." IEEE Sensors Journal (2023).

[13] Gaspar, Gabriel, et al. "Meteorological support in research of forest roads conditions monitoring." 2021 2nd International Conference on Smart Electronics and Communication (ICOSEC). IEEE, 2021.

[14] Dwik, Shaher, G. Sasikala, and S. Natarajan. "Design and Simulation of a Reconfigurable Multifunctional Optical Sensor." Optical Memory and Neural Networks 32.2 (2023): 147-157.

[15] Ghani, Azlinda Abdul, et al. "Effect of epoxidized natural rubber-50 (ENR-50) as compatibilizer in composite." AIP Conference Proceedings. Vol. 2703. No. 1. AIP Publishing, 2023.

[16] Gaspar, Gabriel, et al. "Local weather station for decision making in civil engineering." Computer Science On-line Conference. Cham: Springer International Publishing, 2021.

[17] Dudak, Juraj, et al. "Design of a driver for measurements with piezoelectric elements." 2022 20th International Conference on Mechatronics-Mechatronika (ME). IEEE, 2022.

[18] Clemente, Carmine Stefano, Daniele Davino, and Vincenzo Paolo Loschiavo. "Energy balance of a continuous structural health monitoring system based on energy harvesting." IOP Conference Series: Materials Science and Engineering. Vol. 949. No. 1. IOP Publishing, 2020.

[19] George, Anna Merine, et al. "Indoor PV-Based Power Management System for Connected Lighting and Shading Control." Sustainable Energy and Technological Advancements: Proceedings of ISSETA 2021. Singapore: Springer Singapore, 2022. 759-771.

[20] TEKİN, Nazlı. ENERGY HARVESTING WIRELESS MULTIMEDIA SENSOR NETWORKS IN INDUSTRIAL ENVIRONMENTS. MS thesis. Abdullah Gül Üniversitesi, Fen Bilimleri Enstitüsü, 2020.

[21] Di Buono, Antonio, et al. "The effects of Total Ionizing Dose irradiation on supercapacitors deployed in nuclear decommissioning environments." Journal of Power Sources 479 (2020): 228675.

[22] Byamukama, Maximus, et al. "Powering environment monitoring Wireless Sensor Networks: A review of design and operational challenges in Eastern Africa." EAI Endorsed Transactions on Internet of Things 4.14 (2018): e1-e1.

[23] Staaf, Henrik. Conjoined piezoelectric harvesters and carbon supercapacitors for powering intelligent wireless sensors. Chalmers Tekniska Hogskola (Sweden), 2018.

[24] Li, Qi. Electrochemical Capacitors for Miniaturized Self-Powered Systems: Challenges and Solutions. Diss. Chalmers Tekniska Hogskola (Sweden), 2020.

[25] El Mahboubi, Firdaous. Stockage adaptatif pour noeud de capteur sans fil autonome et sans batterie. Diss. Université Paul Sabatier-Toulouse III, 2018.

[26] Panangala, Samitha Dilhani. High Performance Electrode Materials From Carbon Nanofibers with Tunable Pore Architectures. Diss. 2019.

[27] Lima, David Manuel Cartaxo. Integração Sensorial para o diagnóstico de Transformadores de Distribuição (MT/BT) de Energia Eléctrica. MS thesis. 2018.

[28] Chetto, Maryline, and Rola El Osta. "Earliest Deadline First Scheduling for Real-Time Computing in Sustainable Sensors." Sustainability 15.5 (2023): 3972.

[29] Tropea, Mauro, et al. "Security in wireless sensor networks: A cryptography performance analysis at mac layer." Future Internet 14.5 (2022): 145.

[30] Ďuďák, Juraj, et al. "A Low-Power Data Logger with Simple File System for Long-Term Environmental Monitoring in Remote Areas." IEEE Sensors Journal (2023).

[31] Serianni, Abdon, and Nunzia Palmieri. "A MAC Layer Energy Drain Attack Analysis in WSN." 2022 30th Telecommunications Forum (TELFOR). IEEE, 2022.

[32] Vera-Perez, José, et al. "Safety and Security oriented design for reliable Industrial IoT applications based on WSNs." 2019 24th IEEE International Conference on Emerging Technologies and Factory Automation (ETFA). IEEE, 2019.

[33] Palmieri, Nunzia, and Luis Miguel Samaniego Campoverde. "A MAC layer analysis of an impersonation attack in a wireless sensor network." Autonomous Systems: Sensors, Processing and Security for Ground, Air, Sea, and Space Vehicles and Infrastructure 2023. Vol. 12540. SPIE, 2023.

[34] Fraiji, Yosra. Stratégies de sécurité contextuelle sous contrainte énergétique pour le réseau intra Véhicule Electrique. Diss. Normandie, 2021.

[35] Panahi, Uras, and Cüneyt Bayılmış. "Enabling secure data transmission for wireless sensor networks based IoT applications." Ain Shams Engineering Journal 14.2 (2023): 101866.